

# NASA Contractor Report 4471

## A Stochastic Optimal Feedforward and Feedback Control Methodology for Superagility

Nesim Halyo, Haldun Direskeneli,  
and Deborah B. Taylor  
*Information & Control Systems, Incorporated*  
*Hampton, Virginia*

Prepared for  
Langley Research Center  
under Contract NAS1-19091



National Aeronautics and  
Space Administration  
Office of Management  
Scientific and Technical  
Information Program

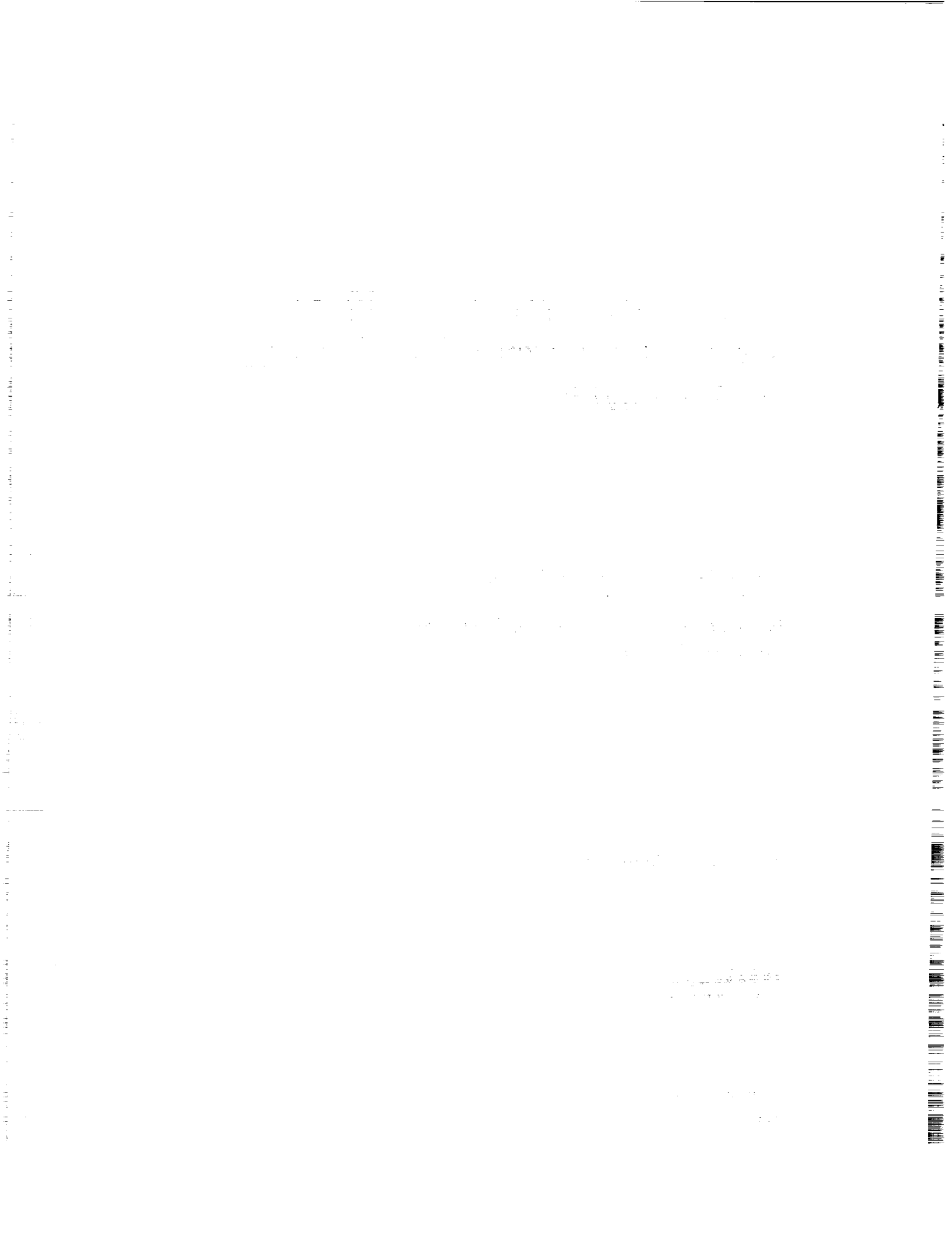
1992

N93-13370

Unclass

H1/63 0131727

(NASA-CR-4471) A STOCHASTIC  
OPTIMAL FEEDFORWARD AND FEEDBACK  
CONTROL METHODOLOGY FOR  
SUPERAGILITY Final Report  
(Information and Control Systems)  
150 p



## FOREWORD

The work described in this report was performed by Information & Control Systems, Incorporated (ICS) under Contract Number NAS1-19091 for the National Aeronautics and Space Administration (NASA), Langley Research Center (LaRC). The work was sponsored under the Small Business Innovation Research (SBIR) program by the Aircraft Guidance & Controls Branch.

Mr. Aaron Ostroff was the NASA Technical Representative for this contract. Dr. Nesim Halyo was the ICS project manager.

All the design, analysis and simulation results shown in this report were obtained using our Computer-Aided Control System Design (CACSD) software package ACET<sup>TM</sup>.

We would like to thank the National Aeronautics and Space Administration for its support of this important work.

## SUMMARY

This work was performed under the NASA SBIR program. ICS plans to market the software developed as a new module in its commercial CACSD software package: ACET. This module will contain algorithms for designing SOFFT control laws, for analyzing command tracking performance with  $Z$ -plots and for simulating SOFFT control systems using the incremental implementation. ICS also plans to market the SOFFT methodology to design flight control systems for high-performance aircraft and in other control applications.

A new control design methodology is proposed: Stochastic Optimal Feedforward and Feedback Technology (SOFFT). Traditional design techniques optimize a single cost function (which expresses the design objectives) to obtain both the feedforward and feedback control laws. Since the feedforward response must be fast while the feedback response must be relatively slow (to attenuate noise), combining these objectives into a single cost function produces conflicting demands; so that neither of the objectives is fully achieved. In the SOFFT approach, two cost functions are defined. The feedforward control law is designed to optimize one cost function, the feedback optimizes the other. By separating the design objectives and decoupling the feedforward and feedback design processes, both objectives can be achieved fully.

The main feedforward design objective is to produce a desirable response in tracking input commands when no random noises and disturbances are present. In particular, a fast and smooth tracking response during the transient phase while performing difficult maneuvers is the goal of the feedforward law. The main feedback design objectives are to suppress sensor noise, accommodate plant disturbances and provide stability in the presence of plant modeling uncertainties.

A new measure of command tracking performance,  $Z$ -plots, was developed. By analyzing these plots at off-nominal operating points, the sensitivity or robustness of the total system in tracking commands can be predicted.  $Z$ -plots provide an important tool for designing robust control systems.

The Variable-Gain SOFFT methodology was used to design a flight control system for the F/A-18 aircraft. The Variable-Gain SOFFT controller can be used to extend the operating regime of the aircraft and to provide greater performance (flying/handling qualities) throughout the extended regime. The angle-of-attack ( $\alpha$ ) command system designed smoothly and quickly brings the aircraft to within 3 degrees of its physical (actuator) limit with an easy maneuver. A detailed nonlinear simulation of the aircraft and control system displays excellent command tracking performance.

An important by-product of the SOFFT approach is that by removing the conflicting demands on the control system, both feedforward and feedback control laws can be designed with less effort and in considerably less time. Our main conclusion is that the concept of separating the feedforward and feedback objectives and decoupling the two design processes works well.

# TABLE OF CONTENTS

<b>FOREWORD</b> .....	iii
<b>LIST OF FIGURES</b> .....	viii
<b>LIST OF TABLES</b> .....	xiii
<b>LIST OF SYMBOLS</b> .....	xiv
<b>I. INTRODUCTION</b> .....	1
<b>II. INTEGRATED FEEDFORWARD AND FEEDBACK (IFF)</b>	
<b>CONTROL DESIGN</b> .....	6
1. Linearization .....	6
2. Time-Invariant SOFFT Control .....	10
3. Feedback Control Design .....	12
4. Feedforward Control Design .....	16
5. Algorithm for Feedforward Gains .....	20
Perfect Tracking .....	21
6. The SOFFT Control Structure .....	22
<b>III. COMMAND TRACKING PERFORMANCE</b> .....	25
1. Z-Plots .....	28
2. F/A-18 Actuator Approximation Design .....	31

# TABLE OF CONTENTS (CONTINUED)

<b>IV. VARIABLE-GAIN SOFFT DESIGN METHODOLOGY</b> .....	<b>37</b>
<b>1. Problem Formulation</b> .....	<b>38</b>
Perfect Tracking .....	41
<b>2. Feedforward Integrators</b> .....	<b>42</b>
<b>3. Algorithm for Gain Computation</b> .....	<b>44</b>
<b>4. Digital Implementation</b> .....	<b>46</b>
Feedforward Control Implementation .....	46
Interpolation of Feedforward Models .....	48
Feedback Control Implementation .....	49
<b>V. F/A-18 SIMULATION</b> .....	<b>51</b>
<b>1. Overview of the Basic Components</b> .....	<b>51</b>
Flight Control System (FCS) Inputs .....	53
Actuator Dynamics .....	53
Engine Dynamics .....	54
Aerodynamic Model .....	55
Kinematics .....	56
Sensor Outputs .....	58
<b>2. Simulation Examples</b> .....	<b>59</b>

# TABLE OF CONTENTS (CONCLUDED)

<b>VI. A VARIABLE-GAIN SOFT FLIGHT CONTROL SYSTEM FOR THE F/A-18</b> .....	68
<b>1. Longitudinal FCS Design</b> .....	68
Feedback .....	69
Feedforward .....	73
<b>2. Lateral FCS Design</b> .....	77
Feedback .....	81
Feedforward .....	84
<b>3. Analysis and Simulation</b> .....	88
Eigenvalues .....	88
Feedback Loop Analysis .....	88
Sensor Noise/Error Suppression .....	92
Plant Disturbance Accommodation .....	95
Command Tracking Performance .....	95
Tracking Performance Sensitivity .....	99
Simulations .....	103
<b>CONCLUSIONS</b> .....	116
<b>REFERENCES</b> .....	119
<b>APPENDIX A</b> .....	122

# LIST OF FIGURES

Figure 1. Error Feedback Controller .....	2
Figure 2. Explicit Model Following Control Law Structure .....	2
Figure 3. SOFFT Integrated Feedforward and Feedback (IFF) Control Structure .....	5
Figure 4. SOFFT Control Law Structure .....	23
Figure 5. $Z_I$ -Plot Interpretation .....	29
Figure 6. $Z_O$ -Plot Interpretation .....	30
Figure 7. Desired Response (Command Model) .....	32
Figure 8. $Z$ -Plots for FB Design 1 .....	33
Figure 9. $Z$ -Plots for FB Design 2 .....	35
Figure 10. Frequency Response from Pitch Command to Thrust Response .....	36
Figure 11. Flight Simulation Diagram .....	52
Figure 12. Longitudinal/Vertical Variables with Longitudinal Variables Perturbed .....	59
Figure 13. Simulation Variables with Lateral Variables Perturbed ...	61
Figure 14. Engine Variables with A Maximum Throttle Pulse Input ..	63



## LIST OF FIGURES (CONTINUED)

<p><b>Figure 15. Simulation Variables for the Same Maximum Engine Throttle Pulse Input as in Figure 14</b> .....</p>	65
<p><b>Figure 16. Frequency-Domain Loop Analysis of <math>\alpha</math>-Command Variable-Gain Feedback Control Law; Model 1; Perspective: Input</b></p>	70
<p><b>Figure 17. Frequency-Domain Loop Analysis of <math>\alpha</math>-Command Variable-Gain Feedback Control Law; Model 2; Perspective: Input</b></p>	71
<p><b>Figure 18. Frequency-Domain Loop Analysis of <math>\alpha</math>-Command Variable-Gain Feedback Control Law; Model 3; Perspective: Input</b></p>	72
<p><b>Figure 19a. Effect of Pitch Rate Gyro Errors on Angle-of-Attack (<math>\alpha</math>) for Model 1</b> .....</p>	74
<p><b>Figure 19b. Effect of <math>\alpha</math>-Vane Errors on Angle-of-Attack (<math>\alpha</math>) for Model 1</b> .....</p>	74
<p><b>Figure 20a. Effect of Pitch Rate Gyro Errors on for Model 2</b> .....</p>	75
<p><b>Figure 20b. Effect of <math>\alpha</math>-Vane Errors on Angle-of-Attack (<math>\alpha</math>) for Model 2</b> .....</p>	75
<p><b>Figure 21a. Effect of Pitch Rate Gyro Errors on Angle-of-Attack (<math>\alpha</math>) for Model 3</b> .....</p>	76
<p><b>Figure 21b. Effect of <math>\alpha</math>-Vane Errors on Angle-of-Attack (<math>\alpha</math>) for Model 3</b> .....</p>	76

## LIST OF FIGURES (CONTINUED)

Figure 22a. Effect of Plant Disturbance (at Input) on Pitch Rate ( $q$ ) for Model 1 .....	78
Figure 22b. Effect of Plant Disturbance (at Input) on Angle-of-Attack ( $\alpha$ ) for Model 1 .....	78
Figure 23a. Effect of Plant Disturbance (at Input) on on Pitch Rate ( $q$ ) for Model 2 .....	79
Figure 23b. Effect of Plant Disturbance (at Input) Angle-of-Attack ( $\alpha$ ) for Model 2 .....	79
Figure 24a. Effect of Plant Disturbance (at Input) on on Pitch Rate ( $q$ ) for Model 3 .....	80
Figure 24b. Effect of Plant Disturbance (at Input) Angle-of-Attack ( $\alpha$ ) for Model 3 .....	80
Figure 25a. Desired Frequency Response of Angle-of-Attack ( $\alpha$ ) to Pilot Inputs .....	82
Figure 25b. Actual Frequency Response of Angle-of-Attack ( $\alpha$ ) to Pilot Inputs for Model 1 .....	82
Figure 25c. Actual Frequency Response of Angle-of-Attack ( $\alpha$ ) to Pilot Inputs for Model 2 .....	83
Figure 25d. Actual Frequency Response of Angle-of-Attack ( $\alpha$ ) to Pilot Inputs for Model 3 .....	83

# LIST OF FIGURES (CONTINUED)

Figure 26a. Command Tracking Performance for Model 1: $z$ -Norm (Unweighted) .....	89
Figure 26b. Command Tracking Performance for Model 1: Weighted $z$ -Norm .....	89
Figure 27a. Command Tracking Performance for Model 2: $z$ -Norm (Unweighted) .....	90
Figure 27b. Command Tracking Performance for Model 2: Weighted $z$ -Norm .....	90
Figure 28a. Command Tracking Performance for Model 3: $z$ -Norm (Unweighted) .....	91
Figure 28b. Command Tracking Performance for Model 3: Weighted $z$ -Norm .....	91
Figure 29. Command Tracking Performance Sensitivity: $p_{true} = 30^\circ$ , $p_{est} = 20^\circ$ .....	93
Figure 30. Command Tracking Performance Sensitivity: $p_{true} = 30^\circ$ , $p_{est} = 40^\circ$ .....	94
Figure 31. F/A-18 SOFFT Control Law Simulation: $\alpha$ -Command = $30^\circ$ .....	96
Figure 32. F/A-18 SOFFT Control Law Simulation: $\alpha$ -Command = $40^\circ$ .....	100

# LIST OF FIGURES (CONCLUDED)

<b>Figure 33. F/A-18 SOFFT Control Law Simulation:</b> $\alpha$ -Command = $5^\circ, 55^\circ$ .....	104
<b>Figure 34. F/A-18 SOFFT Control Law Simulation:</b> $\alpha$ -Command = $18.8^\circ$ ; $p$ -Command = DOUBLET; $\beta$ -Command = $0^\circ$ .....	108
<b>Figure 35. F/A-18 Single-Model SOFFT Control Law Simulation:</b> $\alpha$ -Command = $30^\circ$ ; .....	112
<b>Figure 36. F/A-18 Single-Model SOFFT Control Law Simulation:</b> $\alpha$ -Command = $55^\circ$ ; .....	114

# LIST OF TABLES

<b>Table 1. Eigenvalue Analysis: Model 1 Open-Loop Equivalent <math>s</math>-Plane Eigenvalues</b> .....	<b>85</b>
<b>Table 2. Eigenvalue Analysis: Model 1 Closed-Loop Equivalent <math>s</math>-Plane Eigenvalues</b> .....	<b>85</b>
<b>Table 3. Eigenvalue Analysis: Model 2 Open-Loop Equivalent <math>s</math>-Plane Eigenvalues</b> .....	<b>86</b>
<b>Table 4. Eigenvalue Analysis: Model 2 Closed-Loop Equivalent <math>s</math>-Plane Eigenvalues</b> .....	<b>86</b>
<b>Table 5. Eigenvalue Analysis: Model 3 Open-Loop Equivalent <math>s</math>-Plane Eigenvalues</b> .....	<b>87</b>
<b>Table 6. Eigenvalue Analysis: Model 3 Closed-Loop Equivalent <math>s</math>-Plane Eigenvalues</b> .....	<b>87</b>

## LIST OF SYMBOLS

$A$	State matrix
$A(p)$	State matrix for operating point $p$
$A_x(p)$	State matrix for operating point $p$
$B$	Control effectiveness matrix or input matrix
$B(p)$	Control effectiveness matrix for operating point $p$
$b_x$	measurement bias vector
$\tilde{b}_x$	unknown portion of measurement bias; $\tilde{b}_x = b_x - b_x^*$
$b_x(p)$	measurement bias for operating point $p$
$B_x(p)$	Control effectiveness (input) matrix for operating point $p$
$b_x^*$	Measurement bias in feedforward law
$C$	Output matrix
$C_c$	Output matrix of feedback dynamic compensator
$C_c(p_k)$	Output matrix of feedback dynamic compensator for operating point $p_k$
$C_I$	Output matrix of integral error feedback
$C_I(p_k)$	Output matrix of integral error feedback for operating point $p_k$
$c_k$	Dynamic compensator state vector
$\tilde{c}_k$	Tracking error in dynamic compensator state at $t_k$
$C_u$	Output matrix for control rate commands (CRC)
$C_u(p_k)$	Output matrix for control rate commands (CRC) for operating point $p_k$
$C_u^*$	Output matrix for CRC in feedforward law
$C_x$	Plant output matrix
$C_x(p)$	Plant output matrix for operating point $p$
$C_x^*$	Plant output matrix in feedforward law
$C_x^*(p)$	Plant output matrix in feedforward law for operating point $p$
$C_z^*$	Plant output matrix for command state in feedforward law
$d$	Plant disturbance vector
$D$	Direct transfer matrix
$d(p)$	Plant disturbance for operating point $p$
$d_x$	Plant disturbance vector
$D_x$	Direct transfer matrix
$d_x(p)$	Plant disturbance vector for operating point $p$
$d_x^*$	Plant disturbance vector in feedforward law
$D_x^*$	Direct transfer matrix in feedforward law

## LIST OF SYMBOLS (CONTINUED)

$E$	Expectation operator
$e(p, k)$	Tracking error at time $t_k$ for operating point $p$
$e^*(p, k)$	Tracking error in feedforward law at time $t_k$ for operating point $p$
$e_k$	Tracking error at time $t_k$
$e_k^*$	Tracking error in feedforward law at time $t_k$
$H_c$	Matrix defining the integrated compensator variables
$H_u$	Matrix defining the integrated control variables
$H_x$	Matrix defining the tracking variables
$H_y$	Matrix defining the tracking variables
$H_z$	The command model output matrix
$I$	Identity matrix
$I_k$	Integrator state vector at time $t_k$
$I^*(p, k)$	Integrator state vector at time $t_k$ for operating point $p$
$\tilde{I}_k$	Tracking error in integrator state at time $t_k$
$I_x$	Moment of inertia about $x$ -body axis
$I_y$	Moment of inertia about $y$ -body axis
$I_z$	Moment of inertia about $z$ -body axis
$I_{xy}$	Product of inertia about $x$ and $y$ axes
$I_{yz}$	Product of inertia about $y$ and $z$ axes
$I_{zx}$	Product of inertia about $z$ and $x$ axes
$J$	Cost function for feedback law
$J^*$	Cost function for feedforward law
$J^*(p)$	Local feedforward cost at operating point $p$
$K$	Feedback gain matrix
$k$	Dummy integer variable (usually counts sampling instants)
$K^*(p)$	Gain matrix in feedforward law at operating point $p$
$K_c$	Dynamic compensator feedback gain matrix
$K_{cc}$	Dynamic compensator feedback gain
$K_{cc}(p_k)$	Dynamic compensator feedback gain for operating point $p$
$K_{cI}$	Feedback gain from integrator state to dynamic compensator
$K_{cI}(p_k)$	Feedback gain from integrator state to dynamic compensator for operating point $p_k$
$K_{cu}$	Feedback gain from control command dynamic compensator
$K_{cu}(p_k)$	Feedback gain from control command dynamic compensator for operating point $p_k$
$K_{cx}$	Feedback gain from plant output to dynamic compensator
$K_{cx}(p_k)$	Feedback gain from plant output to dynamic compensator for operating point $p_k$

## LIST OF SYMBOLS (CONTINUED)

$K_I$	Integral feedback gain matrix
$K_I^*$	Integral feedforward gain matrix
$K_I^*(p)$	Integral feedforward gain matrix for operating point $p$
$K_u$	Control command feedback gain matrix
$K_u(p)$	Control command feedback gain matrix for operating point $p$
$K_{uj}$	Feedforward variable-gain matrix for $p(j); 0 \leq j \leq n_p$
$K_x$	Plant state feedback gain matrix
$K_x^*$	Plant state feedforward gain matrix
$K_x^*(p)$	Plant state feedforward gain matrix for operating point $p$
$K_{xc}$	Feedback gain from dynamic compensator state to plant
$K_{xc}(p_k)$	Feedback gain from dynamic compensator state to plant for operating point $p_k$
$K_{xI}$	Feedback gain from integrator state to plant
$K_{xI}(p_k)$	Feedback gain from integrator state to plant for operating point $p_k$
$K_{xj}^*$	Feedforward variable-gain matrix for $p(j); 0 \leq j \leq n_p$
$K_{xu}$	Feedback gain from control command state to plant
$K_{xu}(p_k)$	Feedback gain from control command state to plant for operating point $p_k$
$K_{xx}$	Feedback gain from plant output state to plant
$K_{xx}(p_k)$	Feedback gain from plant output state to plant for operating point $p_k$
$K_z$	Command state feedforward gain matrix
$K_z(p)$	Command state feedforward gain matrix for operating point $p$
$K_{zj}$	Feedforward variable-gain matrix for $p(j); 0 \leq j \leq n_p$
$L$	Rolling moment
$M$	Pitching moment
$N$	Yawing moment
$n_c$	Order of dynamic compensator
$n_I$	Order of integrator feedback
$n_{mod}$	Number of plant models
$n_p$	Dimension of $p$
$n_r$	Dimension of $u_k$ and $\tilde{u}_k$



## LIST OF SYMBOLS (CONTINUED)

$n_{u_x}$	Number of plant controls; dimension of $u_x$
$n_{u_c}$	Number of command model inputs; dimension of $u_c$
$n_{v_c}$	Number of dynamic compensator controls; dimension of $v_c$
$n_x$	Dimension of plant state; plant order; dimension of $x$
$n_{y_x}$	Number of plant outputs or sensors; dimension of $y_x$
$n_z$	Order of command model; dimension of $z$
$o_x^2(t)$	Remainder term in $2^{nd}$ -order Taylor series expansion of $x(t)$
$o_y^2(t)$	Remainder term in $2^{nd}$ -order Taylor series expansion of $y(t)$
$p$	Parameter vector denoting operating point; its components are the gain scheduling variables; roll rate
$p(j)$	$j^{th}$ component of $p$
$p^i$	Value of parameter vector, $p$ , for $i^{th}$ operating point or for $i^{th}$ model
$p_k$	Value of $p$ at time $t_k$
$q$	Pitch rate
$Q$	State penalty matrix in feedback cost function
$Q^*$	State penalty matrix in feedforward cost function
$Q^*(p)$	Local state penalty matrix in feedforward cost function for operating point $p$
$Q_1^*$	State penalty matrix in feedforward cost function excluding tracking error
$Q_1^*(p)$	Local state penalty matrix in feedforward cost function excluding tracking error for operating point $p$
$Q_I$	Integrator state penalty matrix in feedback cost function
$Q_I(p)$	Integrator state penalty matrix in feedback cost function for operating point $p$
$r$	Yaw rate
$R$	Control penalty matrix in feedback cost function
$R^*$	Control penalty matrix in feedforward cost function
$R_1^*$	Control penalty matrix in feedforward cost function
$R_1^*(p)$	Control penalty matrix in feedforward cost function for operating point $p$
$s$	Laplace transform variable

## LIST OF SYMBOLS (CONTINUED)

$t$	time
$T(\omega)$	Transfer function matrix from $u_{zk}$ to $y_{zk}$ at frequency $\omega$
$T^*(\omega)$	(Desired or commanded) transfer function matrix from $u_{zk}$ to $y_{zk}^*$ at frequency $\omega$
$t_k$	$k^{th}$ sampling instant
$T_{ij}(\omega)$	$i - j$ element of $T(\omega)$
$u'$	Forward speed along $x$ body-axis
$\tilde{u}_k$	Tracking error in control rate command state
$u_{zk}$	Plant control (input) vector
$\tilde{u}_{zk}$	Portion of plant control due to feedback of tracking error
$u_x(p, k)$	Variable-gain plant control vector for operating point $p$ at time $t_k$
$u_x(t)$	Continuous plant control vector
$u_x^*$	Constant portion of feedforward control law
$u_x^*(p)$	Constant portion of feedforward control law for operating point $p$
$u_x^*(p, k)$	Variable-gain feedforward control vector for operating point $p$ at time $t_k$
$u_{zk}^*$	Feedforward control vector at time $t_k$
$u_z(p, k)$	Command model input vector for operating point $p$ at time $t_k$
$u_{zk}$	Command model input vector at time $t_k$
$v$	Lateral speed
$\tilde{v}_k$	Feedback design model control vector
$\tilde{v}_{ck}$	Dynamic compensator feedback control vector
$\tilde{v}_{zk}$	Feedback control vector for plant
$w_k$	Discrete plant noise
$w_n$	Natural frequency
$\bar{w}_x(t)$	Continuous plant noise
$w_x(p, k)$	Plant noise for operating point $p$ at time $t_k$
$w_z(p, k)$	Augmented command model noise
$w_{ck}$	Dynamic compensator "plant noise"
$w_{Ik}$	Integrator "plant noise"
$w_{uk}$	Control rate command "plant noise"
$w_{zk}$	Plant noise

## LIST OF SYMBOLS (CONTINUED)

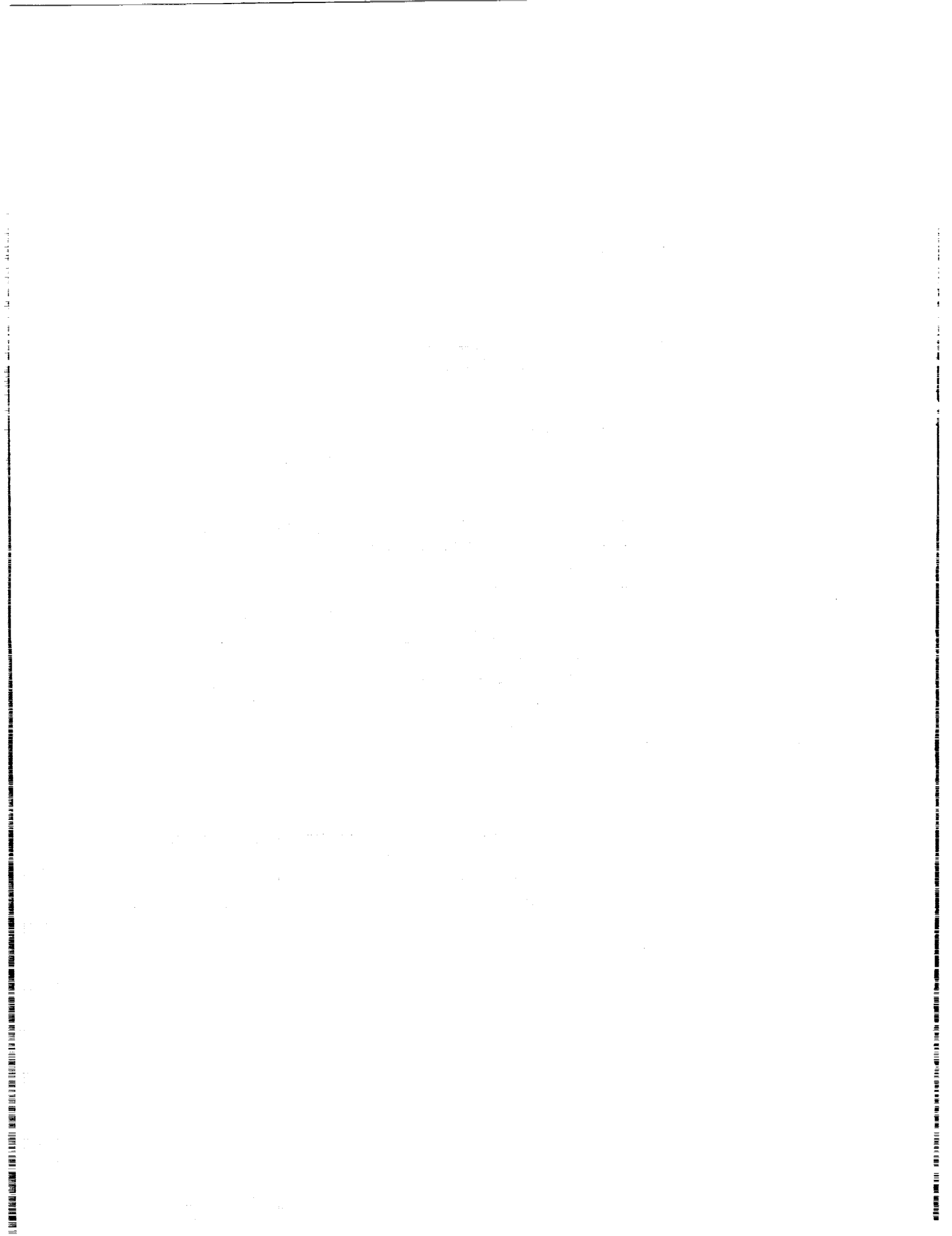
$x(p, k)$	Plant state vector for operating point $p$ at time $t_k$
$x(t)$	Plant state vector at time $t$
$x^*(p, k)$	Feedforward plant state for operating point $p$ at time $t_k$ (star-trajectory)
$X^*(p, k)$	Augmented plant state for operating point $p$ at time $t_k$
$x_k^*$	Feedforward plant state at time $t_k$ (star-trajectory)
$x_k$	Plant state vector
$\tilde{x}_k$	Tracking error in plant state
$\tilde{X}_k$	Tracking error in (augmented) feedback design model state
$Y^*(p, k)$	Augmented feedforward output vector for operating point $p$ at time $t_k$
$\tilde{y}_{ck}$	Tracking error in dynamic compensator output vector
$\tilde{y}_{Ik}$	Tracking error in integrator output vector
$\tilde{Y}_k$	Tracking error in feedback design model output vector
$\tilde{y}_{uk}$	Tracking error in control rate command output vector
$\tilde{y}_{xk}$	Tracking error in plant output vector
$y_x(p, k)$	Plant output vector for operating point $p$ at time $t_k$
$y_x(t)$	Plant output vector at time $t_k$
$y_x(\omega)$	Discrete Fourier transform of $\{y_{xk}\}$
$y_x^*(p, k)$	Feedforward plant output vector of operating point $p$ at time $t_k$
$y_x^*(\omega)$	Discrete Fourier transform of $\{y_{xk}^*\}$
$y_{xk}$	Plant output vector at time $t_k$
$y_{xk}^*$	Feedforward plant output vector at time $t_k$
$y_{zk}$	Command model output vector at time $t_k$
$z(p, k)$	Command model state vector
$Z(p, k)$	Augmented command model state vector
$Z_c(\omega)$	Cross-talk $Z$ -matrix
$Z_I(\omega)$	Input $Z$ -matrix
$z_k$	Command model state vector
$Z_O(\omega)$	Output $Z$ -matrix
$Z_{ij}(\omega)$	$i - j$ element of a $Z$ -matrix
$Z_{max}(\omega)$	Upper bound of $Z$ -matrix
$Z_{min}(\omega)$	Lower bound of $Z$ -matrix

## LIST OF SYMBOLS (CONTINUED)

$\alpha$	Angle-of-attack
$\alpha^*(s)$	Laplace transform of desired angle-of-attack
$\beta$	Sideslip angle
$\Gamma$	Discrete control effectiveness (input) matrix
$\Gamma(p)$	Discrete control effectiveness (input) matrix for operating point $p$
$\Gamma_c$	Input matrix for dynamic compensator
$\Gamma_c(p_k)$	Input matrix for dynamic compensator for operating point $p$
$\Gamma_{cx}$	Input matrix from $\tilde{v}_{xk}$ to dynamic compensator
$\Gamma_{cx}(p_k)$	Input matrix from $\tilde{v}_{xk}$ to dynamic compensator for operating point $p$
$\Gamma_r$	Input matrix control rate commands
$\Gamma_x$	Plant input matrix
$\Gamma_x(p)$	Plant input matrix for operating point $p$
$\Gamma_x^*$	Feedforward plant input matrix
$\Gamma_x^*(p_k)$	Feedforward plant input matrix for operating point $p$
$\Gamma_z$	Command model input matrix
$\Gamma_z(p)$	Command model input matrix at operating point $p$
$\Gamma_Z(p)$	Augmented command model input matrix at operating point $p$
$\delta A$	Aileron position
$\delta A_L$	Left aileron position
$\delta A_R$	Right aileron position
$\delta R$	Rudder position
$\delta R_L$	Left rudder position
$\delta R_R$	Right rudder position
$\delta_s$	Stabilator position
$\Delta \tilde{c}_k$	Incremental dynamic compensator state tracking error
$\Delta t$	Sampling period
$\Delta u_{xk}^*$	Incremental feedforward control vector
$\Delta u_{zk}$	Incremental command model input vector
$\Delta x_k^*$	Incremental feedforward plant state vector
$\Delta y_{xk}$	Incremental plant output vector
$\Delta y_{xk}^*$	Incremental feedforward plant output vector
$\Delta z_k$	Incremental command model state vector
$\theta$	Pitch angle

## LIST OF SYMBOLS (CONCLUDED)

$\nu_{ck}$	Dynamic compensator measurement noise
$\nu_k$	Measurement noise
$\nu_x(p, k)$	Plant measurement noise at operating point $p$
$\nu_x(t)$	Continuous plant measurement noise
$\bar{\nu}_x(t)$	Continuous plant measurement noise
$\nu_{Ik}$	Integrator measurement noise
$\nu_{uk}$	Control command feedback noise
$\nu_{xk}$	Discrete plant measurement noise
$\bar{p}$	Barometric pressure
$p_j(p)$	Metric for distance between operating points $p^j$ and $p$
$\phi$	Roll angle
$\phi(p)$	Design model state transition matrix for operating point $p$
$\phi_c$	Dynamic compensator open-loop state transition matrix
$\phi_c(p_k)$	Dynamic compensator open-loop state transition matrix for operating point $p_k$
$\phi_{cu}$	Dynamic compensator open-loop input matrix from $\tilde{u}_k$
$\phi_{cu}(p_k)$	Dynamic compensator open-loop input matrix from $\tilde{u}_k$ for operating point $p_k$
$\phi_{cy}$	Dynamic compensator open-loop input matrix from $\tilde{y}_{xk}$
$\phi_{cy}(p_k)$	Dynamic compensator open-loop input matrix from $\tilde{y}_{xk}$ for operating point $p_k$
$\phi_x$	Plant state transition matrix
$\phi_x(p)$	Plant state transition matrix for operating point $p$
$\phi_x^*$	Feedforward plant state transition matrix
$\phi_x^+(p)$	Feedforward plant state transition matrix for operating point $p$
$\phi_{xi}^*$	Feedforward plant model state transition matrix for $i^{th}$ model
$\phi_z$	Command model state transition matrix
$\phi_z(p)$	Command model state transition matrix for operating point $p$
$\phi_Z(p)$	Augmented command model state transition matrix for operating point $p$
$\omega$	Frequency



## I. INTRODUCTION

While the feedback control problem has been studied extensively (e.g. [1]-[12]), the feedforward control problem has received less attention [13], [14], [8]. Stochastic optimization methods are often used for feedback control law design (e.g., Linear-Quadratic-Gaussian (LQG), Stochastic Output Feedback, etc.). However, stochastic optimization of feedforward control systems has not been exploited to its full potential.

In this report, we propose a new control design methodology, namely the Stochastic Optimal Feedforward and Feedback Technique, or simply SOFFT. The work was performed within the context of the SBIR program, and describes the research and development activities undertaken. SOFFT is an Integrated Feedforward and Feedback (IFF) design approach. Unlike currently used techniques such as model following, in SOFFT the feedforward and feedback control laws are designed independently of one another. The feedforward and feedback control laws are then integrated using the SOFFT structure. In explicit model following, the feedforward and feedback control laws are obtained from the optimization of a single criterion in which the performances of the feedforward and feedback control laws are jointly evaluated. As a result, the optimized criterion results in a compromise between the performance of the feedforward and feedback control laws.

In other cases, the designer tries to meet all the control objectives by appropriate design of the feedback control law. Generally, this results in the error feedback structure shown in Figure 1. Trying to achieve all the control objectives using feedback alone places conflicting demands on the control law, making it difficult and sometimes impossible to achieve all of the objectives. Some undesirable and unnecessary compromises may have to be made with time-consuming trial-and-error designs.

Thus, both in the error feedback approach and in model following, the design is the result of compromising feedforward and feedback objectives. However, is such a compro-

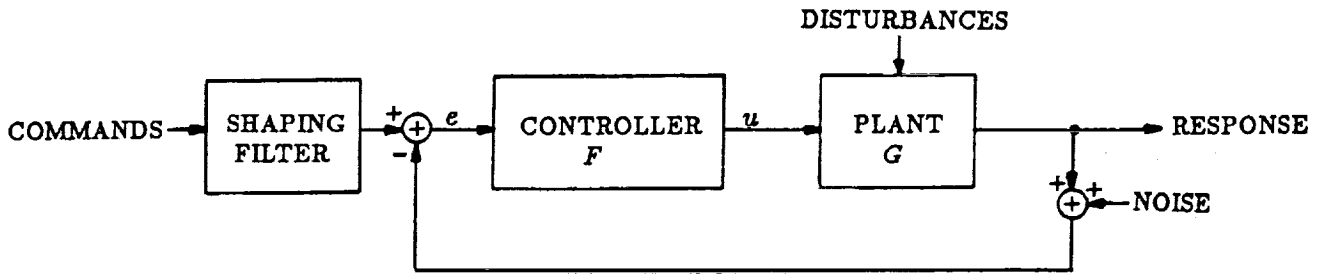


Figure 1. Error feedback controller

mise really necessary? The SOFFT approach decouples the feedforward and feedback control design process by separating the feedforward and feedback control objectives. In the SOFFT approach, a compromise between feedforward and feedback is not necessary.

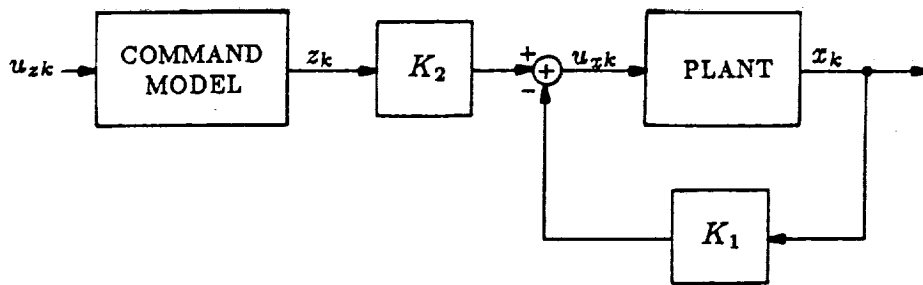


Figure 2. Explicit model following control law structure

In the explicit model following approach, the resulting system structure has a feedforward control law as shown in Figure 2. It is desired that the system respond like the command model which is now shown explicitly. On the other hand, the error feedback form may implicitly contain a desired command model, but the system response is determined by the closed-loop system time constants and natural frequencies.

Consider the model following problem



$$x_{k+1} = \phi_x x_k + \Gamma_x u_{zk} + w_{zk} \quad (1)$$

$$z_{k+1} = \phi_z z_k + \Gamma_z u_{zk} \quad (2)$$

$$e_k = H_x x_k - H_z z_k \quad (3)$$

$$J = \lim_{N \rightarrow \infty} \frac{1}{2(N+1)} E \sum_{k=0}^N e_k^T Q e_k + u_{zk}^T R u_{zk} \quad (4)$$

where  $E$  denotes the statistical expectation operator.

An explicit model following problem is defined by the plant in (1), the command model in (2), the error defined by (3) and the cost or objective function given by (4). Assuming that  $\{w_{zk}, k \geq 0\}$  and  $\{u_{zk}, k \geq 0\}$  are independent gaussian white noise sequences results in an optimization problem. The optimal control law has the structure shown in Figure 2 and is given by ([11] pp. 548-549)

$$u_{zk} = -K_1 x_k + K_2 z_k \quad (5)$$

Note that the feedback and feedforward gain matrices  $K_1$  and  $K_2$  are not independently designed, but are highly interdependent. In fact, both depend on the weighting matrices  $Q$  and  $R$ . Note how conflicting demands are placed by  $Q$  and  $R$ . Increasing  $Q$  means that tracking the input commands is more important relative to the control effort expended to achieve the tracking performance. As long as the control penalty term  $R$  is present, there will be tracking error even for constant commands in steady state.

Now suppose that a difficult maneuver requiring high control effort is commanded. As long as actuator limits are not exceeded, we see no reason for the feedforward controller to sacrifice agility or tracking performance in order to minimize the control effort. We think

that the feedforward control should expend the necessary control effort and perform the maneuver with as much accuracy as possible. However, in the explicit model following approach, such a feedforward control would also result in a feedback control law with very high gains and very little filtering or disturbance robustness. It is difficult to make sure that both a robust feedback control and a fast-response feedforward control are obtained by minimizing a single cost function weighting the tracking error and control effort.

While a particular control design problem may contain additional objectives, most designs try to achieve the following overall control objectives:

1. Quick response to input (e.g., pilot) commands during fast maneuvers
2. Desired overshoot and damping characteristics
3. Attenuation of (low response to) sensor noises and high frequency disturbances (e.g., turbulence)
4. Non-oscillatory response to large disturbances (e.g., high gusts, shear winds, etc.)
5. Maintain the above tracking and disturbance characteristics despite uncertainties, variations and nonlinearities in the plant, actuators and sensors.

The error feedback controller structure is unable to achieve all of the above objectives. In particular, objectives 1 and 3 (and often 5) place conflicting demands on the feedback controller. For example, suppose that the input command is a step or a pulse. Initially, the error  $e$  which drives the controller ( $F$ ), will suddenly increase. In this scenario, the controller must let this sudden (high-frequency) command pass through so that a quick response to this command can be achieved (objective 1).

Now consider the scenario in which the command remains constant but the measurement noise has a random spike. The error,  $e$ , will again suddenly increase. However, in this case, the controller must not pass this signal through to the response; it must in fact attenuate it (objective 3). Thus, conflicting demands are being placed on the controller,  $F$ . Clearly, the error feedback controller cannot meet both objectives. Therefore, a compromise must be reached in which neither objective is completely achieved.

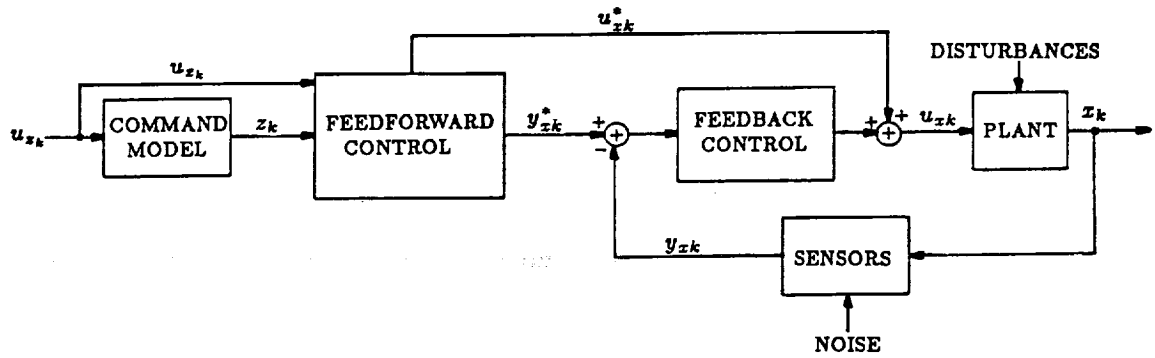


Figure 3. SOFFT integrated feedforward and feedback (IFF) control structure

In the SOFFT approach, the control objectives are separated into two groups. Objectives related to the system response to tracking commands are met by the feedforward controller. Objectives related to disturbance accommodation, noise reduction, and stability are met by the feedback controller. Robustness is a control objective for both controllers. Conversely, SOFFT provides a methodology in which the feedforward control law is designed with one cost function while the feedback control law is designed with a different cost function. The two controllers are combined into the SOFFT control structure (see Figure 3 above and Figure 4 on page 23) so as to cooperate with each other and achieve all the control objectives.

## II. INTEGRATED FEEDFORWARD AND FEEDBACK (IFF) CONTROL DESIGN

In general, a control system contains both a feedforward and feedback control law. We will define the feedforward control law to be the part which depends only on the command variables. The feedback control law is the remaining part which depends on the plant output with or without random noises and disturbances. For linear systems, these definitions uniquely specify the feedforward and feedback control laws. For nonlinear systems, some ambiguity may remain depending on the particular system.

With notable exceptions [6], [8], [13], [14], the feedforward control design problem has received little attention while the feedback control problem has been studied extensively. This asymmetry has resulted in design techniques and methodologies which attempt to meet all the control objectives using only feedback control laws. This approach places an unnecessary burden on the feedback law which must try to achieve conflicting objectives.

By an integrated feedforward and feedback (IFF) control, we mean a control law in which the feedforward and feedback are designed so as to cooperate with each other. It is to be hoped that an IFF control law does not place conflicts between feedforward and feedback.

### 1. Linearization

In the SOFFT approach, we often model the plant by a linear system of the form

$$x_{k+1} = \phi_x x_k + \Gamma_x u_{xk} + w_{xk} + d_x \quad , \quad (6)$$

$$y_{xk} = C_x x_k + \nu_{xk} + b_x \quad (7)$$

where  $x_k$  is the  $n_x$ -component state vector,  $u_{xk}$  the  $n_{ux}$ -component control vector,  $y_{xk}$  the  $n_{yx}$ -component measurement or feedback vector;  $w_{xk}$  and  $v_{xk}$  are Gaussian white noise sequences representing system noise and measurement errors, respectively;  $d_x$  is a constant vector which may represent a constant disturbance or the constant term resulting from linearizing a nonlinear system about a given operating point. Similarly,  $b_x$  represents the bias error in the measurement coupled with the constant term from the linearization of a nonlinear sensor. We may sometimes assume that the actual values of  $b_x$  and  $d_x$  are selected according to a Normal or Gaussian distribution function.

In most applications, the plant and sensors are nonlinear systems. The motivation for using a linear formulation as shown in (6) and (7) comes from the linearization of nonlinear systems.

The class of linearizable systems plays an important role in atmospheric flight vehicle dynamics. For example, the system parameters such as the coefficients of lift and drag are defined and determined from given flight condition data; i.e., a linearization about a given operating point. The kinematics can be expressed analytically but can also be linearized. Thus, the class of linearizable systems is large and contains important application systems.

Consider the nonlinear system

$$\frac{dx(t)}{dt} = \dot{x}(t) = f(x(t), u_x(t), \bar{w}_x(t)) \quad (8)$$

$$y_x(t) = g(x(t), \bar{v}_x(t)) \quad (9)$$

where  $x(t)$  is the  $n_x$ -component state vector,  $u_x(t)$  is the  $n_{ux}$ -component control vector,  $\bar{w}_x(t)$  is a second-order Gaussian white noise process with zero mean and is assumed to be independent of the Gaussian initial condition  $x(0)$ . The functions  $f$  and  $g$  are, in general, nonlinear functions of their arguments.  $f$  describes the plant, actuators, random disturbances and sensor dynamics, while  $g$  models a nonlinear sensor or feedback vector,

$y_x(t)$ . The measurement noise  $\bar{v}_x(t)$  is also assumed to be a Gaussian white noise process with zero mean, statistically independent of  $\bar{w}_x(t)$  and  $x(0)$ .

Assume that the system is linearizable or that  $f$  and  $g$  have Taylor series expansions of the form

$$\begin{aligned} \dot{x}(t) = & f(x_0, u_{x0}, 0) + \frac{\partial f}{\partial x^T}(x_0, u_{x0}, 0) [x(t) - x_0] + \frac{\partial f}{\partial u_x^T}(x_0, u_{x0}, 0) [u_x(t) - u_{x0}] \\ & + \frac{\partial f}{\partial \bar{w}_x^T}(x_0, u_{x0}, 0) [\bar{w}_x(t) - 0] + o_x^2(t) \end{aligned} \quad (10)$$

$$y_x(t) = g(x_0, 0) + \frac{\partial g}{\partial x^T}(x_0, 0) [x(t) - x_0] + \frac{\partial g}{\partial \bar{v}_x^T}(x_0, 0) \bar{v}_x(t) + o_y^2(t) \quad (11)$$

where  $x_0$  and  $u_{x0}$  are arbitrarily selected state and control vectors respectively,  $o_x^2(t)$  and  $o_y^2(t)$  are the remainder terms of the series and are of  $2^{nd}$  order in the perturbed variables.  $(x_0, u_{x0})$  determine a particular operating point or condition. It is important to note that  $f(x_0, u_{x0}, 0)$  need not be zero in this formulation. Thus, both steady-state conditions ( $f(x_0, u_{x0}, 0) = 0$ ) and unsteady conditions can be accommodated in this formulation.

In a given problem, some of the components of  $(x_0, u_0)$  may remain constant. Furthermore, not all the components of  $(x_0, u_0)$  may affect the plant dynamics ( $f(x, u, w)$ ) in a nonlinear manner. The remaining components of the operating condition  $(x_0, u_{x0})$  which have significant variations for a given problem are included as components in the parameter vector,  $p$ . Thus, the parameter vector has  $n_p$  components where

$$n_p \leq n_x + n_{ux} \quad (12)$$

Usually,  $n_p$  would be much smaller than the right-hand-side (RHS) of (12), as only few components of interest are varying for a particular problem.

The parameter vector  $p$  represents the operating point of the system. When designing a variable-gain control law for a nonlinear system (see Sections IV and V), the parameter

vector,  $p$ , plays an important role. Various plant models are selected to cover a range of operating conditions. These plant models correspond to appropriate values of the parameter vector,  $p$ . Thus, a clear understanding of the relationship between  $p$  and the physical variables  $(x_0, u_0)$  is necessary.

Now collecting terms and rewriting (10), (11), we get

$$\dot{x} = A_x(p) x + B_x(p) u_x + w_x + d_x(p) \quad (13)$$

$$y_x = C_x(p) x + \nu_x + b_x(p) \quad (14)$$

where the independent variable  $t$  has been dropped for notational convenience. The remaining terms can be found by equating terms with (10), (11).

$$A_x(p) = \frac{\partial f}{\partial x^T}(x_0, u_{x0}, 0) \quad (15)$$

$$B_x(p) = \frac{\partial f}{\partial u_x^T}(x_0, u_{x0}, 0) \quad (16)$$

$$C_x(p) = \frac{\partial g}{\partial x^T}(x_0, 0) \quad (17)$$

$$w_x(t) = \frac{\partial f}{\partial w_x^T}(x_0, u_{x0}, 0) \bar{w}_x(t) + o_x^2(t) \quad (18)$$

$$\nu_x(t) = \frac{\partial g}{\partial \nu_x^T}(x_0, 0) \bar{\nu}_x(t) + o_y^2(t) \quad (19)$$

$$d_x(p) = f(x_0, u_{x0}, 0) - [A_x(p) x_0 + B_x(p) u_{x0}] \quad (20)$$

$$b_x(p) = g(x_0, 0) - C_x(p) x_0 \quad (21)$$

Finally, the system in (13), (14) can be described by discrete system [10] when  $u_x(t)$  remains constant from one sample to the next while  $p$  remains constant over the sampling period,

$$x_{k+1} = \phi_x(p) x_k + \Gamma_x(p) u_{xk} + w_{xk} + d_x(p) \quad (22)$$

$$y_{xk} = C_x(p) x_k + \nu_{xk} + b_x(p) \quad (23)$$

where  $\phi_x(p)$  is the state transition matrix and  $\Gamma_x(p)$  the control effectiveness matrix as given by [10].

If the operating point parameter vector  $p$  varies over time, then (22), (23) represent a time-varying linear system. When the operating point remains near a given point, the system in (22), (23) becomes a time-invariant linear system such as (6), (7). Both cases will be considered in the following sections.

It is important to note that in this formulation,  $x_k$ ,  $y_{xk}$  and  $u_{xk}$  represent the total state, sensor measurements and control commands; they are not the more commonly seen perturbed variables. Also note that the plant noise  $w_x$  contains two effects: random disturbances such as wind gusts, electronic or other noises, etc., and second order nonlinear effects which come in due to the linearization of the system.

## 2. Time-Invariant SOFFT Control

When the operating point parameter vector  $p$  remains near a given operating condition, the linearized system given by (22), (23) becomes time-invariant and can be described by (6) and (7). In this section, we will summarize the SOFFT approach for linear time-invariant (LTI) systems. The details of the development can be found in the Phase I report\*.

---

\*Halyo, N., "A Stochastic Optimal Feedforward and Feedback Control Methodology for



In the SOFFT approach, we separate the feedforward and feedback control objectives into two groups. Then we optimize each group of objectives to obtain each controller. This also implies separating the design of the feedforward and feedback control systems as is described below.

The overall control objective is to enable the plant (an aircraft or other vehicle or process), to closely track the input commands at every instant in the presence of disturbances, despite uncertainties about the plant, within digital implementation constraints and other system limitations. The standard regulator problem is obtained when the input commands are zero, so that a feedforward controller is not needed. The feedback control law stabilizes the plant and maintains the system state near zero. The set point regulation problem is obtained when the input commands are constant. The most general case where the plant state tracks the input commands at every instant is considered in this work. The commands may take the plant from one operating point to another, constantly maneuvering in a transient rather than steady state condition.

In the SOFFT approach, the feedforward control has the objective of tracking the input commands and producing the desired transient response to commands (overshoots, damping, etc.) assuming no measurement noises nor plant disturbances. On the other hand, the feedback control law has the objectives of measurement and plant noise (disturbance) suppression and stability within considerations that uncertainties and variations in the plant, actuator and sensor subsystems will be present.

Thus, the feedback gains should be high enough for disturbance suppression consistent with low noise feedback and robustness with respect to unmodeled dynamics or parameter uncertainty. On the other hand, the feedforward control is not concerned with noise

---

*Superagility*", ICS FR-689102, Information & Control Systems, Incorporated, 28 Research Drive, Hampton, VA, 1989.

feedback problems as it is completely implemented on a digital control computer and generates a "perfect trajectory" which will be described later.

Consider the plant given by (6) and (7). Now suppose that we want to achieve a trajectory which we denote by  $\{y_{xk}^*, k \geq 0\}$ . Let  $\{u_{xk}^*, k \geq 0\}$  be the control sequence which produces the desired trajectory when no random noise (plant or measurement noise) is present in the system. Accordingly, we must have

$$x_{k+1}^* = \phi_x x_k^* + \Gamma_x u_{xk}^* + d_x \quad (24)$$

$$y_{xk}^* = C_x x_k^* + b_x \quad (25)$$

### 3. Feedback Control Design

The actual plant output trajectory  $\{y_{xk}, k \geq 0\}$  will be perturbed by plant disturbances and measurement errors. So that the actual trajectory will differ from the desired trajectory in (24), (25). In the SOFFT design methodology, we want to design a feedback control law which will keep the actual plant output trajectory  $y_{xk}$  close to the desired trajectory  $\{y_{xk}^*, k \geq 0\}$  at all times and despite plant uncertainties.

Thus, define the tracking error variables

$$\tilde{x}_k = x_k - x_k^* \quad (26)$$

$$\tilde{u}_{xk} = u_{xk} - u_{xk}^* \quad (27)$$

$$\tilde{y}_{xk} = y_{xk} - y_{xk}^* \quad (28)$$

Using (6), (7), (24) and (25), the tracking error variables are seen to satisfy

$$\tilde{x}_{k+1} = \phi_x \tilde{x}_k + \Gamma_x \tilde{u}_{xk} + w_{xk} \quad (29)$$

$$\tilde{y}_{xk} = C_x \tilde{x}_k + \nu_{xk} \quad (30)$$

Now suppose that the desired output  $y_{xk}^*$  is available at the  $k^{th}$  sampling instant  $t_k$ . Since the actual output  $y_{xk}$  is also available from sensor readings, the output tracking error  $\tilde{y}_{xk}$  is available for use in the feedback control law.

If  $\tilde{u}_{xk}$  can be chosen (designed) appropriately to achieve plant noise or disturbance suppression, sensor noise attenuation and stability under plant uncertainties, then the tracking error will be small. The input commands, the command model variables or the desired  $*$ -trajectories are not directly involved in the design of the feedback control law. Note that the feedforward control has not entered into the feedback control design. What is of interest is to keep the error variables small. This is quite different than the explicit model following approach described in the Introduction where the feedback and feedforward control laws are designed simultaneously to minimize a single objective function given in (4).

In order to achieve the feedback objectives, the designer may decide to use instantaneous output feedback, control rate commands, reduced-order dynamic compensation, as well as integral error feedback. Selecting the feedback control structure which builds the control design model is one of the most important parts of the design process. In general, the feedback control structure will be of the form

$$\tilde{u}_{k+1} = \tilde{u}_k + \Delta t \Gamma_r \tilde{v}_{xk} + w_{uk} \quad (31)$$

$$\tilde{c}_{k+1} = \phi_c \tilde{c}_k + \phi_{cy} \tilde{y}_{xk} + \phi_{cu} \tilde{u}_k + \Delta t \Gamma_{cx} \tilde{v}_{xk} + \Delta t \Gamma_c \tilde{v}_{ck} + w_{ck} \quad (32)$$

$$\tilde{I}_{k+1} = \tilde{I}_k + \Delta t(H_y \tilde{y}_{xk} + H_u \tilde{u}_k) + w_{Ik} \quad (33)$$

$$\tilde{u}_{xk} = C_r \tilde{u}_k + D_r \tilde{v}_{xk} \quad (34)$$

where  $\tilde{u}_k$  is the  $n_r$ -component vector of control variables which use a rate command structure (i.e., not all controls need have this structure),  $\tilde{v}_{xk}$  is the  $n_{ux}$ -component vector containing the rate commands for the applicable components while the remaining components are the same as in the original control vector  $\tilde{u}_{xk}$ ,  $\tilde{c}_k$  is the  $n_c$ -component dynamic compensator state vector,  $\tilde{v}_{ck}$  is the  $n_{vc}$ -component compensator control (design) vector,  $\tilde{I}_k$  is the  $n_I$ -component integrator state and  $\Delta t$  is the sampling period. In (33),  $H_y$  and  $H_u$  define the variables fed into the integral error feedback subsystem. In general, we will use  $H$  with a subscript to define tracking error variables and command variables; we will use  $C$  with a subscript to denote the feedback variables; i.e., the output or feedback vector (see (38), (39), (42)). The number of commands is  $n_H$ . When integral error feedback is used, the number of integrators  $n_I$  equals  $n_H$ ; otherwise (integral error is not fed back)  $n_I = 0$  and (33) vanishes. The vector sequences  $\{w_{uk}\}$ ,  $\{w_{ck}\}$  and  $\{w_{Ik}\}$  are assumed to be Gaussian white noise random processes which can be used as design parameters to achieve various objectives.

When the designer selects to command the rate of change of all the control variables in  $\tilde{u}_{xk}$ , then

$$\Gamma_r = C_r = I \quad , \quad D_r = 0 \quad , \quad n_r = n_{ux} \quad . \quad (35)$$

If the designer does not select a control rate structure, then  $n_r$  and  $\tilde{u}_k$  vanish and  $D_r$  is the identity matrix. When the designer selects to command the rate of some control components while commanding the actual position value of the remaining control components  $\Gamma_r$ ,  $C_r$  and  $D_r$  are correspondingly determined.

The dynamic compensator can be forced to be a reduced-order estimator of some unmeasured state variables by appropriate selection of the cost matrices  $Q, R$ , in the objective function. Alternately, the dynamic compensator may be used for other purposes such as signal shaping and stability margin.

Finally, the integrated tracking error can be fed back to achieve a type-1 response for the closed-loop system. The tracking error is modeled as  $H_y \tilde{y}_{xk}$ , and will be discussed further later.

The control feedback structure given in (31) - (34) forms the feedback design model. The design model is the augmented system given by

$$\begin{pmatrix} \tilde{x}_{k+1} \\ \tilde{u}_{k+1} \\ \tilde{c}_{k+1} \\ \tilde{I}_{k+1} \end{pmatrix} = \begin{pmatrix} \phi_x & \Gamma_x C_r & 0 & 0 \\ 0 & I & 0 & 0 \\ \phi_{cy} C_x & \phi_{cu} & \phi_c & 0 \\ \Delta t H_y C_x & \Delta t H_u & 0 & I \end{pmatrix} \begin{pmatrix} \tilde{x}_k \\ \tilde{u}_k \\ \tilde{c}_k \\ \tilde{I}_k \end{pmatrix} + \begin{pmatrix} \Gamma_x D_r & 0 \\ \Delta t \Gamma_r & 0 \\ \Delta t \Gamma_{cx} & \Delta t \Gamma_c \\ 0 & 0 \end{pmatrix} \begin{pmatrix} \tilde{v}_{xk} \\ \tilde{v}_{ck} \end{pmatrix} + \begin{pmatrix} w_{xk} \\ w_{uk} \\ w_{ck} \\ w_{Ik} \end{pmatrix} \quad (36)$$

$$\begin{pmatrix} \tilde{y}_{xk} \\ \tilde{y}_{uk} \\ \tilde{y}_{ck} \\ \tilde{y}_{Ik} \end{pmatrix} = \begin{pmatrix} C_x & 0 & 0 & 0 \\ 0 & C_u & 0 & 0 \\ 0 & 0 & C_c & 0 \\ 0 & 0 & 0 & C_I \end{pmatrix} \begin{pmatrix} \tilde{x}_k \\ \tilde{u}_k \\ \tilde{c}_k \\ \tilde{I}_k \end{pmatrix} + \begin{pmatrix} \nu_{xk} \\ \nu_{uk} \\ \nu_{ck} \\ \nu_{Ik} \end{pmatrix} \quad (37)$$

$$\tilde{X}_{k+1} = \phi \tilde{X}_k + \Gamma \tilde{v}_k + w_k \quad (38)$$

$$\tilde{Y}_k = C \tilde{X}_k + \nu_{xk} \quad (39)$$

$$\tilde{X}_k = \begin{pmatrix} \tilde{x}_k \\ \tilde{u}_k \\ \tilde{c}_k \\ \tilde{I}_k \end{pmatrix}, \quad \tilde{Y}_k = \begin{pmatrix} \tilde{y}_{xk} \\ \tilde{y}_{uk} \\ \tilde{y}_{ck} \\ \tilde{y}_{Ik} \end{pmatrix}, \quad \tilde{v}_k = \begin{pmatrix} \tilde{v}_{xk} \\ \tilde{v}_{ck} \end{pmatrix} \quad (40)$$

$$w_k = \begin{pmatrix} w_{xk} \\ w_{uk} \\ w_{ck} \\ w_{Ik} \end{pmatrix}, \quad \nu_k = \begin{pmatrix} \nu_{xk} \\ \nu_{uk} \\ \nu_{ck} \\ \nu_{Ik} \end{pmatrix} \quad (41)$$

The feedback control law is of the form

$$\tilde{v}_k = -K \tilde{Y}_k = -K C \tilde{X}_k - K \nu_{xk} \quad (42)$$

The feedback gain matrix,  $K$ , can be partitioned so as to be compatible with the partition of  $\tilde{Y}_k$  in (40).

$$K = \begin{pmatrix} K_{xx} & K_{xu} & K_{xc} & K_{xI} \\ K_{cx} & K_{cu} & K_{cc} & K_{cI} \end{pmatrix} \quad (43)$$

The general formulation described above is highly versatile. You can select practically any feedback structure to achieve almost any control objective. Building and optimizing the feedback design model is made quite easy by a software product (ACET) developed in conjunction with SOFFT methodology.

The following feedback cost function can be used to optimize the parameters (i.e., the gain matrix  $K$ ) of the feedback control system.

$$J = \lim_{N \rightarrow \infty} \frac{1}{2(N+1)} E \sum_{k=0}^N \{ \tilde{X}_k^T Q \tilde{X}_k + 2 \tilde{X}_k^T M \tilde{v}_k + \tilde{v}_k^T R \tilde{v}_k \} \quad (44)$$

Minimizing this cost function requires the use of the Stochastic Output Feedback algorithm.

#### 4. Feedforward Control Design

In the SOFFT methodology, the objective of the feedforward control law is to track the input commands and produce the desired transient response (e.g., overshoots or critical damping) when no random disturbances or noises are present. For example, if a fast maneuver is commanded, we would like for the control to move as fast as allowed by the plant's physical constraints to achieve the maneuver.

A high-gain feedback control law has disadvantages such as insufficient sensor noise attenuation as well as lack of robustness to plant variations and nonlinearities. Thus, the

feedback control law must be selected with care not to result in too high a loop gain. On the other hand, the feedforward control law has no such constraint. It is completely implemented on a digital computer and except for round-off error, it has no random noise or plant nonlinearities to contend with. Furthermore, if a fast and large input command is given, it is supposed to produce a fast and large control to produce the response. Thus, the feedforward control law is supposed to be a high-gain system, but one which does not have the associated disadvantages of high-gain feedback.

Consider a command model of the form

$$z_{k+1} = \phi_z z_k + \Gamma_z u_{zk} \quad (45)$$

$$y_{zk} = H_z z_k \quad (46)$$

where the command model state  $z_k$  has  $n_z$ -components which will usually be different (smaller) than the plant model state dimension  $n_x$ . The command model input,  $u_z$ , is assumed to be a Gaussian white noise sequence with zero mean independent of the initial condition  $z_0$ . Thus,  $z_k$  and  $y_{zk}$  are random processes.

Two somewhat different interpretations of the command model are possible. In one case, the command input  $u_{zk}$  is the actual input to the compensated system, such as the pilot stick input to the aircraft. In this case, the command model output  $y_{zk}$  represents the desired output of some plant variables. This case will be used to design a flight control system for the F/A-18 aircraft in a subsequent section.

In the other case,  $u_{zk}$  does not represent a physical variable which is measured. The command model simply represents a class of responses one of which will be commanded. For example,  $y_{zk}$  may represent a flight path generated by a flight management computer according to certain rules. Accordingly, we can devise a command model  $(\phi_z, \Gamma_z, H_z)$  which is statistically representative of this class of paths. Then  $u_{zk}$  can be computed from

the given path and the command model selected. In both applications, the design of the feedforward control law follows the same procedure.

We will assume that at time  $k\Delta t$ , only the current and past values of the commands are known for use in the feedforward controller; i.e.,  $\{z_k, z_{k-1}, \dots, z_0\}$  and  $u_{zk}$  are known at the  $k^{\text{th}}$  sampling instant. This constraint is necessary to design a realizable or causal control law which can be implemented in real-time. If the commands were known for all future values of  $k$ , then the feedforward problem would become deterministic. Optimal tracking techniques are available for such deterministic cases [15]. However, the result of the optimization is an open-loop control sequence rather than a feedforward control law. In special cases, it is possible to obtain a control law by making appropriate approximations. The CGT [13], [14], [15], belongs to this latter class, as it obtains the feedforward control gains by assuming that  $u_{zk}$  is a constant vector for all  $k$ . However, then it uses this feedforward law in cases where  $u_{zk}$  varies. This and other approximations in the CGT largely account for its unpredictable tracking performance. The SOFFT approach avoids making such approximations by casting the problem as a stochastic one in which the constraint of causality can be naturally incorporated.

Recall that we must find the desired control and output trajectories  $u_{zk}^*$  and  $y_{zk}^*$  which satisfy (24) and (25) in order to separate the feedback design problem (defined by (26) - (30)) from the feedforward control problem. Since the feedforward objective is to track the commands, particularly during transient maneuvers, we want to minimize the tracking error at every instant. Let

$$e_k^* = H_y y_{zk}^* - H_z z_k \quad , \quad k \geq 0 \quad (47)$$

Thus, we would like to maintain  $e_k^*$  at very low values for all  $k \geq 0$ . If  $e_k^*$  vanishes for  $k \geq 0$ , then we have the "perfect tracking" case. Note that this applies only to the feedforward since plant and sensor noises will result in less than perfect tracking in the actual system.



We select a quadratic cost function in  $e_k^*$  and include further terms to accommodate any objectives other than tracking.

$$J^* = \lim_{N \rightarrow \infty} \frac{1}{2(N+1)} E \sum_{k=0}^N \{ \|e_k^*\|_2^2 + x_k^{*T} Q_1^* x_k^* + u_{zk}^{*T} R_1^* u_{zk}^* \} \quad (48)$$

Thus, we would like to minimize the cost function  $J^*$  subject to the constraints

$$x_{k+1}^* = \phi_x x_k^* + \Gamma_x u_{zk}^* + d_x \quad (49)$$

$$z_{k+1} = \phi_z z_k + \Gamma_z u_{zk} \quad (50)$$

Since  $u_{zk}$  is a Gaussian white noise sequence, (48) - (50) pose a discrete LQG problem with an unstable and uncontrollable part. The solution to this problem is given in [5], [6]. The resulting control law is

$$u_{zk}^* = -K_x^* x_k^* - K_z z_k - K_u u_{zk} + u_x^* \quad (51)$$

where  $u_x^*$  is a constant vector depending linearly on  $d_x$  and  $b_x$ . As we will use an incremental implementation for the feedforward controller, the actual values of  $u_x^*$ ,  $d_x$  and  $b_x$  will not be needed.

Thus, we can determine the desired control trajectory,  $u_{zk}^*$  from (51). Then, using (24), (25) we can determine the desired output trajectory,  $y_{zk}^*$ , iteratively. Since we now know  $u_{zk}^*$  and  $y_{zk}^*$ , we can feed these values into the feedback control system to determine the feedback control  $\tilde{u}_{zk}$  and obtain the total control command to be sent to the plant. Thus both feedback and feedforward can be designed separately, each optimizing its own set of objectives.

## 5. Algorithm for Feedforward Gains

To obtain the optimal feedforward gains  $K_x^*$ ,  $K_z$  and  $K_u$ , the necessary conditions for optimality may be solved. From [5], these equations can be found to be

$$K_x^* = [\Gamma_x^T P_{xx}^* \Gamma_x + R_1^*]^{-1} \Gamma_x^T P_{xx}^* \phi_x \quad (52)$$

$$P_{xx}^* = [\phi_x - \Gamma_x K_x^*]^T P_{xx}^* [\phi_x - \Gamma_x K_x^*] + K_x^{*T} R_1^* K_x^* + H_x^T H_x + Q_1^* \quad (53)$$

$$K_z = [\Gamma_z^T P_{zz}^* \Gamma_z + R_1^*]^{-1} \Gamma_z^T P_{zz}^* \phi_z \quad (54)$$

$$P_{zz}^* = [\phi_z - \Gamma_z K_z^*]^T P_{zz}^* \phi_z - H_z^T H_z \quad (55)$$

$$K_u = [\Gamma_x^T P_{xx}^* \Gamma_x + R_1^*]^{-1} \Gamma_x^T P_{xx}^* \Gamma_z \quad (56)$$

where

$$H_x = H_y C_x \quad (57)$$

The first two equations (52) and (53) are seen to be the standard full-state linear quadratic regulator (LQR) necessary conditions when the state and control penalty matrices  $Q$  and  $R$  for the problem are set by

$$Q = H_x^T H_x + Q_1^* \quad , \quad R = R_1^* \quad (58)$$

where  $Q_1^*$  and  $R_1^*$  correspond to (48). A standard LQR algorithm can be used to compute  $K_x^*$  and  $P_{xx}^*$ . It is important to note that most algorithms will generate a critical point rather than the absolute minimum.

The necessary conditions for the remaining gains  $K_z$  and  $K_u$  are seen to be linear equations.  $P_{zz}^*$  is the solution of the discrete Lyapunov equation given in (55).  $K_z$  and  $K_u$  can be easily computed from (54) and (56), respectively.

### Perfect Tracking

We define perfect tracking as the case where  $H_y y_{zk}^* = H_z z_k$  for all  $k$  and all commands,  $u_{zk}$ . When  $Q_1^*$  and  $R_1^*$  vanish, the optimal solution will often produce perfect tracking. However, when perfect tracking is not possible, there may continue to exist an optimal solution which will approximately track the commands.

When the matrix  $[H_x \Gamma_x]$  is non-singular, perfect tracking is possible and the feedforward gains can be obtained with greater ease. In this case, we have

$$K_x^* = [H_x \Gamma_x]^{-1} H_x \phi_x \quad (59)$$

$$K_z = -[H_x \Gamma_x]^{-1} H_z \phi_z \quad (60)$$

$$K_u = -[H_x \Gamma_x]^{-1} H_z \Gamma_z \quad (61)$$

Substitution of these gains into (52) - (56) shows that the necessary conditions for optimality are satisfied. While these gains produce the feedforward control necessary for perfect tracking, they may produce high gain values and their use should be examined on a case by case basis. Thus, when  $H_x \Gamma_x$  is nearly singular, the perfect tracking capability of the system may be limited due to control authority limitations. In such cases, a different tracking variable may be selected.

## 6. The SOFFT Control Structure

The control command sent to the plant is the sum of two components, one generated by the feedforward controller,  $u_{xk}^*$ , the other by the feedback controller,  $\tilde{u}_{xk}$ . The feedforward control  $u_{xk}^*$  is determined by (24), (25), (50) and (51). The feedback control  $\tilde{u}_{xk}$  is determined by (31) - (34) and (42). An incremental implementation is recommended for the actual digital implementation of the SOFFT control law.

Combining both feedforward and feedback control laws results in a system structure depicted by the block diagram in Figure 4. This diagram shows the feedforward control law in greater detail. Considering only the structure, of the SOFFT control law, rather than the methodology, we note that the SOFFT structure has

- 1) feedforward dynamic compensation beyond the command model,
- 2) two feedforward links to the feedback loop:  $u_{xk}^*$  and  $y_{xk}^*$

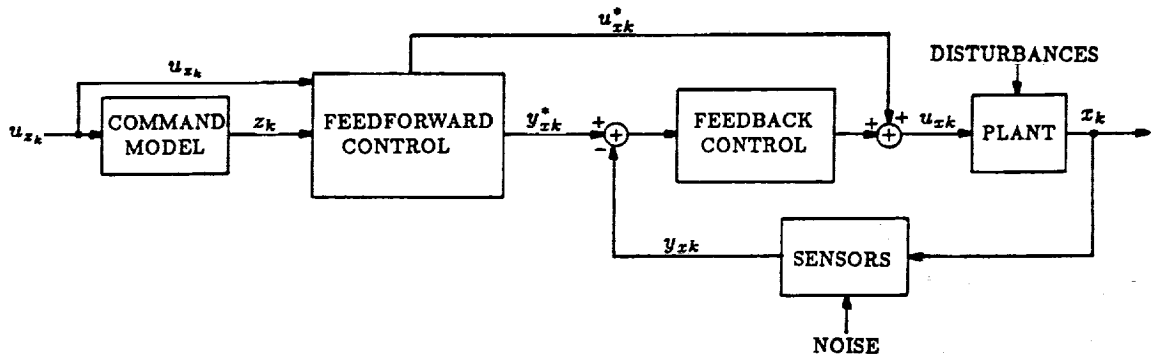


Figure 3. SOFFT integrated feedforward and feedback (IFF) control structure

It is also important to note that these two feedforward links ( $u_{xk}^*$ ,  $y_{xk}^*$ ) are highly correlated. As can be seen from Figures 3 and 4, the correlation is introduced by the plant and sensor models used in the feedforward control system. When these models perfectly match the actual plant and sensors, then the actual and desired outputs  $y_{xk}$  and  $y_{xk}^*$  match at every instant and no feedback correction  $\tilde{u}_{xk}$  is needed. When the feedforward models

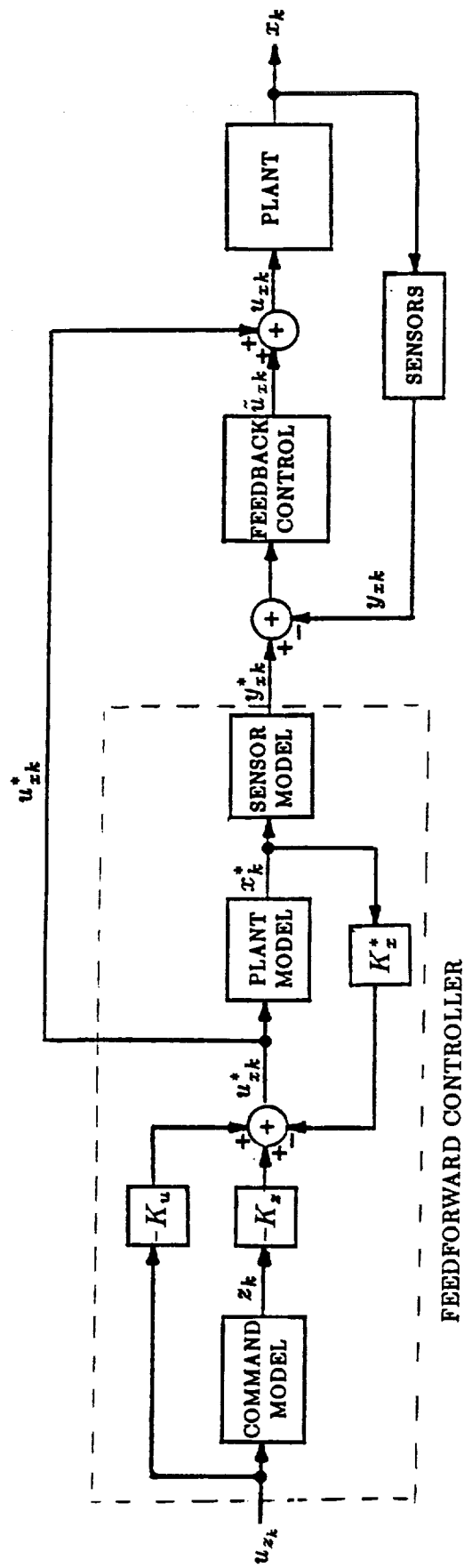


Figure 4. SOFTT Control Law Structure

do not match the actual plant and sensors, whether due to random noises or modeling errors, the outputs  $y_{xk}$  and  $y_{xk}^*$  do not match and the feedback control system produces a corrective action,  $\tilde{u}_{xk}$ . Thus, the feedforward and feedback systems are integrated so that they cooperate in trying to achieve all the control objectives.

It is important to note that neither the error feedback structure shown in Figure 1 nor the explicit model follower structure shown in Figure 2 match the SOFFT structure. In comparison to the Command Generator Tracker (CGT), note that SOFFT uses a dynamic compensator while the corresponding CGT feedforward control law consists of a gain matrix. Also note that the CGT and the model follower structures do not feed  $u_{zk}$  directly.

The SOFFT control law does not require full-state feedback. It accommodates any sensor configuration by using stochastic output feedback. Further note that the number of controls and the number of outputs or feedback variables do not have to match, but are arbitrary.

Finally, the SOFFT structure appears to be a combination of the model follower and error feedback structures in that it feeds forward both  $y_{xk}^*$  and  $u_{zk}^*$ .

### III. COMMAND TRACKING PERFORMANCE

Most current measures of robustness treat the sensitivity of the feedback control law. For example, the classical phase and gain margins provide an excellent measure of stability robustness for single-input single-output (SISO) systems. The loop gain and phase may vary by the respective margins before the closed-loop system becomes unstable. For multi-input multi-output (MIMO) systems, similar stability margin criteria have been developed using  $\sigma$ -plots or the singular values of the return difference matrix.  $\sigma$ -plots also provide a measure of the error in a MIMO error feedback control system.

While the analysis of the feedback loops provides invaluable information, it analyzes only one part of the total system. When the system has a feedforward control law reaching the feedback loops at more than one point, it is desirable to have a measure of the error in tracking which can handle the total system.

In this section, we will develop a measure of command tracking performance (CTP) or the ability of the compensated system to track input commands. We call these analysis tools  $Z$ -plots.

First we develop a mathematical model of the complete SOFFT control law including the feedforward and feedback control laws in their general form. Here we will allow for the plant and sensor models used in designing the feedforward control law to be different than the ones used in designing the feedback control law, both of which may be different than the actual plant and sensor model. We will denote the feedforward models with the superscript " \* " while the actual models will not have this superscript.

There are a large number of state vector selections which can be reasonably selected to describe the system. All of these are valid. Here, we have selected the following form of the feedforward and feedback systems compensating the plant.

$$\begin{aligned} & z_{k+1} = \phi_z z_k + \Gamma_z u_{zk} & (62) \\ \text{FEEDFORWARD} & \left\{ \begin{aligned} x_{k+1}^* &= [\phi_x^* - \Gamma_x^* K_x^*] x_k^* - \Gamma_x^* K_z^* z_k \\ &\quad - \Gamma_x^* K_u^* u_{zk} + (d_x^* + \Gamma_x^* u_x^*) & (63) \\ u_{zk}^* &= -K_x^* x_k^* - K_z^* z_k - K_u^* u_{zk} + u_x^* & (64) \\ y_{zk}^* &= C_x^* x_k^* + D_x^* u_{zk}^* + C_z^* z_k + C_u^* u_{zk} + b_x^* & (65) \end{aligned} \right. \end{aligned}$$

$$\begin{aligned} \text{PLANT} & \left\{ \begin{aligned} x_{k+1} &= \phi_x x_k + \Gamma_x u_{zk}^* + \Gamma_x \tilde{u}_{zk} + w_{zk} + d_x & (66) \\ y_{zk} &= C_x x_k + D_x u_{zk} + \nu_{zk} + b_x & (67) \end{aligned} \right. \end{aligned}$$

$$\begin{aligned} & \tilde{u}_{k+1} = \tilde{u}_k + \Delta t \Gamma_r \tilde{v}_{zk} + w_{uk} & (68) \\ \text{FEEDBACK} & \left\{ \begin{aligned} \tilde{c}_{k+1} &= \phi_c \tilde{c}_k + \phi_{cu} \tilde{u}_k + \phi_{cy} \tilde{y}_{zk} + \Delta t \Gamma_c \tilde{v}_{ck} \\ &\quad + \Delta t \Gamma_{cx} \tilde{v}_{zk} + w_{ck} & (69) \\ \tilde{I}_{k+1} &= \tilde{I}_k + \Delta t [H_y \tilde{y}_{zk} + H_u \tilde{u}_k] + w_{Ik} & (70) \\ \tilde{u}_{zk} &= C_r \tilde{u}_k + D_r \tilde{v}_{zk} & (71) \end{aligned} \right. \end{aligned}$$

$$\begin{aligned} \text{CONTROL} & \left\{ \begin{aligned} \tilde{v}_k &= \begin{pmatrix} \tilde{v}_{zk} \\ \tilde{v}_{ck} \end{pmatrix} = -K_x [y_{zk} - y_{zk}^*] - K_u \tilde{u}_k \\ &\quad - K_c \tilde{c}_k - K_I \tilde{I}_k & (72) \end{aligned} \right. \end{aligned}$$

$$\begin{aligned} \text{SYSTEM} & \left\{ \begin{aligned} H_y y_{zk} &= H_y C_x x_k + H_y \nu_{zk} + H_y b_x & (73) \end{aligned} \right. \\ \text{OUTPUT} & \end{aligned}$$

$$\begin{aligned} \text{TRACKING} & \left\{ \begin{aligned} H_y \tilde{y}_{zk} &= H_y [y_{zk} - y_{zk}^*] & (74) \\ \text{ERROR} & \end{aligned} \right. \end{aligned}$$

where the gain matrices  $K_x, K_u, K_c$  and  $K_I$  are partitions of the feedback gain matrix  $K$  in (42) and (43).

$$K = (K_x \quad K_u \quad K_c \quad K_I) = \begin{pmatrix} K_{xx} & K_{xu} & K_{xc} & K_{xI} \\ K_{cx} & K_{cu} & K_{cc} & K_{cI} \end{pmatrix}$$

Note that although  $D_x$  and  $D_x^*$  have been neglected (assumed null) in the development of the SOFFT feedforward control law, we are including them in this formulation to obtain a more general analysis tool. Also note that some notational changes have been made in



comparison to our Phase I final reports, such as  $v_{uk}$  and  $\Gamma_{cu}$  have been renamed  $v_{zk}$  and  $\Gamma_{cz}$ , respectively.

After some manipulation the system equations (62) - (74) can be put in state space form as follows.

$$\begin{pmatrix} z_{k+1} \\ x_{k+1}^* \\ x_{k+1} \\ \tilde{u}_{k+1} \\ \tilde{c}_{k+1} \\ \tilde{I}_{k+1} \end{pmatrix} = \begin{pmatrix} \phi_z & 0 & 0 & 0 & 0 & 0 \\ -\Gamma_x^* K_z & (\phi_x^* - \Gamma_x^* K_x^*) & 0 & 0 & 0 & 0 \\ -\Gamma_x K_z & -\Gamma_x K_x^* & \phi_x & \Gamma_x C_r & 0 & 0 \\ 0 & 0 & 0 & I & 0 & 0 \\ -\phi_{cy} \bar{C}_z^* & -\phi_{cy} \bar{C}_x^* & \phi_{cy} C_x & (\phi_{cu} + \phi_{cy} D_x C_r) & \phi_c & 0 \\ -\Delta t H_y \bar{C}_z^* & -\Delta t H_y \bar{C}_x^* & \Delta t H_y C_x & \Delta t (H_u + H_y D_x C_r) & \Delta t H_c & I \end{pmatrix} \begin{pmatrix} z_k \\ x_k^* \\ x_k \\ \tilde{u}_k \\ \tilde{c}_k \\ \tilde{I}_k \end{pmatrix} \\ + \begin{pmatrix} 0 & 0 \\ 0 & 0 \\ \Gamma_x D_r & 0 \\ \Delta t \Gamma_r & 0 \\ (\Delta t \Gamma_{cz} + \phi_{cy} D_x D_r) & \Delta t \Gamma_c \\ \Delta t H_y D_x D_r & 0 \end{pmatrix} \begin{pmatrix} \tilde{v}_{zk} \\ \tilde{v}_{ck} \end{pmatrix} + \begin{pmatrix} \Gamma_z \\ -\Gamma_x^* K_u \\ -\Gamma_x K_u \\ 0 \\ -\phi_{cy} \bar{C}_u^* \\ -\Delta t H_y \bar{C}_u^* \end{pmatrix} u_{zk} \quad (75)$$

$$\begin{pmatrix} \tilde{y}_{zk} \\ \tilde{y}_{uk} \\ \tilde{y}_{ck} \\ \tilde{y}_{Ik} \end{pmatrix} = \begin{pmatrix} -\bar{C}_z^* & -\bar{C}_x^* & C_x & D_x C_r & 0 & 0 \\ 0 & 0 & 0 & C_u & 0 & 0 \\ 0 & 0 & 0 & 0 & C_u & 0 \\ 0 & 0 & 0 & 0 & 0 & C_I \end{pmatrix} \begin{pmatrix} z_k \\ x_k^* \\ x_k \\ \tilde{u}_k \\ \tilde{c}_k \\ \tilde{I}_k \end{pmatrix}$$

$$+ \begin{pmatrix} D_x D_r & 0 \\ 0 & 0 \\ 0 & 0 \\ 0 & 0 \end{pmatrix} \begin{pmatrix} \tilde{v}_{zk} \\ \tilde{v}_{ck} \end{pmatrix} + \begin{pmatrix} -\bar{C}_u^* \\ 0 \\ 0 \\ 0 \end{pmatrix} u_{zk} \quad (76)$$

$$\begin{aligned} \bar{C}_z^* &= C_z^* + \bar{D}_z K_z & \bar{D}_z &= D_x - D_x^* \\ \bar{C}_x^* &= C_x^* + \bar{D}_x K_x^* & \bar{b}_x &= b_x - b_x^* \\ \bar{C}_u^* &= C_u^* + \bar{D}_x K_u \end{aligned} \quad (77)$$

where the constant forcing terms related to  $d_x, b_x, d_x^*$ , etc. and random noises have been neglected as they will not impact the desired transfer functions.

Using the state-space model above, frequency response from the input command  $u_{zk}$  to the outputs  $H_y y_{zk}$  and  $H_x y_{zk}^*$  can be computed with any selection of the parameters, with

the feedback loops open or closed. In these computations, it is assumed that  $D_x D_r = 0$ .

The outputs are obtained using

$$\begin{pmatrix} y_{zk} \\ y_{zk}^* \end{pmatrix} = \begin{pmatrix} -D_x K_z & -D_x K_z^* & C_z & D_x C_r & 0 & 0 \\ \hat{C}_z^* & \hat{C}_z^* & 0 & 0 & 0 & 0 \end{pmatrix} \begin{pmatrix} z_k \\ x_k^* \\ x_k \\ \bar{u}_k \\ \bar{c}_k \\ \bar{I}_k \end{pmatrix} + \begin{pmatrix} -D_x K_u \\ \hat{C}_u^* \end{pmatrix} u_{zk} \quad (78)$$

$$\begin{aligned} \hat{C}_z^* &= C_z^* - D_x^* K_z \\ \hat{C}_z^* &= C_z^* - D_x^* K_z^* \\ \hat{C}_u^* &= C_u^* - D_x^* K_u \end{aligned} \quad (79)$$

## 1. Z-Plots

Let  $T(\omega)$  be the transfer function matrix from the pilot command input  $u_z(\omega)$  to the plant output or feedback vector,  $y_z(\omega)$ ; i.e.,

$$y_z(\omega) = T(\omega) u_z(\omega) \quad (80)$$

Let the desired or commanded plant outputs,  $y_z^*(\omega)$ , be given by

$$y_z^*(\omega) = T^*(\omega) u_z(\omega) \quad (81)$$

When we have more sensors (plant outputs) than commands, the corresponding transfer functions from  $u_z(\omega)$  to the commanded output are  $H_y T(\omega)$  and  $H_y T^*(\omega)$ . We assume that there are as many pilot inputs ( $n_{u_x}$ ) as there are commanded plant outputs; i.e.,  $H_y T(\omega)$  is  $n_{u_x} \times n_{u_x}$ . We will further assume that  $H_y T^*(\omega)$  is invertible, a.e.

We define the  $Z$ -matrices as

$$Z_I(\omega) = [H_y T^*(\omega)]^{-1} [H_y T(\omega)] \quad (82)$$

$$Z_O(\omega) = [H_y T(\omega)] [H_y T^*(\omega)]^{-1} \quad (83)$$

To understand the meaning of the  $Z$ -matrices, first note that

$$Z_I(\omega) = Z_O(\omega) = I \quad , \quad \text{when} \quad H_y T(\omega) = H_y T^*(\omega) \quad . \quad (84)$$

Thus, when the actual response equals the desired response, the  $Z$ -matrices are unity.

Now define the  $u_z(\omega)$ ,  $u_z^*(\omega)$ ,  $y(\omega)$ ,  $y^*(\omega)$  as follows,

$$u_z^*(\omega) = Z_I(\omega) u_z(\omega) \quad (85)$$

$$y(\omega) = Z_O(\omega) y^*(\omega) \quad (86)$$

These definitions lead to the following interpretations when  $T(\omega) \neq T^*(\omega)$ ; i.e., when off-nominal conditions are being analyzed.

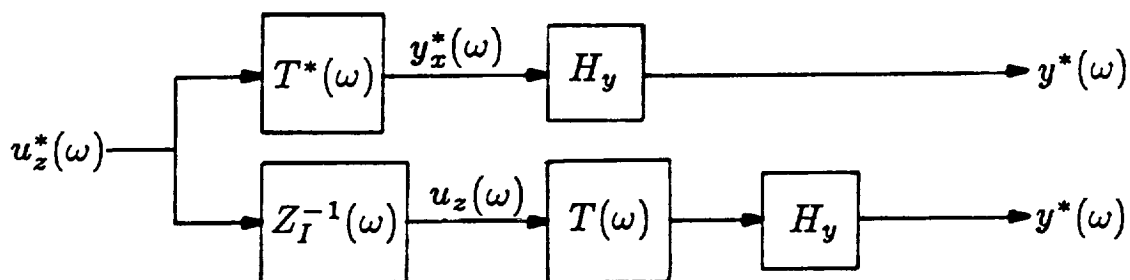


Figure 5.  $Z_1$ -Plot interpretation

The system response to a pilot input varies from the ideal response in off-nominal conditions to achieve the desired response  $y^*(\omega)$ , the pilot constantly varies his input commands  $u_z(\omega)$ . If the pilot has to vary his inputs drastically, the system is not robust.

Conversely, if only small adjustments in the pilot input are needed, the system's tracking performance is robust. Note how this is related to pilot workload.

Figure 5 shows the effect of  $Z_I(\omega)$  in terms of block diagrams. It is seen that if the pilot compensates for the off-nominal condition by including  $Z_I^{-1}(\omega)$  as a transfer function, he will produce perfect tracking. Thus, both the magnitude and the frequency content of  $Z_I^{-1}(\omega)$  is important as a measure of the amount of work the pilot must do to compensate for off-nominal conditions.

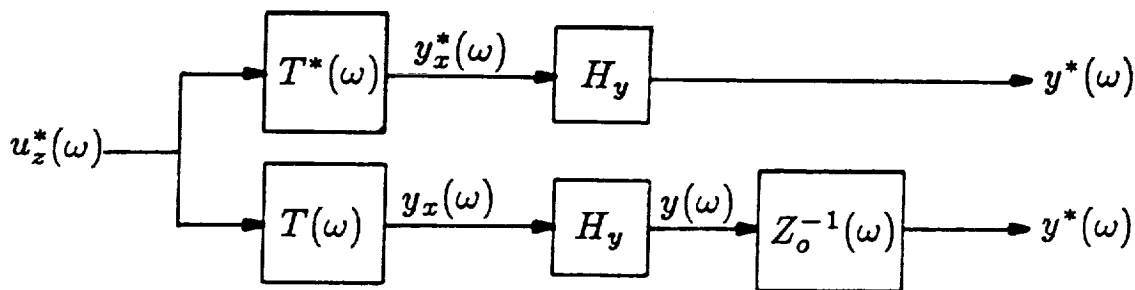


Figure 6.  $Z_O$ -Plot interpretation

While  $Z_I(\omega)$  is a measure of the input sensitivity,  $Z_O(\omega)$  is a measure of the output sensitivity. If a pilot input  $u_z^*(\omega)$  produces the output  $[H_y y_z^*(\omega)] = y^*(\omega)$  with the nominal aircraft, then the same pilot input will result in the response  $[H_y y_x(\omega)] = y(\omega)$  when the aircraft is in off-nominal conditions. Thus,  $Z_O(\omega)$  measures the sensitivity of the commanded plant outputs to off-nominal conditions when the pilot makes no effort to adapt to these conditions. Figure 6 shows the effect of  $Z_O(\omega)$  in terms of block diagrams. When the control system (feedforward and feedback) does not vary,  $Z_O(\omega)$  depends only on the feedback loop parameters (plant and feedback controller). On the other hand,  $Z_I(\omega)$  depends both on the feedforward and feedback loop parameters. We will refer to  $Z_I(\omega)$  and  $Z_O(\omega)$  as the  $Z$ -matrices and refer to the analysis plots obtained from them as  $Z$ -plots, for convenience. We think that the  $Z$ -matrices and the transfer function  $T$ -matrices,  $T(\omega)$ , provide highly useful information for the analysis and design of MIMO control systems.

Now define the following measures

$$Z_{max}(\omega) = \|Z(\omega)\|_2 \quad (87)$$

$$Z_{min}(\omega) = \|Z^{-1}(\omega)\|_2^{-1} \quad (88)$$

$$Z_c(\omega) = 1 + \|Z(\omega) - \text{diag}\{Z(\omega)\}\|_2 \quad (89)$$

Recall that ideally the  $Z$ -matrices (and their inverses) should equal the identity matrix. This can be seen from Figures 5 and 6 and from (84). Thus, for a robust MIMO system, the diagonal elements of the  $Z$ -matrix should be close to 1, while the off-diagonal elements should be small. As defined above,  $Z_{max}(\omega)$  and  $Z_{min}(\omega)$  bound the  $Z$ -matrix above and below, whereas  $Z_c(\omega)$  provides a measure of the magnitude of the off-diagonal elements. Thus,  $Z_c(\omega)$  isolates the magnitude of cross-talk; e.g., the impact of command 1 on output 2. Note that for a SISO system,  $Z_c(\omega)$  vanishes as there are no off-diagonal elements.

These measures are conservative. They display the worst case scenario for all the loops. It is often important to look at the individual elements of the  $Z$ -matrices and the  $T$ -matrices. This is particularly necessary when the system loop characteristics are different; e.g., when the desired bandwidth for two loops is significantly different. Thus  $Z_{ij}(\omega)$  and  $T_{ij}(\omega)$  are also important.

## 2. F/A-18 Actuator Approximation Design

To illustrate the techniques developed a longitudinal flight control system design for the F/A-18 was obtained at a single flight condition. The intent was to test the methodologies developed for approximation of actuators (or more generally the plant model) during the feedforward controller design, and also to test the usefulness of the sensitivity measures developed.

These considerations led us to a MIMO SOFFT design. The flight condition used was level flight at  $20^\circ$  angle-of-attack. The controls were the throttle and stabilator. The sensors used were a pitch rate gyro, an angle-of-attack vane and the thrust level. Although three sensors are fed back, the pilot can command only two variables independently since there are only two independent controls. The commanded plant outputs were selected to be: 1)  $q + \frac{1}{2} \alpha$  (i.e., a pitching command), 2)  $\delta T$  (i.e., a thrust level command). The command model for the pitching command was chosen to be the short-period mode approximation. For the second command, a 1<sup>st</sup> order model with 2 sec. time constant was used.

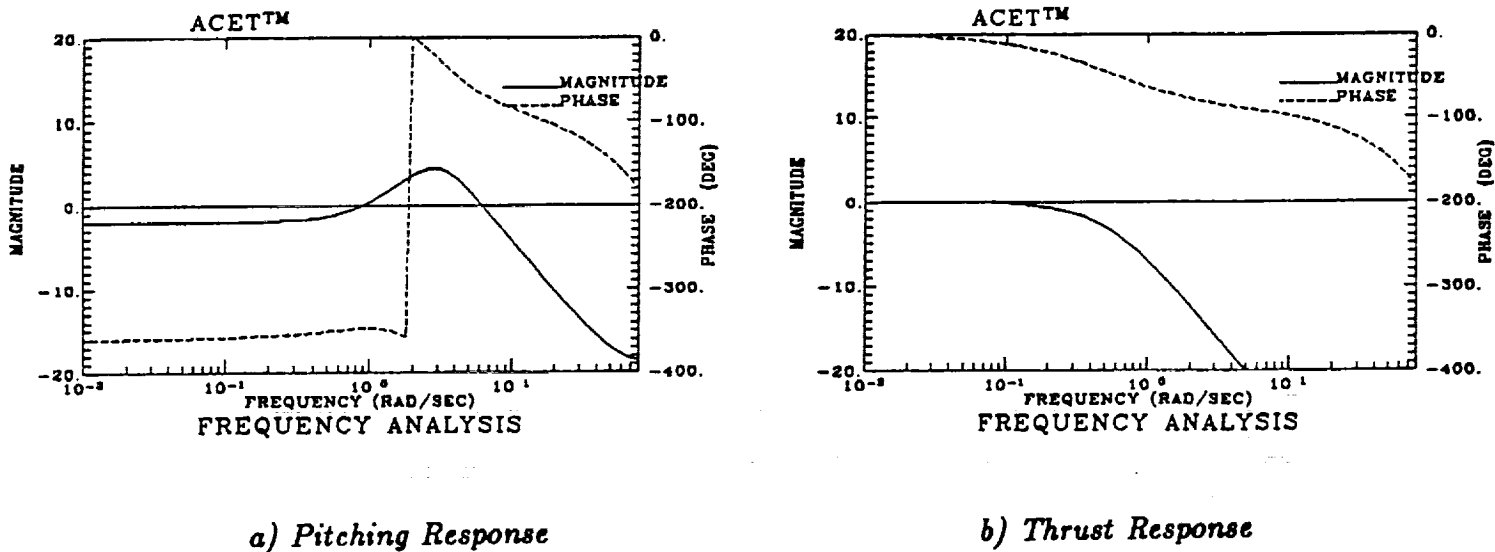
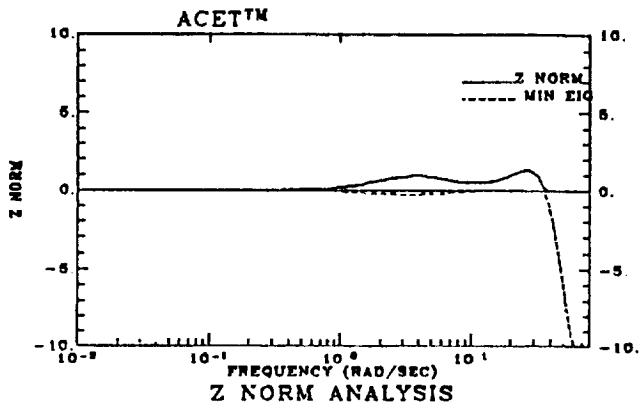


Figure 7. Desired response (command model)

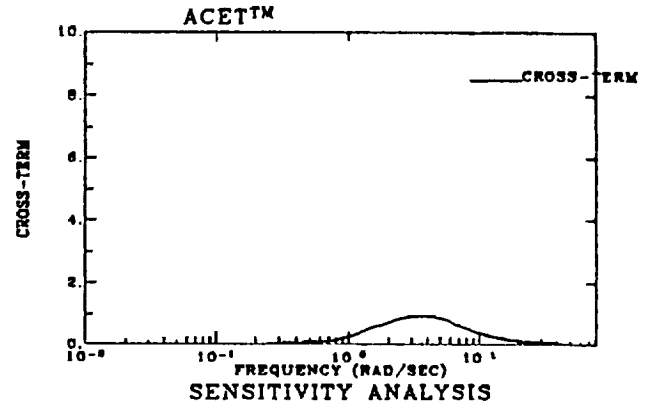
Using the design approach developed, a digital feedback control law with a PIF\* structure was designed at a 25 Hz sampling rate. The feedback design included actuator

---

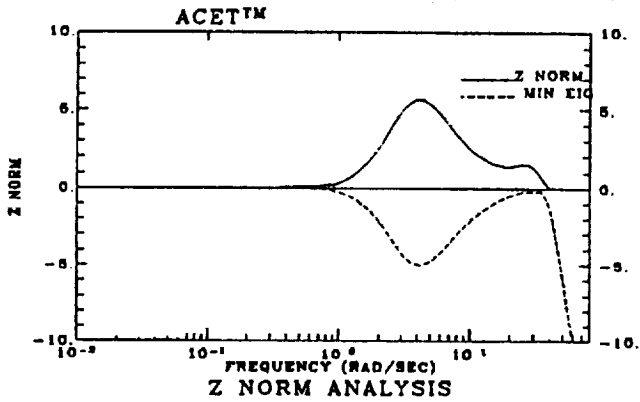
\*The PIF structure consists of a proportional feedback portion, an integrated error feedback portion and a filter portion which weighs the control rate. Thus, the PIF structure can filter out high frequencies, produce type 1 behavior and adjust time constants. It has been successfully used in various control laws including [14], [17], [25].



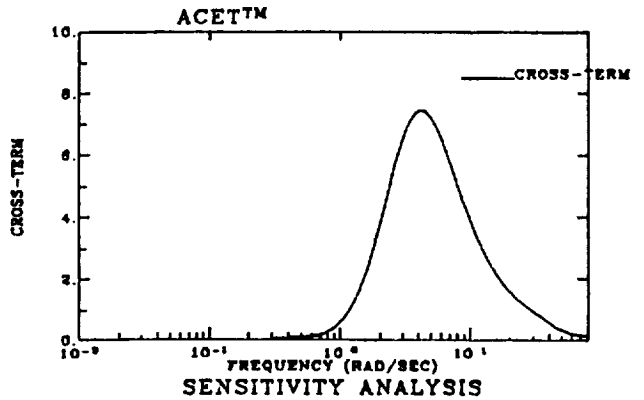
a)  $Z_0$ -Plot:  $Z_{0max}(\omega)$  and  $Z_{0min}(\omega)$



b)  $Z_0$ -Plot:  $Z_{0c}(\omega)$



c)  $Z_I$ -Plot:  $Z_{Imax}(\omega)$  and  $Z_{Imin}(\omega)$



d)  $Z_I$ -Plot:  $Z_{Ic}(\omega)$

Figure 8. Z-Plots for FB design 1

models for both the thrust and stabilator. On the other hand, in the feedforward design, the stabilator actuator was neglected from the plant model. The throttle-to-thrust model was kept since this has a long 2 sec. time constant.

The desired response to pitching and thrust commands is shown in Figure 7. All plots are shown in db for amplitudes and degrees for phase. Two feedback designs were made. Feedback (FB) Design 1 was the first design made. Using a "perfect tracking" feedforward design (without stabilator actuator), a SOFFT controller was obtained. Figure 8 shows the  $Z$ -plots for this design. From Figure 8a, we see that the pitching and thrust response will be within 1 or 2 db of the ideal or desired response for any pilot command until 40 rad/sec. However, some cross-talk is apparent from Figure 8b.

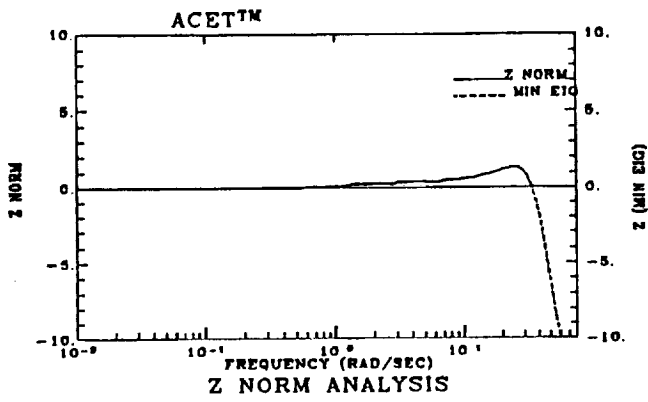
Figures 8c and 8d show a higher level sensitivity. If the pilot were to try to compensate his input commands so as to achieve the ideal response, significant adjustment would be needed in the higher frequency range above 1 rad/sec.

After some trial-and-error, we obtained Feedback (FB) Design 2. The  $Z$ -plots for this design are shown in Figure 9. While the  $\|Z_O\|_2$  has been reduced modestly, the "loop cross-talk" has been reduced impressively for both  $Z_I$  and  $Z_O$ . The cross-talk from the pitching command  $u_{z_1}$  to the thrust response is responsible for the difference.

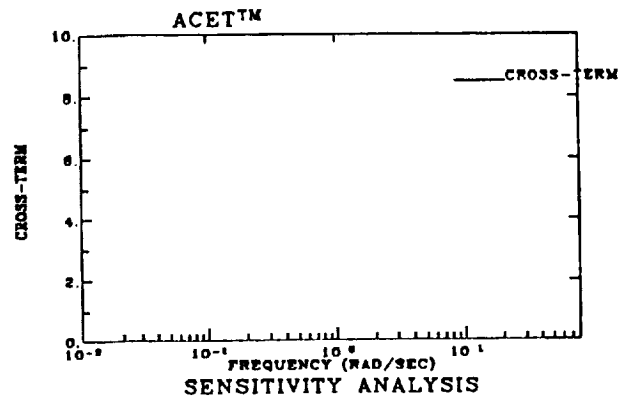
From Figure 10, it is seen that the maximum level has been reduced by 40 db, from -20 db to -60 db near 2 rad/sec. Actually, depending on the design goals, both designs display characteristics. However, the  $Z$ -plots seem to show specifically what's good and what's not as good. We are working on some small extensions of the concepts.

The individual elements of the  $Z$ -matrices are not shown here. Our experience so far with  $Z$ -plots and  $T$ -plots have been rewarding. These measures seem to provide important information about the tracking performance of the system. The sensitivity of the command tracking performance of a SOFFT design will be analyzed using  $Z$ -plots in section VI.

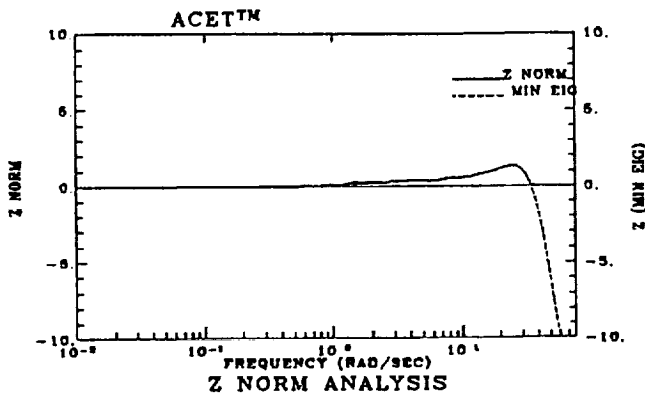




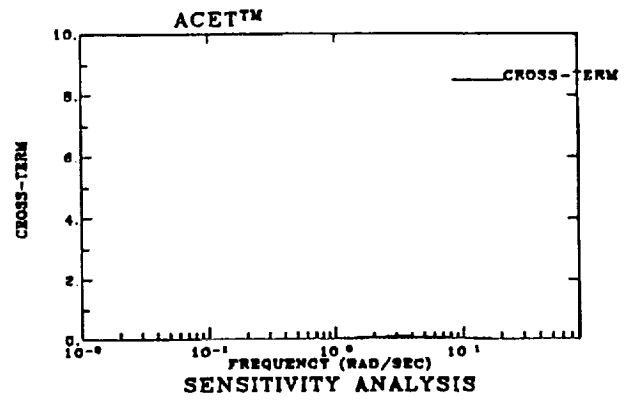
a)  $Z_0$ -Plot:  $Z_{0max}(\omega)$  and  $Z_{0min}(\omega)$



b)  $Z_0$ -Plot:  $Z_{0c}(\omega)$

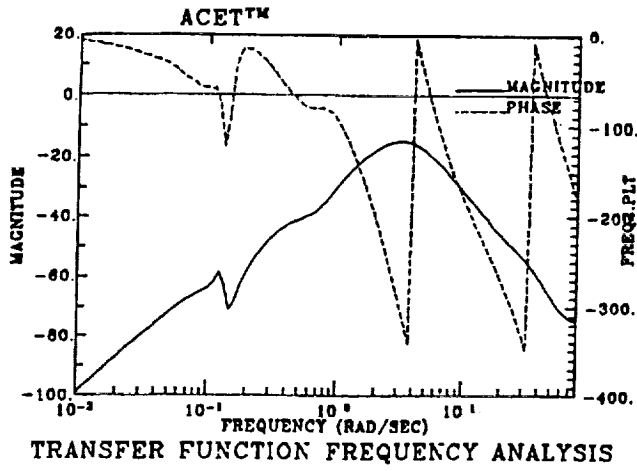


c)  $Z_I$ -Plot:  $Z_{Imax}(\omega)$  and  $Z_{Imin}(\omega)$

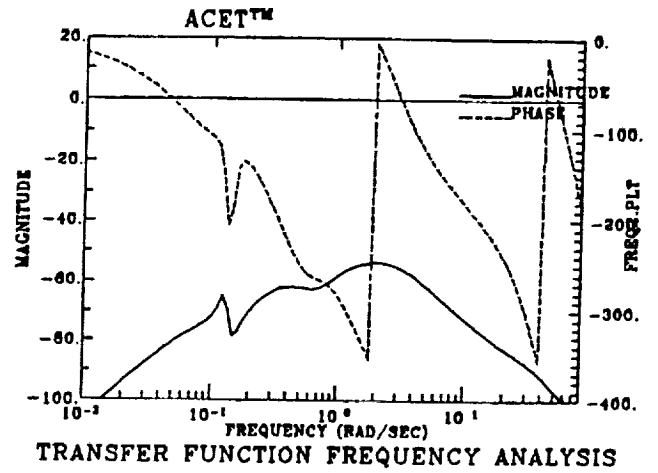


d)  $Z_I$ -Plot:  $Z_{Ic}(\omega)$

Figure 9. Z-Plots for FB design 2



a) *FB Design 1*



b) *FB Design 2*

Figure 10. Frequency response from pitching command ( $u_{z_1}$ ) to thrust response

#### IV. VARIABLE-GAIN SOFFT DESIGN METHODOLOGY

In the preceding sections, we have dealt with linear time-invariant systems. Of course, the time-invariant or single-model SOFFT control law tends to be very robust. So that it can control a nonlinear plant over a wide range of operating points even though the design model corresponds to a single operating point.

As the actual operating point moves away from the design condition, the assumptions used in the design methodology become less valid. And although the performance of the single-model SOFFT control law may still be acceptable, it is clear that a design based on the current operating point can have higher performance. Furthermore, by adapting to the current operating point, we can extend the operating regime of the plant indefinitely within the physical constraints of the plant. Thus, extending the operating range and having greater performance throughout the operating range are the major motivating factors for the Variable-Gain SOFFT design methodology.

For aircraft, the operating point is the flight condition of interest. To produce high levels of agility or maneuverability, it is necessary to move from one flight condition to another with great ease and high flight path accuracy. When the flight conditions are relatively close, a robust control system can provide satisfactory performance within a small flight regime. However, when the flight regime extends beyond certain limits, a constant-gain control system no matter how robust cannot maintain the necessary levels of agility. Or conversely, a control system with a variable-gain structure can provide greater agility when appropriately designed.

In this section, we will develop the design methodology for Variable-Gain SOFFT control laws. Given the successful applications [23], [24], [27] of the Variable-Gain Output Feedback design methodology [17], [18], we expect that Variable-Gain SOFFT will also provide a successful method for extending the flight regime with improved flying qualities.

## 1. Problem Formulation

In section II.1, the nonlinear plant and sensor models in (8) and (9) were linearized and discretized resulting in the discrete system given by (22) and (23).

When the operating point varies, it is necessary to linearize the plant about a new operating point  $(x_0, u_0, 0)$  or  $p$  at every iteration. As long as the sampling interval, say  $\Delta t$ , is selected sufficiently small, the operating point parameter vector  $p$  remains near its initial value over the interval. Thus, the linearization about the new plant, say  $p_k$ , is valid, and the original nonlinear system can now be described by the plant and measurement model

$$x_{k+1} = \phi_x(p_k) x_k + \Gamma_x(p_k) u_{xk} + w_{xk} + d_x(p_k) \quad (90)$$

$$y_{xk} = C_x(p_k) x_k + \nu_{xk} + b_x(p_k) \quad (91)$$

To design a control law for this system, consider the following class of time-invariant systems.

$$x(p, k + 1) = \phi_x(p) x(p, k) + \Gamma_x(p) u_x(p, k) + w_x(p, k) + d_x(p) \quad (92)$$

$$y_x(p, k) = C_x(p) x(p, k) + \nu_x(p, k) + b_x(p) \quad (93)$$

where  $p$  is a parameter vector of  $n_p$  components which represents the particular flight condition or operating point. For a fixed  $p$ , (92) and (93) represent a linear time-invariant system. The parameter vector  $p$  can be chosen by the designer in the way that best suits the particular problem under investigation. In particular,  $p$  may be a nonlinear function of the state vector or the measurement vector; or it may represent an unmeasured parameter

of the system. In all cases, the vector  $p$  must be either measured or estimated using a filter or other parameter estimation technique.

The system matrices  $\phi(p)$ ,  $\Gamma(p)$ , etc. can be arbitrary functions of  $p$ ; however, they must be known functions of  $p$ . For example, we can define these matrices by specifying them at several critical flight conditions, and then defining them by linear interpolation in between these flight conditions. Of course, the matrices can also be defined analytically when such expressions are available. Finally, note that the variables  $x(p, k)$ ,  $y_x(p, k)$ ,  $u_x(p, k)$  represent total quantities rather than perturbations of the physical variables. This is achieved by appropriate interpretation of the terms  $d_x(p)$  and  $b_x(p)$ .

In the Variable-Gain Control formulation, we shall allow the command model to vary with the operating point parameter vector  $p$ .

$$z(p, k + 1) = \phi_z(p) z(p, k) + \Gamma_z(p) u_z(p, k) \quad (94)$$

$$e(p, k) = H_y(p) y_x(p, k) - H_z(p) z(p, k) \quad (95)$$

The ability to vary the command model with the parameter vector provides an important flexibility in the control system. First, it allows the designer to command different variables (or different linear combinations of the variables) as the operating point or flight condition enters significantly different modes of operation; e.g., you can command different variables during normal flight than you would during stall or post-stall operation.

The second flexibility is that the commanded handling qualities can change with the operating point parameter vector  $p$ . Thus, the desired response to a given command can be different according to the value of the parameter vector. Also recall that the parameter vector can be selected arbitrarily. Thus one component of  $p$  may be chosen as a mode selector to represent fast or sluggish handling. Then according to the value set by the pilot, the aircraft would produce a fast or slower response. There are clearly a wide variety of ingenious ways of defining the parameter vector to produce desirable effects.

The objective is for  $H_y(p, k) y_x(p, k)$  to track the commands  $H_z(p, k) z(p, k)$  at every sampling instant. Alternately, the objective is to minimize the tracking error  $e(p, k)$  at every sampling instant.

Following the SOFFT approach for single model time-invariant systems, suppose that the control trajectory  $u_x^*(p, k)$  produces the desired feedforward state trajectory  $x^*(p, k)$ . Then

$$x^*(p, k+1) = \phi_x(p) x^*(p, k) + \Gamma_x(p) u_x^*(p, k) + d_x(p) \quad (96)$$

Now consider the "local" cost function  $J^*(p)$ :

$$J^*(p) = \frac{1}{2} \lim_{N \rightarrow \infty} \frac{1}{N+1} \sum_{k=0}^N E \left\{ \|e^*(p, k)\|_2^2 + x^*(p, k)^T Q_1^*(p) x^*(p, k) + u_x^*(p, k)^T R_1^*(p) u_x^*(p, k) \right\} \quad (97)$$

where  $e^*(p, k)$  is defined in accordance with (47).

When the feedforward objective includes only command tracking, the weighting matrices  $Q_1^*$  and  $R_1^*$  can be set to zero, so that only the tracking error is weighted. In other cases, the feedforward objectives may include additional goals such as keeping the control commands  $u_x^*$  at relatively low values. These can be included using the additional terms  $Q^*$  and  $R^*$ . However, the added objectives will be obtained at the expense of some additional tracking error.

The cost function  $J^*(p)$  describes the local objective at the operating point or flight condition corresponding to the vector  $p$ . Since the real objective is to design a control system for the complete operating range or the flight regime, a global cost function can be defined by a linear combination of the local costs over the region of interest.

$$J^* = \sum_{i=1}^{n_{mod}} f_i J^*(p^i) \quad (98)$$

where  $p^i$  denotes a particular value of the parameter vector  $p$  and determines a particular operating point in the operating range,  $f_i$  is a weighting coefficient which can be selected by the designer to specify the relative importance of the particular local operating point  $p^i$  and  $n_{mod}$  is the number of operating points included in the cost function. Note that  $n_{mod}$  should be chosen so that the complete operating range is represented satisfactorily.

Following the variable-gain output feedback methodology, let us constrain the form of the gain matrices as shown below.

$$K_x^*(p) = K_{x0}^* + \sum_{j=1}^{n_p} p(j) K_{xj}^* \quad (99)$$

$$K_z(p) = K_{z0} + \sum_{j=1}^{n_p} p(j) K_{zj} \quad (100)$$

$$K_u(p) = K_{u0} + \sum_{j=1}^{n_p} p(j) K_{uj} \quad (101)$$

where  $p(j)$  is the  $j^{th}$  component of the parameter vector  $p$ ,  $K_{xj}^*$ ,  $K_{zj}$  and  $K_{uj}$  are constant gain matrices. The control law is of the form

$$u_x^*(p, k) = -K_x^*(p) x^*(p, k) - K_z(p) z(p, k) - K_u(p) u_z(p, k) + u_x^*(p) \quad (102)$$

Thus, the problem is to minimize the global cost  $J^*$  in (98) subject to the constraints of (96), (94) and (102). An algorithm to obtain the gain matrices in (99) – (101) will be described in section IV.3.

### Perfect Tracking

To achieve perfect tracking, the cost function is selected so as to weight only the tracking error  $e^*(p, k)$ . Thus, the matrices  $Q_1^*$  and  $R_1^*$  in the local cost  $J^*(p)$  are set to zero. In this case, the local cost can be minimized subject to the local plant model at each operating point corresponding to  $p$ . Thus, it is not necessary to limit consideration

to a finite number of operating points,  $p^i$ , as in the cost (98). In this case, the complete operating range can be included. The solution is the same as the time-invariant case except that now the plant parameters are functions of  $p$ .

$$K_x^*(p) = [H_x(p) \Gamma_x(p)]^{-1} H_x(p) \phi_x(p) \quad (103)$$

$$K_z(p) = -[H_x(p) \Gamma_x(p)]^{-1} H_z(p) \phi_z(p) \quad (104)$$

$$K_u(p) = -[H_x(p) \Gamma_x(p)]^{-1} H_z(p) \Gamma_z(p) \quad (105)$$

It is important to note that the optimal gain matrices for the perfect tracking case are not of the form shown in (99) - (101). Of course this is not significant as long as the gain matrices can be computed with ease in real time.

Since the plant model matrices are known a priori, the only computational load in obtaining the gain matrices is in inverting the matrices  $[H_x(p) \Gamma_x(p)]$ . The dimension of this matrix is  $n_{yx}$  by  $n_{ux}$ . Thus, it is necessary to invert a matrix of dimension as large as the number of controls ( $n_{ux}$ ) or the number of commands ( $n_{yx}$ ). When the number of controls is small such as 1, 2 or 3, it is possible to invert the matrices analytically. For higher order matrices, inversion routines are available. However, as the dimension increases, the computational load increases as the cube of the dimension and may reach undesirable levels. Also, for high order matrices, the accuracy of the inverse may be called into question. However, for up to third order, the inversion can be accomplished with ease.

## 2. Feedforward Integrators

For single-model designs, it is often possible to achieve perfect tracking in the feedforward control. As before, by perfect tracking we mean that the desired output trajectory matches the command model output at every sampling instant; i.e.,



$$e^*(p, k) = H_y(p) y_z^*(p, k) - H_z(p) z(p, k) = 0 \quad , \quad k \geq 0 \quad (106)$$

In other cases, perfect tracking may not be achieved. For example, in a single-model design in which  $R_1^* > 0$  ( $R_1^*$  is positive definite), perfect tracking will not be obtained even though the tracking error may be small. In the Variable-Gain feedforward formulation given in the previous section, perfect tracking will not be achieved in the general case. For non-minimum phase systems, it may be desirable not to use the perfect tracking solution. Finally, in other cases, the plant's physical constraints such as position and rate limits may make it more desirable not to seek perfect tracking in the feedforward system as well.

Thus, in general  $H_y y_z^*(p, k)$  will not track the commanded  $H_z z(p, k)$  perfectly at every  $k$  and  $p$ . As long as the tracking error is small, this may not be significant. However, in some cases, it is desirable to have no error in steady-state for constant commands. For this purpose, it is possible to introduce integrators into the feedforward control law.

Thus, let

$$I^*(p, k+1) = I^*(p, k) + \Delta t e^*(p, k) \quad (107)$$

$$u_x^*(p, k) = -K_x^*(p) x^*(p, k) - K_z(p) z(p, k) - K_u(p) u_z(p, k) - K_I^*(p) I^*(p, k) + u_x^*(p) \quad (108)$$

Now, we introduce an integral penalty term into the objective or cost function. Now consider the local cost function

$$J^* = \frac{1}{2} \lim_{N \rightarrow \infty} \frac{1}{N+1} \sum_{k=0}^N E \left\{ \|e^*(p, k)\|_2^2 + x^*(p, k)^T Q_1^*(p) x^*(p, k) + u_x^*(p, k)^T R_1^*(p) u_x^*(p, k) + I^*(p, k)^T Q_I I^*(p, k) \right\} \quad (109)$$

while the global cost remains as given by (98).

The result of minimizing the new cost function will be a type-1 behavior in the feedforward system. In the transient, some tracking error will be present, but the error will vanish in steady-state. The algorithm for gain computation is given in the following section.

### 3. Algorithm for Gain Computation

In developing an algorithm for computing the feedforward variable-gain matrices, we will include the case for feedforward integrators. To exclude the integrators, simply neglect the corresponding terms

First consider the augmented command model

$$Z(p, k) = \begin{pmatrix} z(p, k) \\ u_z(p, k) \end{pmatrix} \quad (110)$$

$$Z(p, k + 1) = \phi_Z(p) Z(p, k) + \Gamma_Z(p) w_z(p, k) \quad (111)$$

where  $w_z(p, k)$  is the white noise sequence whose covariance equals that of  $u_z(p, k)$ .

$$\phi_Z(p) = \begin{pmatrix} \phi_z(p) & \Gamma_z(p) \\ 0 & 0 \end{pmatrix}, \quad \Gamma_Z(p) = \begin{pmatrix} 0 \\ I \end{pmatrix} \quad (112)$$

Now, consider the augmented state vector  $X^*(p, k)$ .

$$X^*(p, k) = \begin{pmatrix} x^*(p, k) \\ I^*(p, k) \\ Z(p, k) \end{pmatrix} \quad (113)$$

After some manipulations, it follows that

$$X^*(p, k + 1) = \phi(p) X^*(p, k) + \Gamma(p) u_x^*(p, k) + \Gamma_w(p) w_z(p, k) \quad (114)$$

$$Y^*(p, k) = X^*(p, k) \quad (115)$$

where the augmented matrices can be built as given below

$$\phi(p) = \begin{pmatrix} \phi_x(p) & 0 & 0 \\ \Delta t H_x(p) & I & -\Delta t H_z(p) \\ 0 & 0 & \phi_z(p) \end{pmatrix}, \quad \Gamma(p) = \begin{pmatrix} \Gamma_x(p) \\ 0 \\ 0 \end{pmatrix} \quad (116)$$

$$C = I, \quad D = 0, \quad \Gamma_w(p) = \begin{pmatrix} 0 \\ 0 \\ \Gamma_z(p) \end{pmatrix}, \quad H_z(p) = (H_x(p) \ 0) \quad (117)$$

Now we express the local cost function in terms of the augmented state.

$$Q^*(p) = \begin{pmatrix} H_x^T(p) H_x(p) + Q_1^*(p) & 0 & -H_x^T(p) H_z(p) \\ 0 & Q_I(p) & 0 \\ -H_z^T(p) H_x(p) & 0 & H_z^T(p) H_z(p) \end{pmatrix} \quad (118)$$

$$J^*(p) = \frac{1}{2} \lim_{N \rightarrow \infty} \frac{1}{N+1} \sum_{k=0}^N E \left\{ X^*(p, k)^T Q^*(p) X^*(p, k) + u_z^*(p, k)^T R_1^* u_z^*(p, k) \right\} \quad (119)$$

$$J^* = \sum_{i=1}^{n_{mod}} f_i J^*(p^i) \quad (120)$$

Observing (114) - (120), note that we have embedded the stochastic optimal feedforward control design problem into the Variable-Gain Output Feedback problem treated in [17] and [18].

Thus, the algorithm for the current problem is obtained by building the augmented matrices in (116) - (118) for each of the models considered; i.e., for each value  $p^i$ ,  $i = 1, 2, \dots, n_{mod}$ . Then by using the Variable-Gain Output Feedback algorithm in [18] pp. 28-29, we obtain the optimal feedforward gain.

$$u_z^*(p, k) = -K^*(p) X^*(p, k) \quad (121)$$

$$K^*(p) = (K_x^*(p) \ K_I^*(p) \ K_z(p) \ K_u(p)) = K_0^* + \sum_{j=1}^{n_p} p(j) K_j^* \quad (122)$$

Our experience with this algorithm to date indicates a fast rate of convergence, in fact, much faster than usual variable-gain output feedback problems. We think this is due to the fact that  $C = I$ ; i.e., the feedforward uses a full-state feedback structure.

#### 4. Digital Implementation

The implementation of the SOFFT feedforward control law is intrinsically different than that of feedback control law. In the feedback control law, only those equations involved in computing the control commands,  $u_{zk}$ , are implemented. In particular, the plant state and sensor output vectors are not computed; the actual plant and sensors produce the outputs which are input to the feedback control system.

In the SOFFT feedforward control law, both the control commands,  $u_{zk}^*$ , and the desired trajectory,  $y_{zk}^*$ , are computed in the implementation. Usually, this involves an approximate plant and sensor model. Of course, the command model must also be implemented.

We have developed an incremental implementation obtained by differencing and some approximations. The usual advantages of incremental implementations are that trim values are not needed, that integrator wind-up problems do not occur and limiting is easily handled.

#### Feedforward Control Implementation

Let  $p_k$  be a parameter vector value at the sampling instant  $t_k$ .

$$\Delta u_{zk} = u_{zk} - u_{zk-1} \quad (123)$$

$$\Delta z_{k+1} = \phi_z(p_k) \Delta z_k + \Gamma_z(p_k) \Delta u_{zk} \quad (124)$$

$$z_{k+1} = z_k + \Delta z_{k+1} \quad (125)$$

$$\begin{aligned} \Delta u_{xk}^* = & -K_x^*(p_k) \Delta x_k^* - K_I^*(p_k) \Delta t [H_y(p_k) y_{xk-1}^* - H_z(p_k) z_{k-1}] \\ & - K_z(p_k) \Delta z_k - K_u(p_k) \Delta u_{zk} \end{aligned} \quad (126)$$

$$\Delta x_{k+1}^* = \phi_x^*(p_k) \Delta x_k^* + \Gamma_x^*(p_k) \Delta u_{xk}^* \quad (127)$$

$$\Delta y_{xk+1}^* = C_x^*(p_k) \Delta x_{k+1}^* \quad (128)$$

$$y_{xk+1}^* = y_{xk}^* + \Delta y_{xk+1}^* \quad (129)$$

$$u_{xk}^* = u_{xk-1}^* + \Delta u_{xk}^* \quad (130)$$

Thus, the feedforward control law produces the vectors  $u_{xk}^*$  and  $y_{xk+1}^*$  which are now input to the feedback control law to obtain the complete or combined control law. The gains  $K_x^*(p_k)$ ,  $K_I^*(p_k)$ ,  $K_z(p_k)$  and  $K_u(p_k)$  are computed on line from (99) - (101) or from (103) - (105) for perfect tracking. Note that  $K_I^*(p_k) \equiv 0$  for perfect tracking; otherwise, it has the form shown in (122) or (99) - (101). The plant and command model matrices are also computed on-line using the interpolation algorithm described below. Of course, other interpolations may also be used.

It can be shown that the perfect tracking control law coupled with the above incremental implementation will produce the desired  $y_{xk}^*$  trajectory such that

$$H_y(p_k) \Delta y_{xk+1}^* = H_z(p_k) \Delta z_{k+1} \quad , \quad k \geq 0 \quad (131)$$

When  $H_y$  and  $H_z$  are independent of  $p$ , this results in the perfect tracking trajectory

$$H_y y_{xk+1}^* = H_z z_{k+1} \quad , \quad k \geq 0 \quad (132)$$

provided that the initial conditions match; i.e.,

$$H_y y_{z0}^* = H_z z_0 \quad (133)$$

This produces a type-1 property for steady-state tracking as  $k \rightarrow \infty$ . On the other hand, the same type-1 property does not hold for the optimal tracking option. A constant command may not produce the equality shown in (132) in steady-state (or as  $k \rightarrow \infty$ ). In many cases, this type-1 property may not be necessary as long as the transient behavior is satisfactory. To ensure steady-state tracking with zero error, it is necessary to include integrators in the feedforward control law.

### Interpolation of Feedforward Models

As mentioned earlier, the feedforward control law generates the \*-trajectories using a model of the plant and sensors. In the variable-gain design case, these models are specified at a finite number of operating points sufficient to represent the operating range. In actual operation, the operating point parameter  $p_k$  will naturally have values different than the specified models. To accommodate the complete operating range, it is necessary to interpolate in between these models. The following interpolation algorithm was developed for this purpose.

Let  $p^j$ , for  $j = 1, 2, \dots, M$ , represent the  $j^{\text{th}}$  model parameter vector. Let  $p$  be the current value of the parameter vector. Define the metric  $\rho_j(p)$  as follows:

$$\rho_j(p) = \|p - p^j\| \quad , \quad j = 1, 2, \dots, M \quad (134)$$

where  $\|\cdot\|$  is the 2-norm for vectors. Of course, any norm could be used for this purpose.

### Algorithm

1. Find the  $n$  smallest values of  $\rho_j(p), j = 1, 2, \dots, M$ . If  $\rho_j(p) = 0$  for some  $j$ , then  $\phi_x^*(p) = \phi_{x_j}^*$ ; stop. It may be desirable to also check that the selected  $n$  models are not too close to each other; e.g.,  $\|p^i - p^j\| \geq \epsilon$ .
2. Reorder the models so that the selected models are the first  $n$  models,
3. Compute

$$\bar{\rho}(p) = \frac{1}{\sum_{i=1}^n \frac{1}{\rho_i(p)}} \quad (135)$$

Note:

$$\sum_{i=1}^n \frac{\bar{\rho}(p)}{\rho_i(p)} = 1 \quad (136)$$

4. Compute the interpolated matrices  $\phi_x^*(p), \Gamma_x^*, C_x^*(p)$  using the formula

$$\phi_x^*(p) = \sum_{i=1}^n \frac{\bar{\rho}(p)}{\rho_i(p)} \phi_{x_i}^* \quad , \quad \phi_{x_i}^* = \phi_x^*(p^i) \quad (137)$$

Note: When  $n = 2, n_p = 1$ , this algorithm produces the usual linear interpolation.

### Feedback Control Implementation

The feedback control uses the sensor measurements  $y_{xk}$  and the feedforward variables  $y_{xk}^*, u_{xk}^*$ , etc.

$$\Delta y_{xk} = y_{xk} - y_{xk-1} \quad (138)$$

$$\begin{aligned} \tilde{v}_{xk} = & [I - \Delta t K_{xu}(p_k) C_u \Gamma_r] \tilde{v}_{xk-1} - K_{xz}(p_k) [\Delta y_{xk} - \Delta y_{xk}^*] - K_{zc}(p_k) C_c(p_k) \Delta \tilde{c}_k \\ & - \Delta t K_{xI}(p_k) C_I(p_k) [H_y(p_k) y_{xk-1} - H_y(p_k) y_{xk-1}^* + H_u(p_k) \tilde{u}_{k-1}] \end{aligned} \quad (139)$$

$$\begin{aligned}
\Delta \tilde{c}_{k+1} = & (\phi_c(p_k) - \Delta t \Gamma_c(p_k) K_{cc}(p_k) C_c(p_k)) \Delta \tilde{c}_k \\
& + (\phi_{cy}(p_k) - \Delta t \Gamma_c(p_k) K_{cx}(p_k)) [\Delta y_{xk} - \Delta y_{xk}^*] \\
& - (\Delta t)^2 \Gamma_c(p_k) K_{cI}(p_k) C_I(p_k) [H_y(p_k) y_{xk-1} - H_y(p_k) y_{xk-1}^* + H_u(p_k) \tilde{u}_{k-1}] \\
& + (\phi_{cu}(p_k) - \Delta t \Gamma_c(p_k) K_{cu}(p_k) C_u(p_k)) \Delta t \Gamma_r \tilde{v}_{xk-1} \\
& + \Delta t \Gamma_{cz}(p_k) (\tilde{v}_{xk} - \tilde{v}_{xk-1})
\end{aligned} \tag{140}$$

$$\tilde{c}_{k+1} = \tilde{c}_k + \Delta \tilde{c}_{k+1} \tag{141}$$

$$\tilde{u}_k = \tilde{u}_{k-1} + \Delta t \Gamma_r \tilde{v}_{xk-1} \tag{142}$$

$$u_{xk} = C_r \tilde{u}_k + D_r \tilde{v}_{xk} + u_{xk}^* \tag{143}$$

The control commands  $u_{xk}$  are now sent to the plant. When  $p_k$  is constant, the implementation reduces to the single-model case.



## V. F/A-18 SIMULATION

A general dynamic flight simulation module was developed to test the new control design methodology proposed in this work. This simulation module incorporates the specific aerodynamic properties of the F/A-18 aircraft, although any other aircraft can also be simulated by inserting the particular aerodynamic and propulsive modules for that aircraft. The non-linear F/A-18 simulation was also integrated into ACET for various platforms. This combination of ACET and non-linear aircraft simulation produces a very powerful tool to design flight control systems.

### 1. Overview of the Basic Components

Figure 11 identifies the basic components of the F/A-18 simulation and the interactions among them. For each integration period,  $\Delta t$ , the aircraft simulation receives the command inputs from the flight control system (FCS), computes the total forces and moments on the aircraft by using engine, actuator and the aerodynamic models of the aircraft, obtains the position and speed components using the aircraft kinematics and produces sensor outputs to be used by FCS. Each dynamical model in the simulation can be improved or simply changed by varying the model dynamics while keeping the structure of the simulation intact. The actual algorithm of the simulation also involves various data exchanges among the basic components. The simulation is intended for arbitrary flight maneuvers in relatively short periods of time, so the body axes components are selected to be computed and the Earth-fixed axes are an inertial frame of reference. The simulation also contains a vectored thrust capability. The control actuator models have linear 1<sup>st</sup>-order dynamics with non-linearities such as rate and position limiters. The kinematics equations for a rigid airplane are solved using a non-linear Runge-Kutta-Fehlberg method for the single step

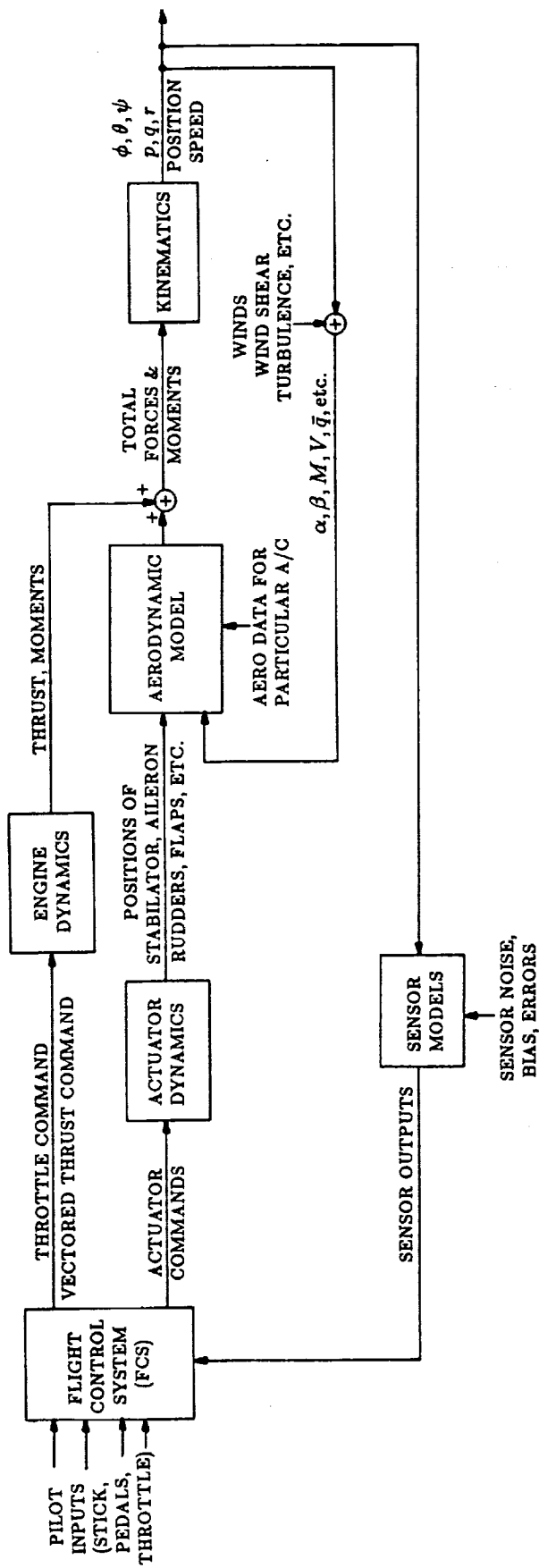


Figure 11. Flight simulation diagram

integration. Since F/A-18 can be simulated in different mission conditions, arbitrary center of gravity locations in the aircraft can be selected. Steady components of wind velocity vector are also included. An ideal sensor model is employed for sensor parameters. The F/A-18 simulation was integrated into ACET for VAX computers on the VMS platform and for IBM-compatible computers with DOS. Combining the model building, control design, analysis, linear simulation, matrix operations, and plotting capabilities of ACET and the non-linear F/A-18 simulation, the integrated product enables the researcher to increase his efficiency in designing flight control systems greatly. Detailed important features of the F/A-18 simulation components are:

### Flight Control System (FCS) Inputs

The FCS module provides the simulation section the necessary pilot input variables such as the control surface actuator commands, engine throttle and vectored thrust commands. The FCS inputs to the simulation as elements of the command input vector,  $U$  and their references are:

$U(1)$  = Stabilator (positive trailing edge down (+TED), deg)

$U(2)$  = Aileron (+TED, deg)

$U(3)$  = Rudder (+TE left, deg)

$U(4)$  = Throttle angle (deg)

$U(5)$  = Pitch vane command for vectored thrust (VT)

$U(6)$  = Yaw vane command for VT

Any combination of the command input variables can be selected with the simulation setting the other input parameters to constant values. The command input variables are computed by FCS for each integration interval,  $\Delta t$ .

### Actuator Dynamics

Actuator dynamics model includes a linear 1<sup>st</sup>-order dynamics for the actuator sur-

faces and non-linearities consisting of position and rate limiters. The actuator commands from FCS are used in a configuration module to obtain the positions of the actuator surfaces. A list of the control actuator surfaces and their references are:

DHTR = Right stabilator (positive trailing edge down, (+TED))

DHTL = Left stabilator (+TED)

DAR = Right aileron (+TED)

DAL = Left aileron (+TED)

DRR = Right rudder (+TE left)

DRL = Left rudder (+TE left)

DTFR = Right trailing edge flap (+TED)

DTFL = Left trailing edge flap (+TED)

DLFR = Right leading edge flap (+TED)

DLFL = Left leading edge flap (+TED)

Speed brakes (0 - 60 deg) (set to 0)

Landing gear (0 - 1 down) (set to 0)

Due to asymmetric position limiters, the stabilators, the ailerons and the all flap surfaces may have asymmetric responses.

### Engine Dynamics

The non-linear engine model for the F/A-18 aircraft was incorporated in the simulation. The engine model is based on data received from DFRF and its implementation in AGCB at LaRC. The engine commands from the FCS include the throttle command which determines the various conditions of the engine such as the flight idle, military power, afterburner on, etc. A vectored thrust capability using pitch and yaw thrust commands also exists.

The engine dynamics are modeled in an engine module which requires angle-of-attack,

mach, altitude and attitude rates and produces total engine forces and moments. The iteration time for the engine is 0.032 sec and it is synchronized with the F/A-18 simulation by using additional iterations if necessary. The engine module accounts for various losses such as ram, inlet/aft body, windmill drags and thrust vectoring losses to compute the net thrust of the engine. The gyroscopic effects are also included in computations.

Static and dynamic tests have been made with the engine module at various throttle level, mach number and other conditions. The rate limit, gyroscopic and other non-linear effects as well as phugoid and short period modes due to attitude changes have been observed in the engine output and are found reasonable.

### **Aerodynamic Model**

The aerodynamic model of the F/A-18 aircraft in the simulation computes the aerodynamic forces and moments using modules supplied by Langley researchers. The model utilizes the control surface actuator positions from the actuator models and the current body axes components from the kinematics modules. The model includes a quasi-static-elastic approximation where the flexible modes are actively modeled to compute the aerodynamic coefficients. The force and moment coefficients and the lift and pitch derivatives are first computed about the aerodynamics reference center (a wind tunnel reference), and then translated into the body axes with respect to center of gravity (CG) location. The model also includes a rolling moment increment for  $\alpha > 40^\circ$  as well as other effects for high  $\alpha$ . Various mission conditions can be employed changing CG location and mass distribution. The simulation employed a default configuration representing an early estimate of F/A-18 HARV. The forces and moments obtained from the aerodynamic and the engine models produce the total forces and moments to be used in the kinematics model.

## Kinematics

The kinematics formulation for the simulation was developed using a six-degree-of-freedom formulation. The equations of motion were derived for a rigid airplane and a quasi-static-elastic approximation was used to compute aerodynamic forces and moments. The motion of the aircraft was computed in the body axes, rather than the stability axes since the simulation was developed for various flight maneuvers rather than a particular flight condition. For the moment equations, symmetry about the  $x-z$  plane was assumed. The simulation was primarily intended for maneuvers occurring in relatively short periods of time, rather than long periods, such as cruise and navigation. Consequently, a flat, non-rotating Earth model was assumed, so that the Earth-fixed axes are an inertial frame of reference and the mass and inertia distribution was assumed to be constant during the simulation not dependent on factors, such as fuel load, weapon adjustments, etc. For each simulation, various mission conditions can be selected with different mass and inertia distributions and center of gravity locations. Gravity is assumed to be constant with the default value selected at sea level. It is also constant over the airplane volume acting as a force at the center of gravity with no moments produced.

The kinematics equations used in the simulation are given below:

$$\dot{u} = -qw + rv - g \sin \theta + \frac{1}{m} F_x \quad (144)$$

$$\dot{v} = pw - ru + g \cos \theta \sin \phi + \frac{1}{m} F_y \quad (145)$$

$$\dot{w} = qu - pv + g \cos \theta \cos \phi + \frac{1}{m} F_z \quad (146)$$

$$\dot{p} = K_1 \left[ \left( \frac{I_y I_z - I_z^2 - I_{zx}^2}{I_x I_z} \right) qr + K_2 pq + \left( \frac{1}{I_x} \right) L + \left( \frac{I_{zx}}{I_x I_z} \right) N \right] \quad (147)$$

$$\dot{q} = \left( \frac{I_z - I_x}{I_y} \right) rp + \left( \frac{I_{zx}}{I_y} \right) (r^2 - p^2) + \left( \frac{1}{I_y} \right) M \quad (148)$$

$$\dot{r} = K_1 \left[ \left( \frac{I_x^2 - I_x I_y - I_{zx}^2}{I_x I_z} \right) p q - K_2 q r + \frac{I_{zx}}{I_x I_z} L + \frac{1}{I_z} N \right] \quad (149)$$

$$\dot{\phi} = p + \sin \phi \tan \theta q + \cos \phi \tan \theta r \quad (150)$$

$$\dot{\theta} = \cos \phi q - \sin \phi r \quad (151)$$

$$\dot{\psi} = \sin \phi \sec \theta q + \cos \phi \sec \theta r \quad (152)$$

$$\begin{aligned} \dot{x} = & (\cos \theta \cos \psi) u + (\sin \phi \sin \theta \cos \psi - \cos \phi \sin \phi) v \\ & + (\cos \phi \sin \theta \cos \psi + \sin \phi \sin \psi) w \end{aligned} \quad (153)$$

$$\begin{aligned} \dot{y} = & (\cos \theta \sin \psi) u + (\sin \phi \sin \theta \sin \psi + \cos \phi \cos \psi) v \\ & + (\cos \phi \sin \theta \sin \psi - \sin \phi \cos \psi) w \end{aligned} \quad (154)$$

$$\dot{z} = -\sin \theta u + \sin \phi \cos \theta v + \cos \phi \cos \theta w \quad (155)$$

where

$$K_1 = \left[ \frac{1}{1 - \left( \frac{I_{zx}^2}{I_x I_z} \right)} \right]$$

$$K_2 = \left[ \frac{I_{zx}}{I_x I_z} (I_x - I_y + I_z) \right]$$

In these equations, the body axes origin is at the center of gravity and the axes are oriented such that  $+x$  is out the nose,  $+y$  is out the right wing and  $+z$  is out the belly. The airplane is assumed to be symmetric about the  $x - z$  plane, therefore,  $I_{xy}$  and  $I_{yz}$  products of inertia are zero and are not included in the kinematics equations.

The kinematic equations are solved using a non-linear single-step integration algorithm employing a seventh-eighth (7,8) order Runge-Kutta-Fehlberg method and a solution for all kinematic parameters are obtained at each simulation step size,  $\Delta t$ . The integration module employs variable internal step sizes depending on the variability of the solutions and adapts to existing singularities and invalid inputs. The simulation options include selecting relative and absolute accuracies. The algorithm was found to be performing well with good numerical stability.

### Sensor Outputs

The F/A-18 simulation was developed to give the option of selecting a number of sensor outputs necessary for the flight control system. An ideal sensor model is employed and any combination of sensor outputs can be fed back to the control system. The available sensor parameters include all the computed kinematic parameters, body angles, body mounted accelerometers, etc. A complete list of available sensor outputs are given below:

$Y(1), \dots, Y(12) = X(1), \dots, X(12)$  From kinematic equations

$Y(13) = V_T$ , True air speed (ft/sec)

$Y(14) = \alpha$ , Angle-of-attack (deg)

$Y(15) = \beta$ , Sideslip angle (deg)

$Y(16) = F_{BX}$ , Body mounted accelerometer in the  $x$ -axis (ft/sec<sup>2</sup>)

$Y(17) = F_{BY}$ , Body mounted accelerometer in the  $y$ -axis (ft/sec<sup>2</sup>)

$Y(18) = F_{BN}$ , Normal body mounted accelerometer (ft/sec<sup>2</sup>)

$Y(19) = \dot{h}$ , Sink rate (ft/sec)

$Y(20) = \gamma$ , Flight path angle (deg)

$Y(21) = \bar{p}$ , Barometric pressure (lbs/ft<sup>2</sup>)

$Y(22) = \rho$ , Air density (slugs/ft<sup>3</sup>)



## 2. Simulation Examples

F/A-18 aircraft simulation had been tested in various static and dynamic conditions. Various modes including phugoid, short period and lateral modes had been analyzed; static tests were compared with the trim conditions given by Langley researchers at various mach numbers and attitudes. Dynamical tests had also been made by using non-trim initial conditions for the aircraft dynamics.

Figure 12 shows the longitudinal/vertical variables where longitudinal variables have perturbed initial conditions. The control inputs are set for a trim condition at  $\alpha = 18.8^\circ$  and mach number = 0.24. The plots indicate a short period mode with a period of 8 or 9 sec., and a phugoid mode with a period of about 40 sec. Both of these natural frequencies are in general agreement with the theoretical values determined from the linearized models. Figure 13 shows the variables in a simulation of the same flight condition where lateral variables have non-trim initial conditions. The natural frequencies of these modes are also in general agreement with the theoretical values.

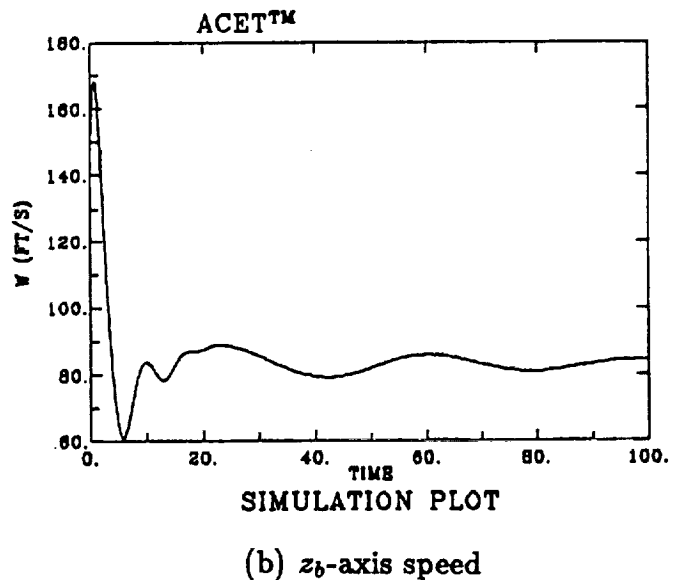
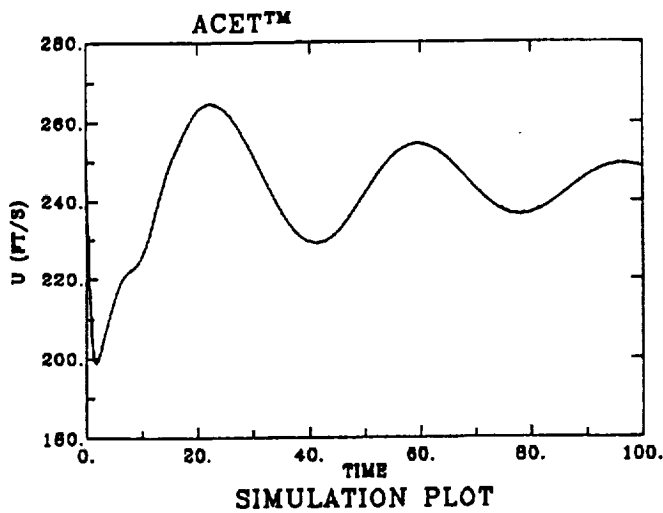
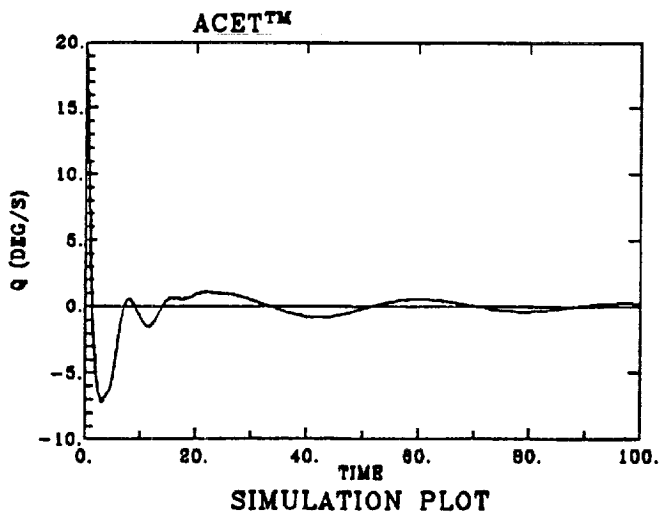
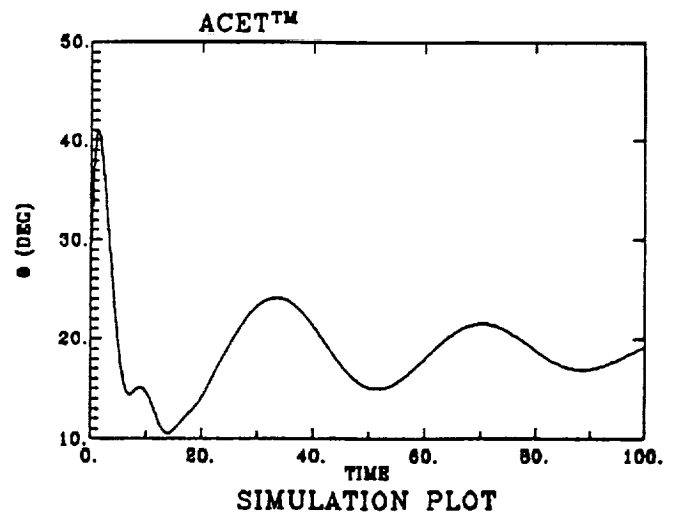


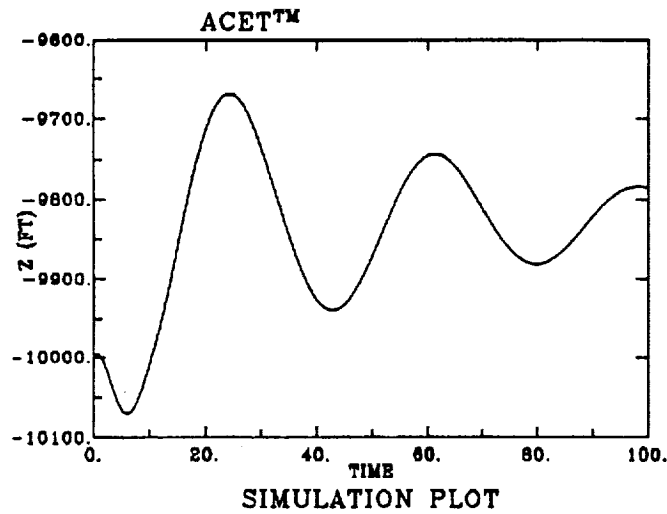
Figure 12. Longitudinal/vertical variables with longitudinal variables perturbed



(c) Pitch rate

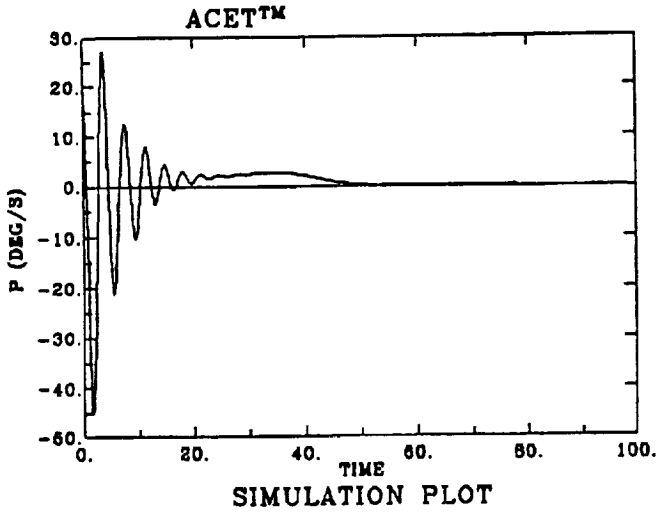


(d) Pitch angle

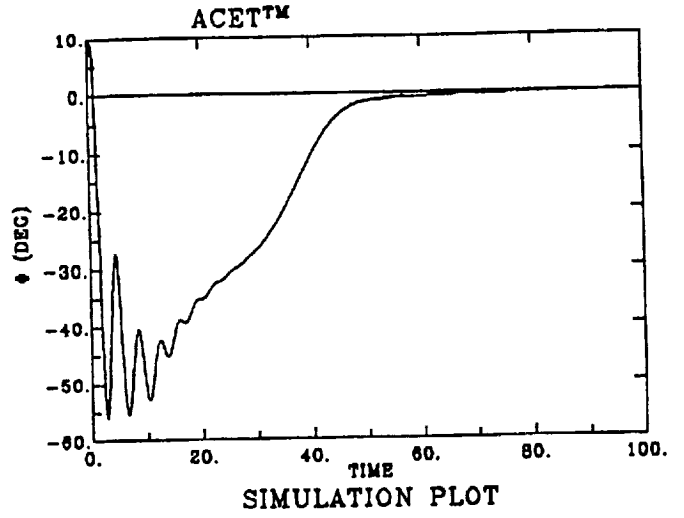


(e) Negative altitude

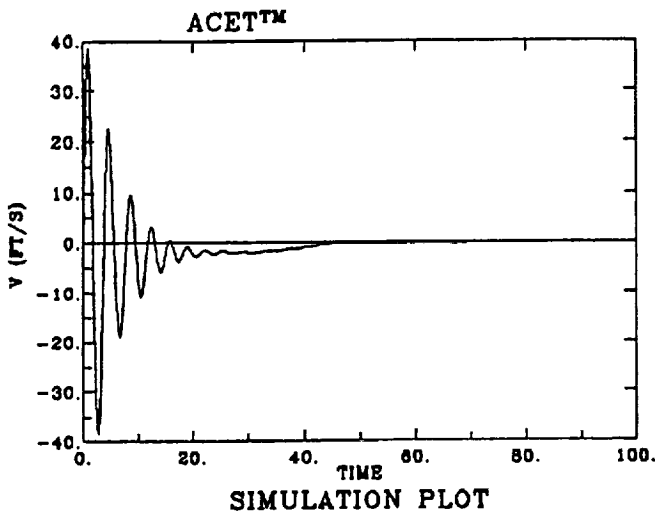
Figure 12. Longitudinal/vertical variables with longitudinal variables perturbed (continued)



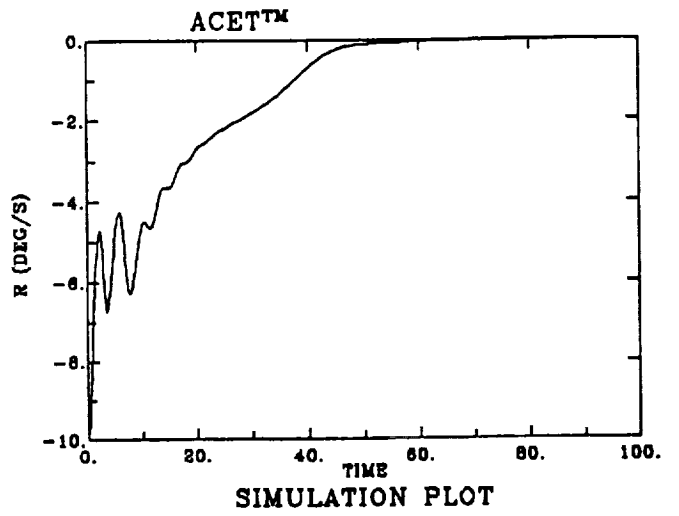
(a) Roll rate



(b) Roll angle

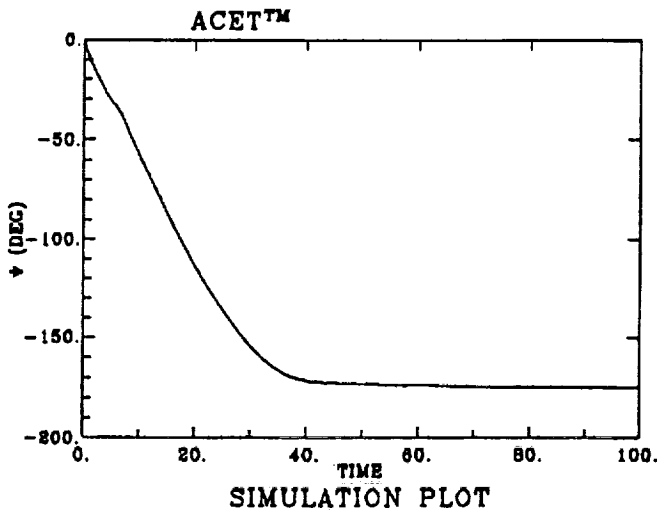


(c) Lateral speed

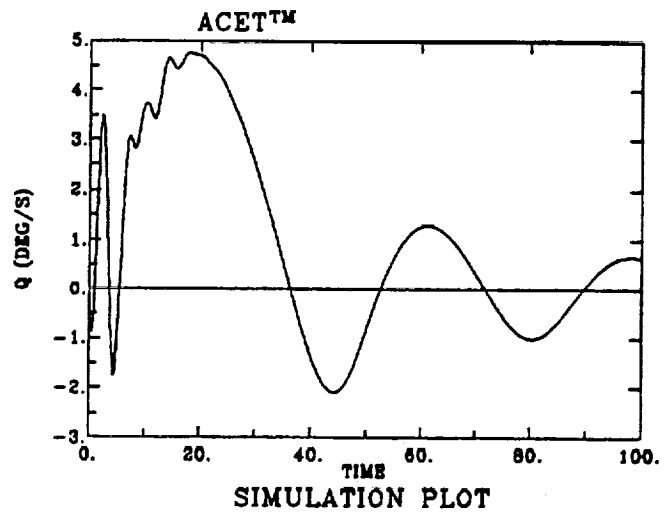


(d) Yaw rate

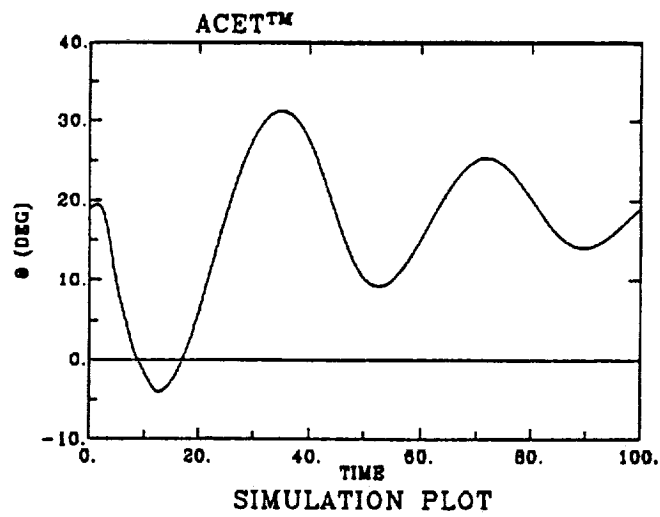
Figure 13. Simulation variables with lateral variables perturbed



(e) Yaw angle



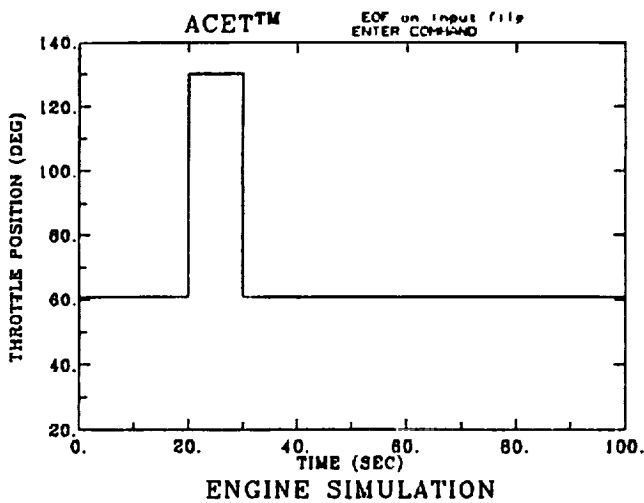
(f) Pitch rate



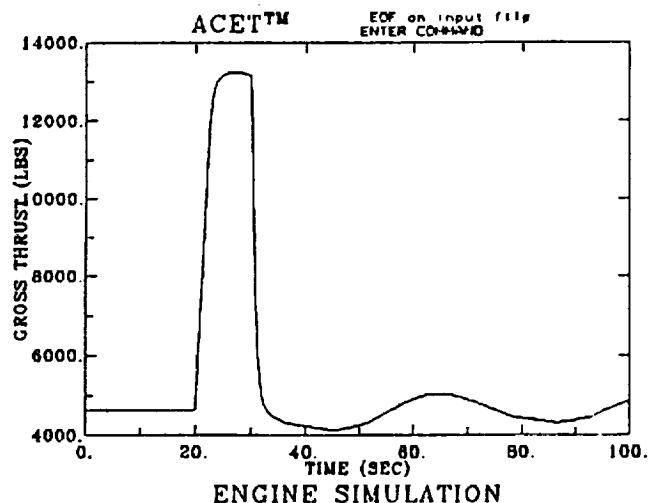
(g) Pitch angle

Figure 13. Simulation variables with lateral variables perturbed (continued)

Figure 14 shows the effects of the nonlinear engine dynamics in the simulation. The aircraft is essentially in trim with level wings as initial condition where the control inputs are set at  $\alpha = 18.8^\circ$  and mach number = 0.24. A large throttle pulse to maximum throttle and back to its trim position is applied as shown in Figure 14(a). The engine gross thrust, the  $x$ -axis thrust and pitching moment are shown in Figures 14(b) - 14(e). Note that the gross thrust oscillates with the phugoid mode, but the  $x$ -axis thrust seems more stable. Also note that the gross thrust is shown for one engine, while the net  $x$ -axis thrust includes the effect of both engines. Rate limit and other nonlinearities are seen in Figure 14(c) which zooms on the leading edge of the pulse.

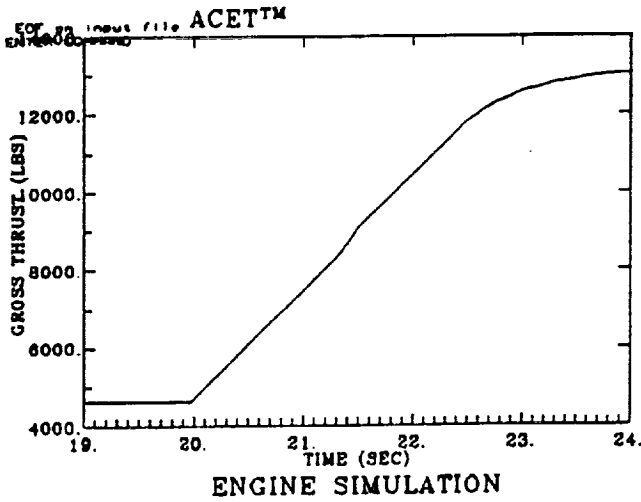


(a) Throttle position input

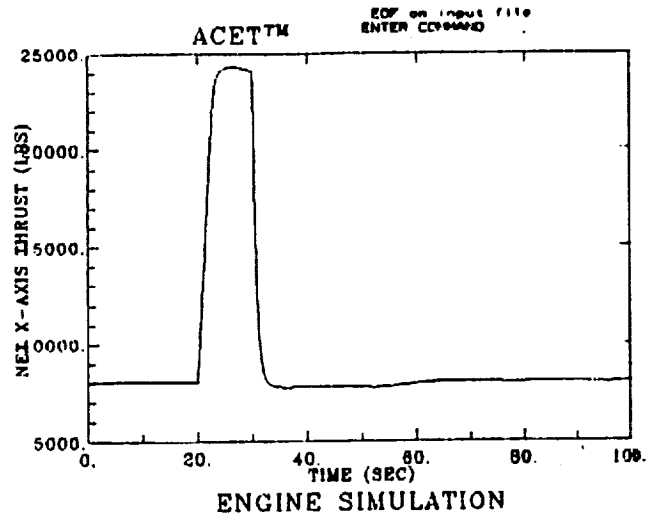


(b) Gross thrust

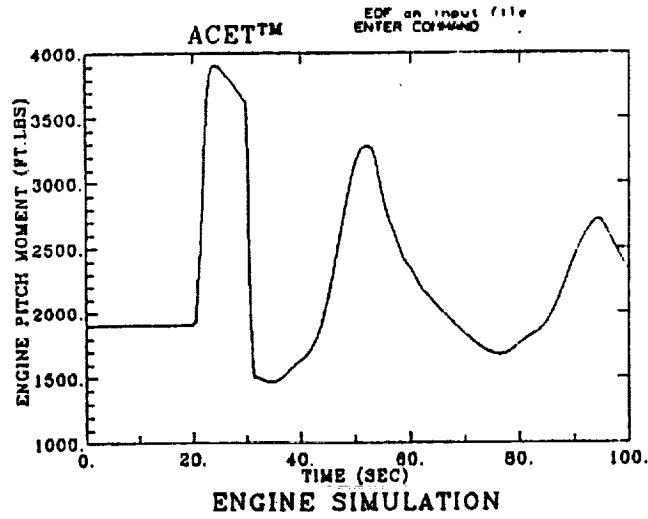
Figure 14. Engine variables with a maximum throttle pulse input



(c) Gross thrust (zoom to see detail)



(d) Net x-axis thrust



(e) Pitching moment produced by engine

Figure 14. Engine variables with a maximum throttle pulse input (continued)

In Figure 15 the simulation plots show that the throttle command excites all the modes of the aircraft dynamics. The phugoid mode is clear in Figure 15, the short period mode rides over the phugoid in Figures 15(d) and 15(e). The gyroscopic effects seem to produce a significant response in the lateral variables as seen in Figures 15(f) – 15(i). The combined response of engine and airframe seem reasonable.

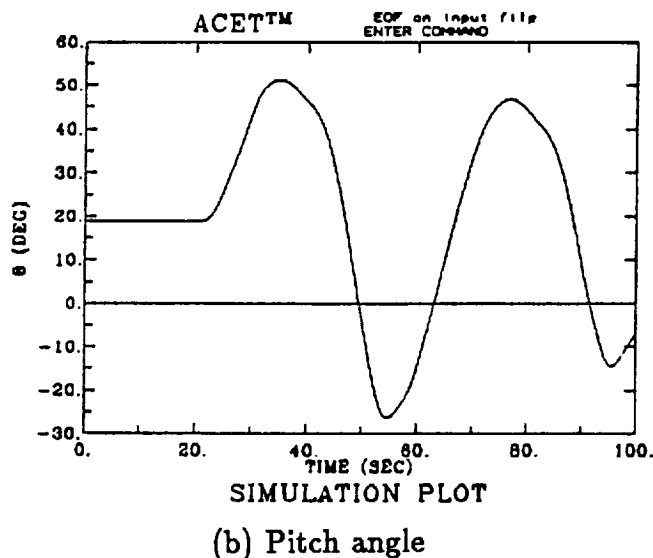
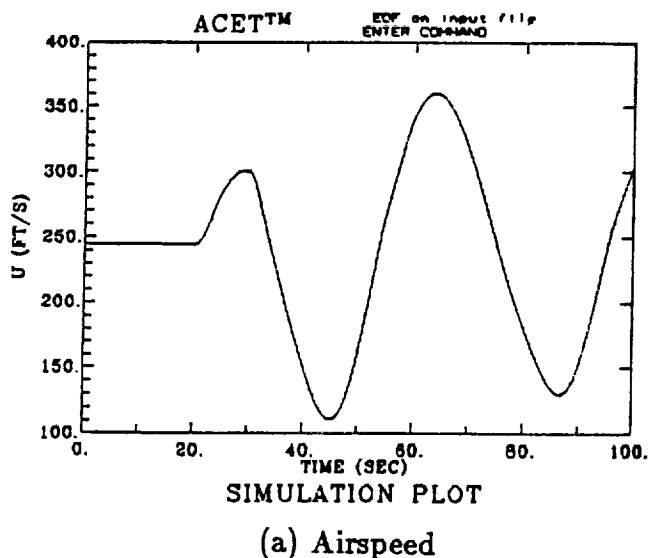
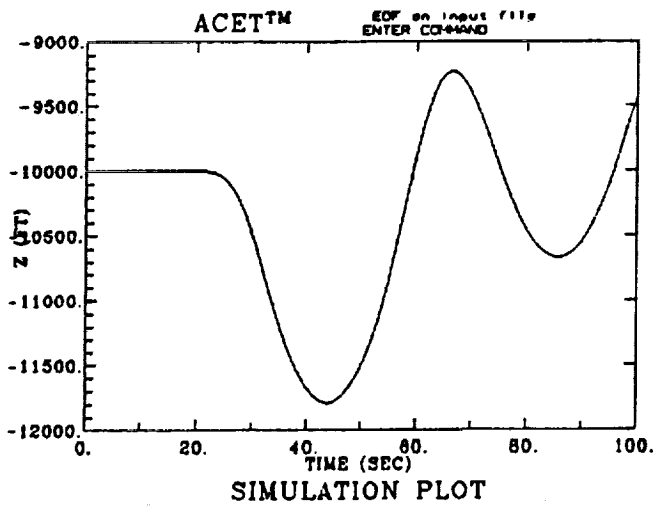
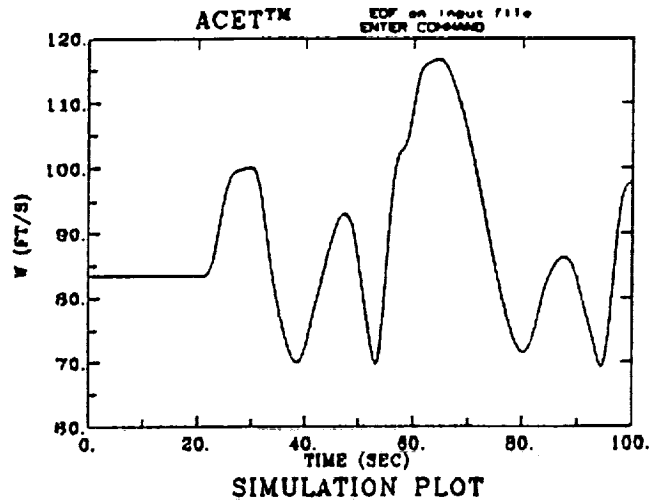


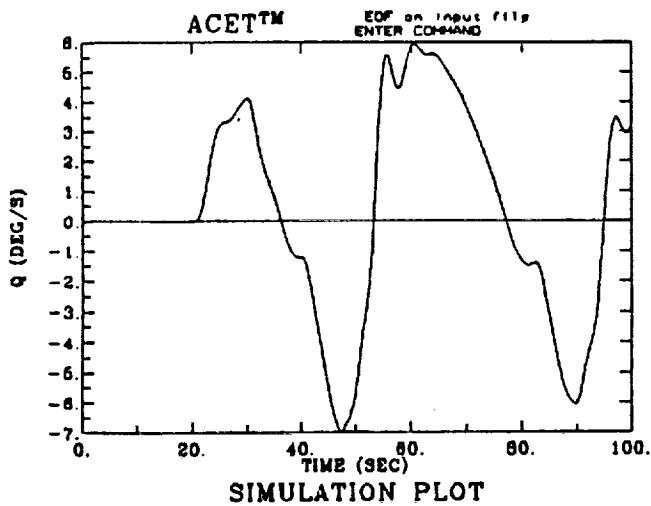
Figure 15. Simulation variables for the same maximum engine throttle pulse input as in Figure 14



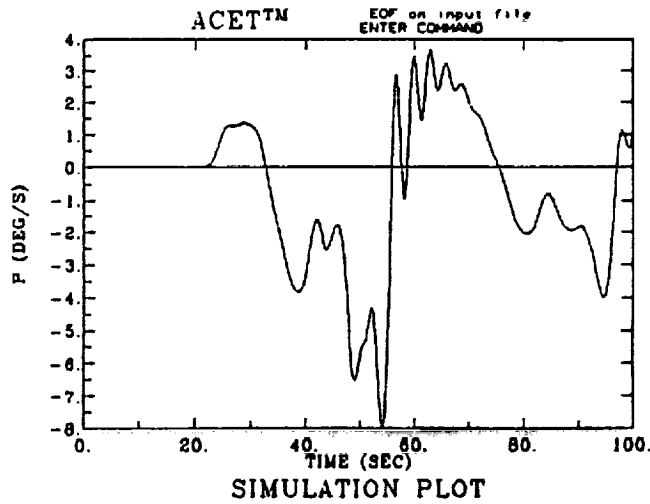
(c) Negative altitude



(d)  $z_b$ -axis speed



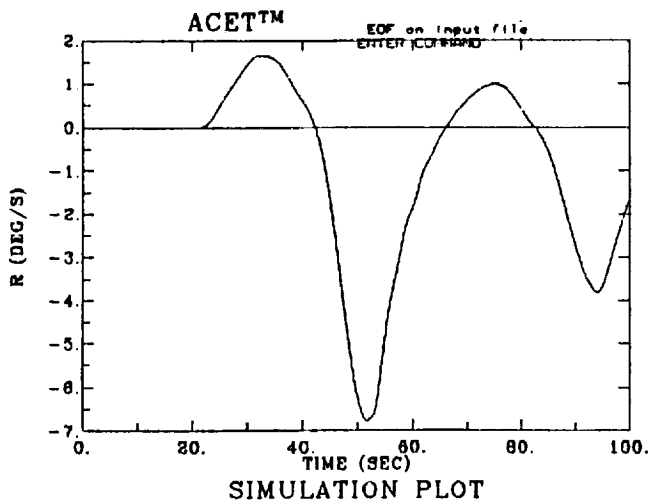
(e) Pitch rate



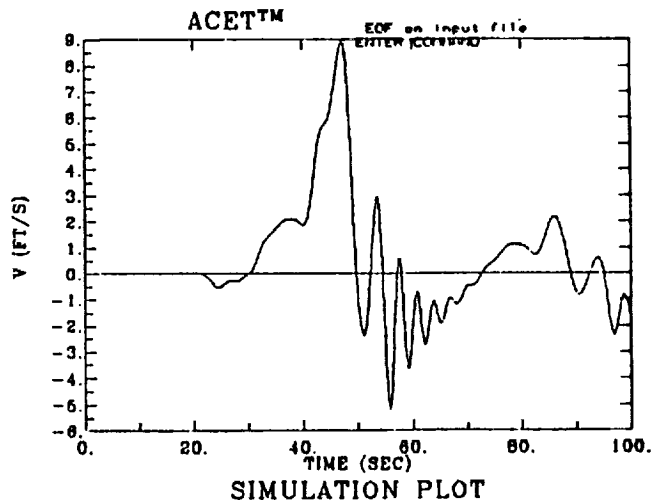
(f) Roll rate

Figure 15. Simulation variables for the same maximum engine throttle pulse input as in Figure 14 (continued)

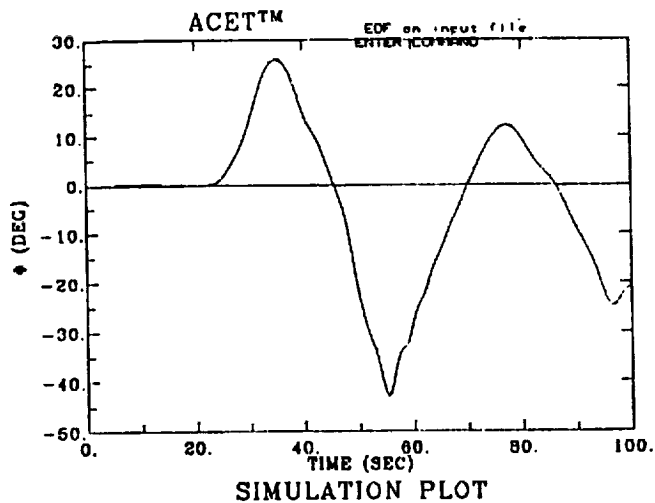




(g) Yaw rate



(h) Lateral speed



(i) Roll angle

Figure 15. Simulation variables for the same maximum engine throttle pulse input as in Figure 14 (continued)

## VI. A VARIABLE-GAIN SOFFT FLIGHT CONTROL SYSTEM FOR THE F/A-18

The SOFFT control design methodology developed in the preceding sections can be applied to any nonlinear system which can be linearized and discretized as described in section II. This class of linearizable systems is quite large and includes very diverse applications from flight controls to robotics, from crystal growth to power transmission networks.

Here we will illustrate the use of the SOFFT design methodology by applying it to a flight control system (FCS) design for the F/A-18 aircraft. The objective is to enable the aircraft to provide high performance with high flying/handling qualities throughout its flight envelope. Alternately, we want to extend the flight regime by improving the aircraft's flying qualities until the physical limitations of the aircraft are reached, such as control authority, rate limits, etc.

### 1. Longitudinal FCS Design

To demonstrate the methodology, a variable-gain SOFFT control law was developed to design an angle-of-attack ( $\alpha$ ) command system for the F/A-18 aircraft. A single-model  $\alpha$ -command system was also designed in the earlier stages of methodology development. This will be used to compare the effect of using variable gain.

The aircraft longitudinal/vertical dynamics was modeled by a 4<sup>th</sup>-order linearized state-space model of the form

$$\dot{x} = A(p)x + B(p)\delta_s + w(p) + d(p) \quad (156)$$

$$x^T = (u' \ \alpha \ q \ \theta) \quad (157)$$

where  $u'$  is the forward speed along the  $x$  body-axis in units of 10 ft/sec,  $\alpha$  is the angle-of-attack in degrees,  $q$  is the pitch rate in deg/sec and  $\theta$  is the pitch angle in degrees. The control is the stabilator ( $\delta_s$ ) or horizontal tail position in degrees.

### Feedback

Both the feedback and feedforward control laws used variable-gain. For this purpose, 3 linearized models corresponding to 3 flight conditions in level flight, with level wings at three different angles-of-attack and airspeed were used. The operating point parameter vector  $p$  was chosen to be the angle-of-attack ( $\alpha$ ). The 3 flight conditions were selected at  $5^\circ$ ,  $20^\circ$  and  $40^\circ$ . Thus,

$$p = \alpha \quad , \quad p^1 = 5 \quad , \quad p^2 = 20 \quad , \quad p^3 = 40 \quad . \quad (158)$$

For the feedback design model, the plant model was augmented by an actuator system for the stabilator. The stabilator actuator dynamics were assumed to be the same for the various flight conditions.

$$\dot{\delta}_s = -30 \delta_s + 30 u_x \quad (159)$$

Using a sampling period ( $\Delta t$ ) of .04 sec (i.e., a sampling frequency of 25 Hz), the augmented system was discretized.

The output or feedback vector  $y_x$  was selected as

$$y_x = \begin{pmatrix} q \\ \alpha \end{pmatrix} + \nu_x + b_x \quad (160)$$

Thus, a pitch rate gyro and an  $\alpha$ -vane were used as sensors for feedback. The main reason for using these sensors is that they are body-mounted, basic measurements. Whereas a pitch gyro may not be as reliable in many maneuvers. Of course, since  $p$  is needed for the adaptive variable gains, a measurement of  $\alpha$  is desirable. The only drawback of this

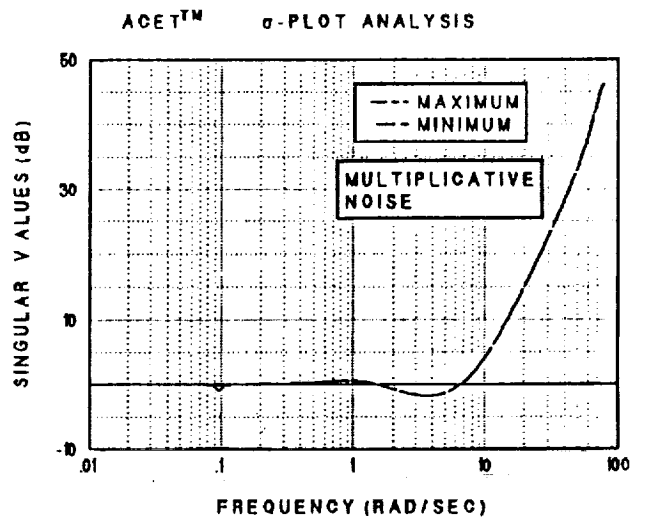
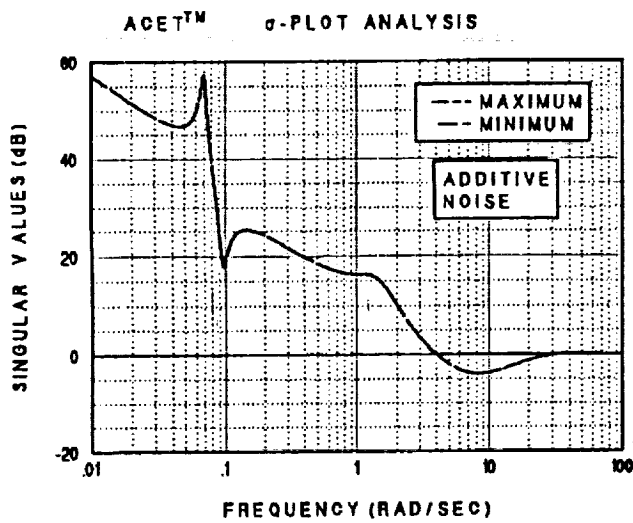
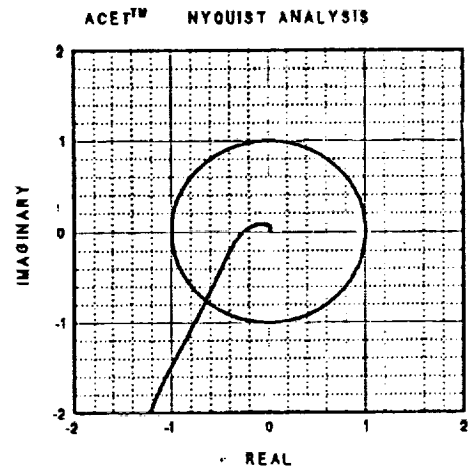
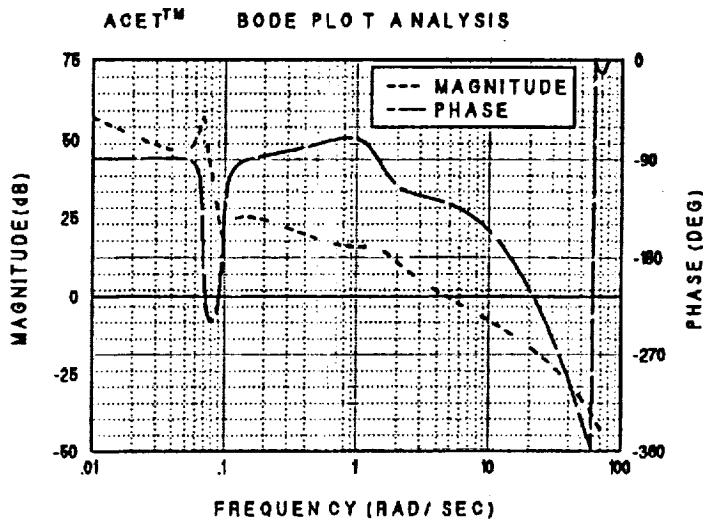


Figure 16. Frequency-domain loop analysis of  $\alpha$ -command variable-gain feedback control law; model 1; perspective: input.

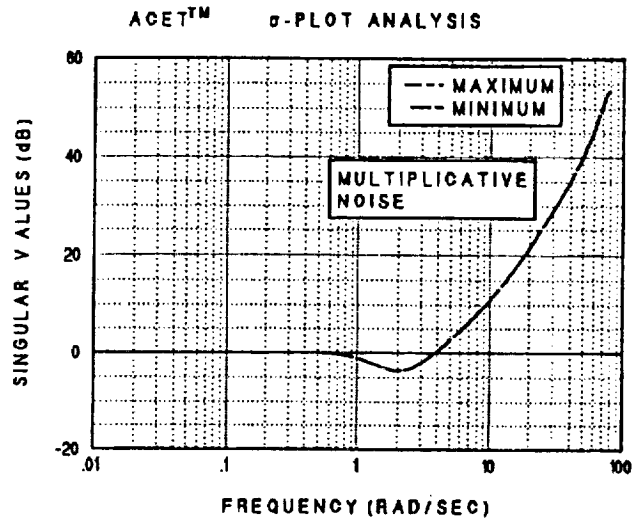
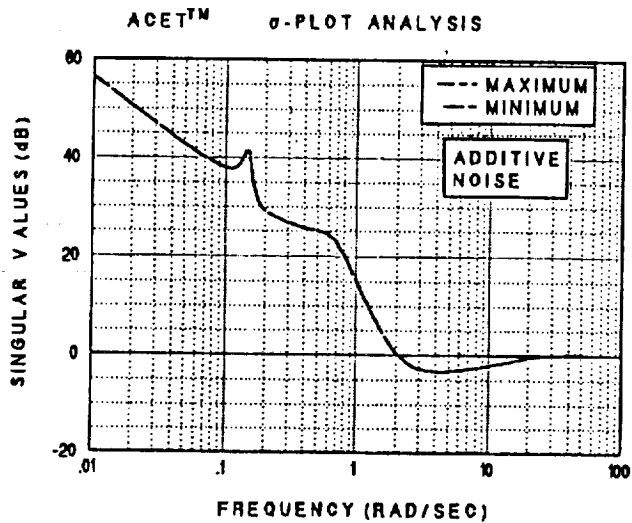
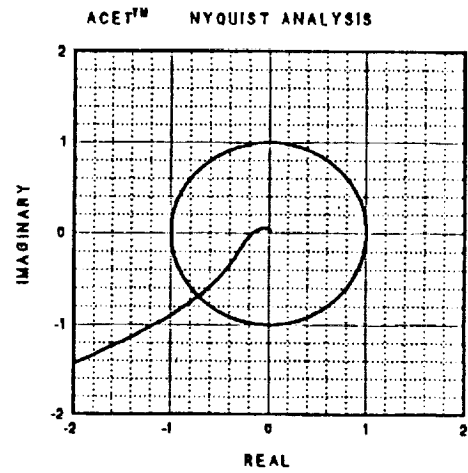
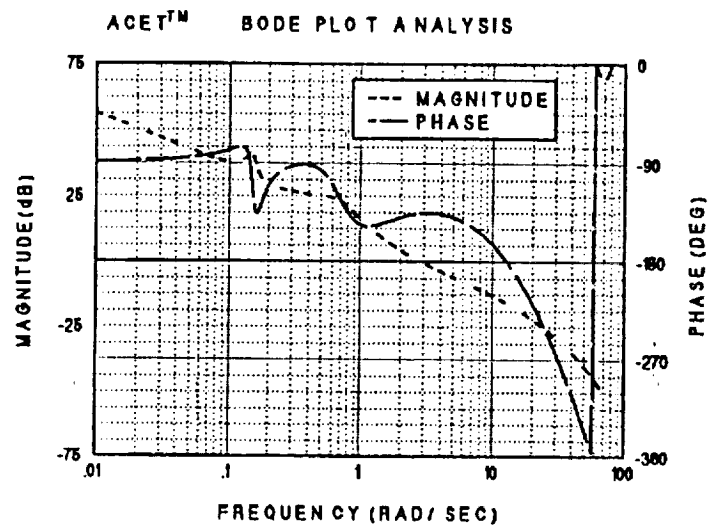


Figure 17. Frequency-domain loop analysis of  $\alpha$ -command variable-gain feedback control law; model 2; perspective: input.

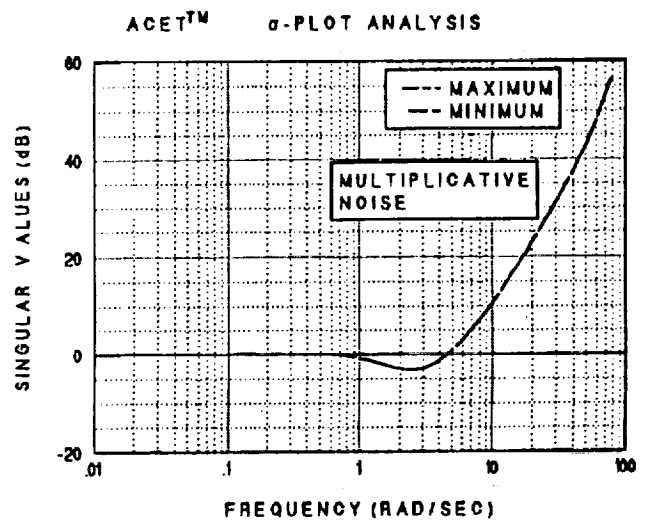
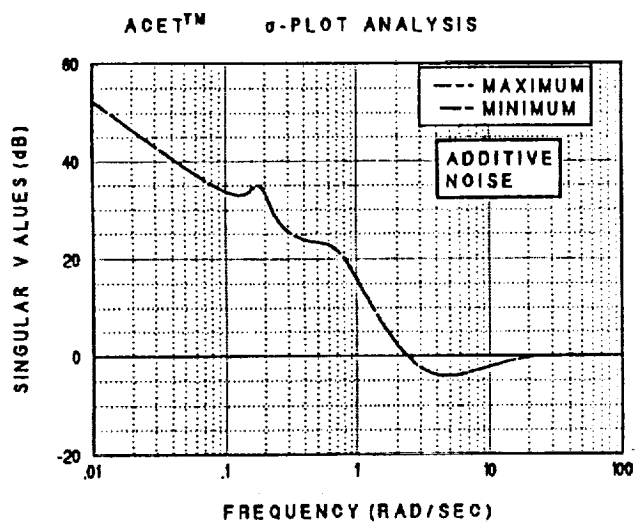
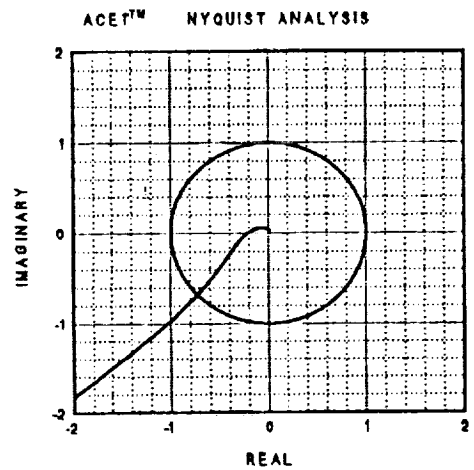
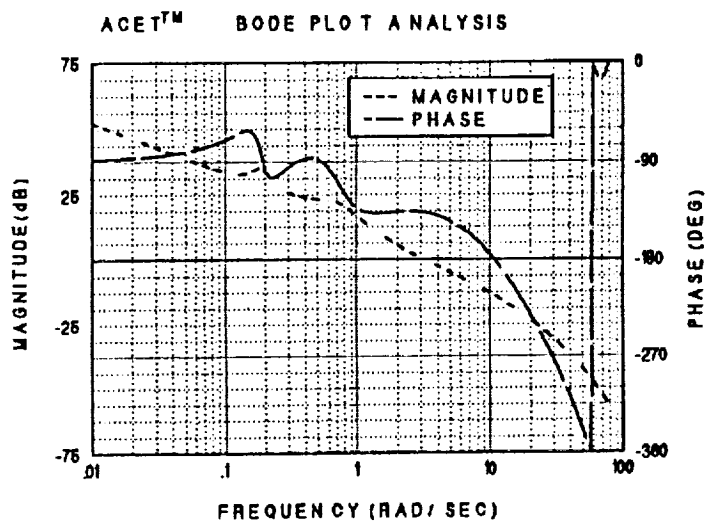


Figure 18. Frequency-domain loop analysis of  $\alpha$ -command variable-gain feedback control law; model 3; perspective: input.

sensor configuration is that the phugoid mode cannot be adequately damped. However, since pilots generally produce phugoid damping often without conscious effort, this is not a significant setback.

A Proportional-Integral-Filter (PIF) structure was used for the feedback control law. This structure produces a type-1 closed-loop control system as well as allowing control rate weighting to achieve the necessary feedback objective of noise suppression. Of course, other feedback structures can also be used to achieve the desired feedback objectives. For the current problem, the PIF structure adds 2 more states (the control  $\tilde{u}_x$  and the  $\alpha$ -integrator  $\tilde{I}$ ) to the longitudinal dynamics and actuator. Thus, the feedback design model has a total of 7 states. A digital Variable-Gain Output Feedback [17], [18] control law was designed using the ACET CACSD tool.

### Feedforward

In the SOFFT approach, the flying qualities are largely achieved by the feedforward control law. This is due to the fact that the SOFFT feedforward law produces the initial system response which is highly weighted in pilot ratings. On the other hand, in the error feedback structure, the feedback produces both the initial and steady-state responses to a given command.

Whereas the stabilator actuator was used in the feedback design model, it was not included in the feedforward design model to reduce the order of the feedforward control law. Thus, the 4<sup>th</sup>-order discretized longitudinal dynamics model was used. It is important to note that a short period approximation of 2<sup>nd</sup>-order can also be used if further order reduction is desired. However, the designer must use  $Z$ -plots to evaluate the consequences of such approximations in terms of command tracking performance.

The command model was selected to produce desirable short period flying qualities. Short period handling qualities are rated "satisfactory" in a small region of the complex plane in the vicinity of a natural frequency of  $\omega_n = 3$  rad/sec and a damping ratio of  $\zeta = 0.7$

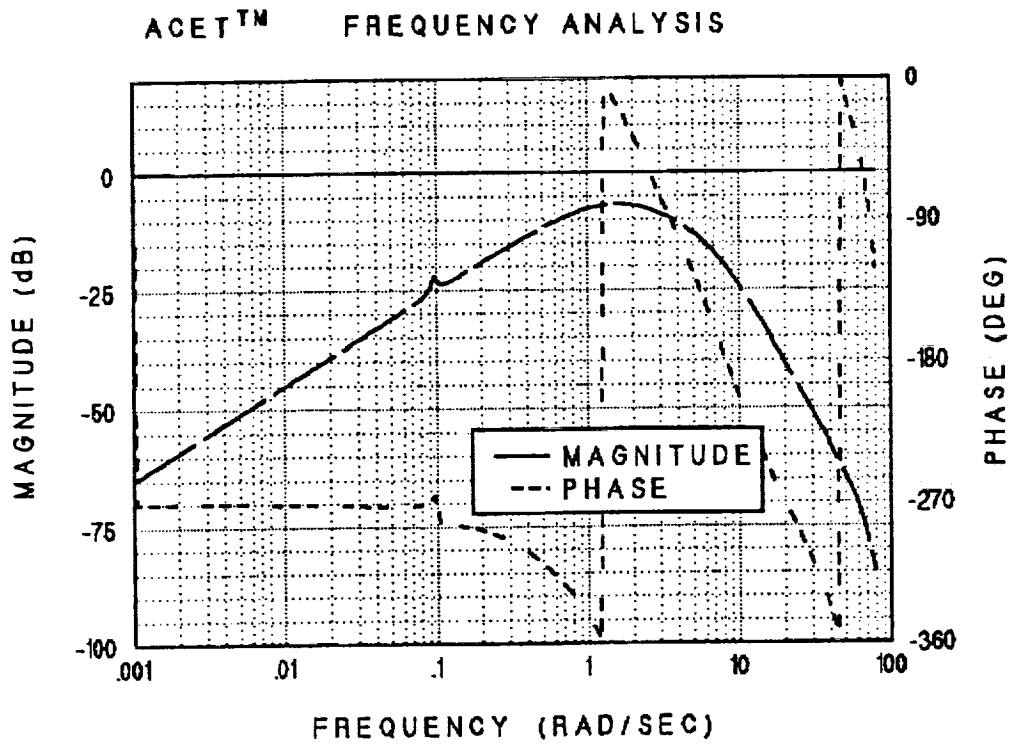


Figure 19a. Effect of pitch rate gyro errors on angle-of-attack ( $\alpha$ ) for Model 1.

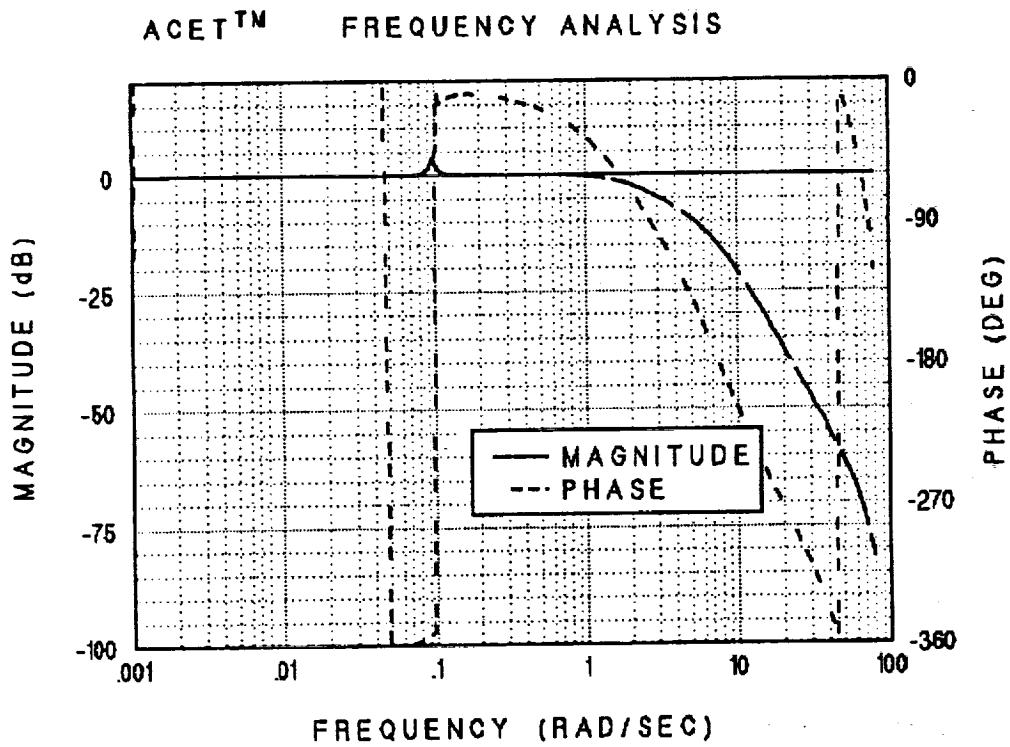


Figure 19b. Effect of  $\alpha$ -vane errors on angle-of-attack ( $\alpha$ ) for Model 1.



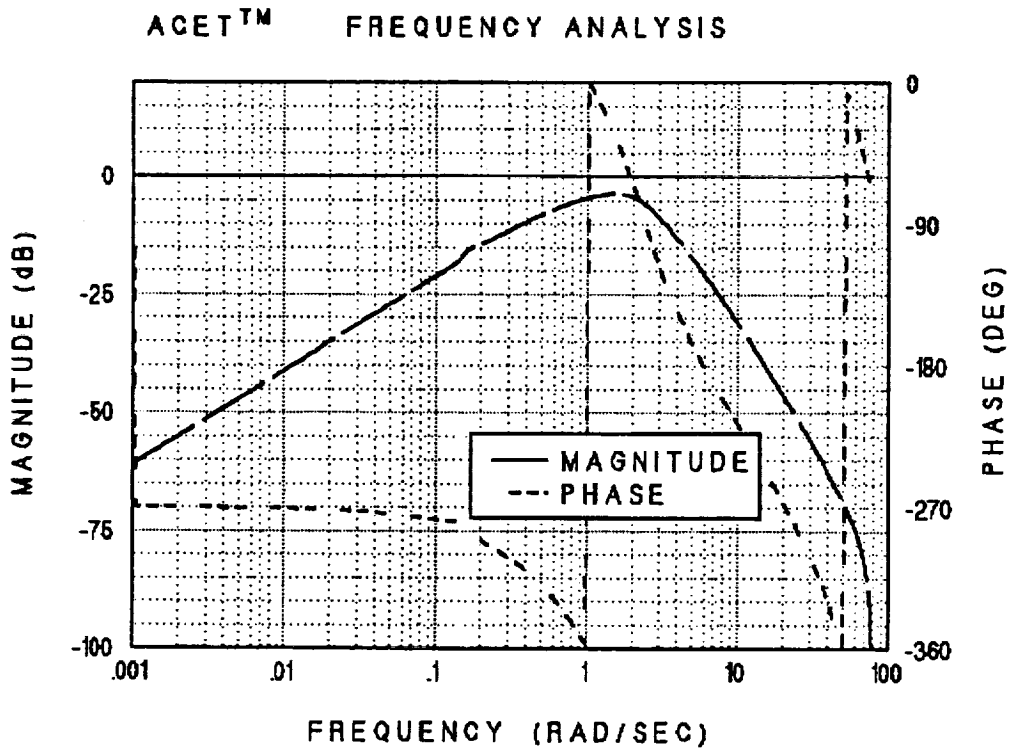


Figure 20a. Effect of pitch rate gyro errors on angle-of-attack ( $\alpha$ ) for Model 2.

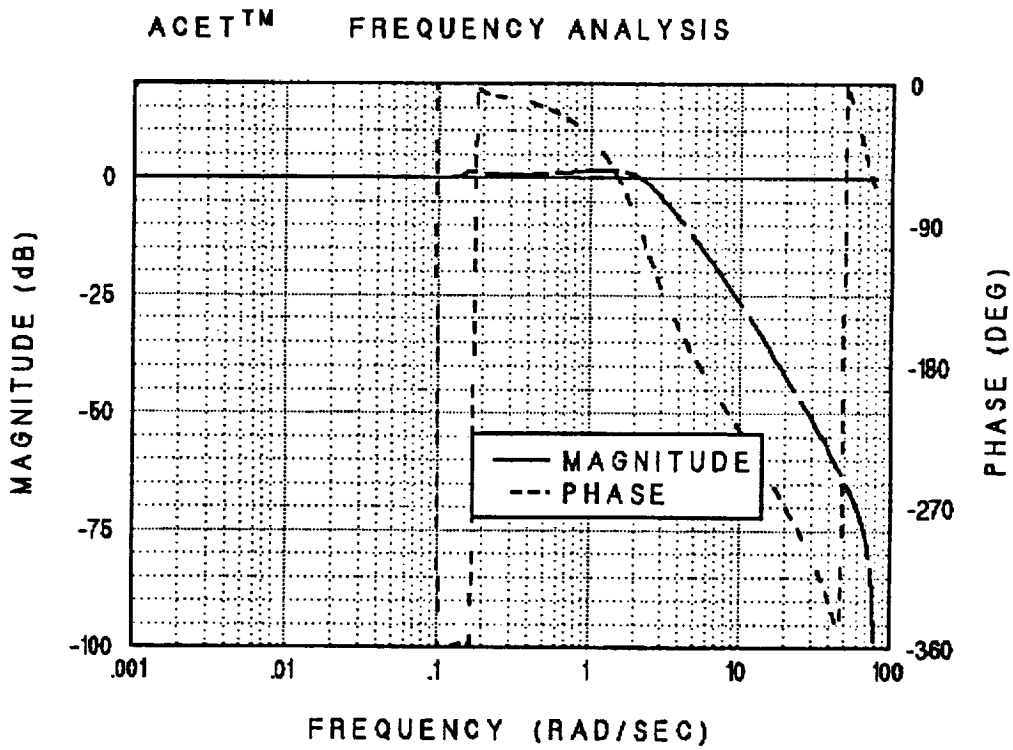


Figure 20b. Effect of  $\alpha$ -vane errors on angle-of-attack ( $\alpha$ ) for Model 2.

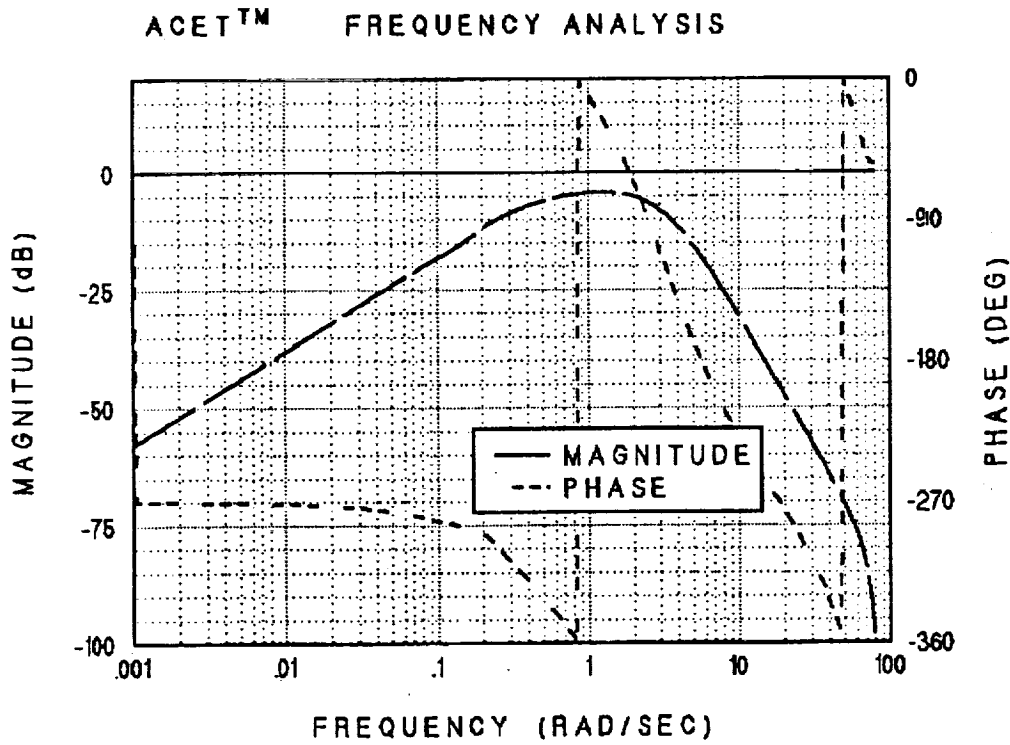


Figure 21a. Effect of pitch rate gyro errors on angle-of-attack ( $\alpha$ ) for Model 3.

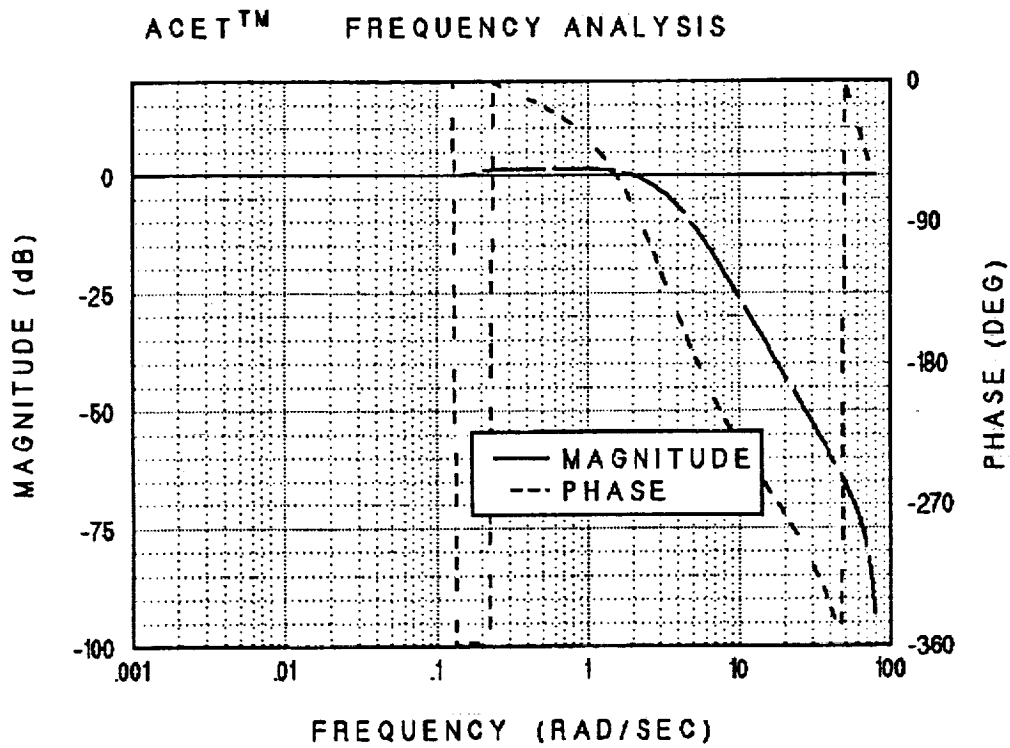


Figure 21b. Effect of  $\alpha$ -vane errors on angle-of-attack ( $\alpha$ ) for Model 3.

(e.g., see [21] pp. 511-518). Thus, the command model was obtained by discretizing the following continuous model at a sampling period of 40 msec.

$$\frac{\alpha^*(s)}{u_z(s)} = \frac{y_z(s)}{u_z(s)} = \frac{w_n^2}{s^2 + 2\zeta w_n s + w_n^2} , \quad w_n = 3 , \quad \zeta = .7 \quad (161)$$

where  $u_z$  is the pilot input command and  $y_z$  is the desired response of the angle-of-attack.

Thus, a 2<sup>nd</sup>-order command model was used. While this methodology allows the command model to vary with the flight condition parameter,  $p$ , we kept it constant.

Using the methods described in section IV, we designed a perfect tracking SOFFT feedforward control law. Using the incremental implementation described, we simulated the variable-gain SOFFT control law.

## 2. Lateral FCS Design

A single-model SOFFT control law was designed to compensate the lateral dynamics. With the variable-gain design methodology having been demonstrated by the longitudinal/vertical  $\alpha$ -command system, the main motivation was to close the loop around the lateral dynamics to perform a complete simulation. A roll rate and sideslip command system was designed for this lateral control law.

A 4<sup>th</sup>-order lateral model was used to design both the feedforward and feedback control laws.

$$\dot{x} = Ax + Bu + w + d \quad (162)$$

$$x^T = (\beta \ p \ r \ \phi) , \quad u^T = (\delta A \ \delta R) \quad (163)$$

where  $\beta$  is the sideslip angle in degrees,  $p$  is the roll rate in deg/sec,  $r$  is the yaw rate in deg/sec,  $\phi$  is the roll angle in degrees,  $\delta A$  is the aileron position in degrees and  $\delta R$  is the rudder position in degrees. Note that the aileron variable  $\delta A$  corresponds to the

ACET™ FREQUENCY ANALYSIS

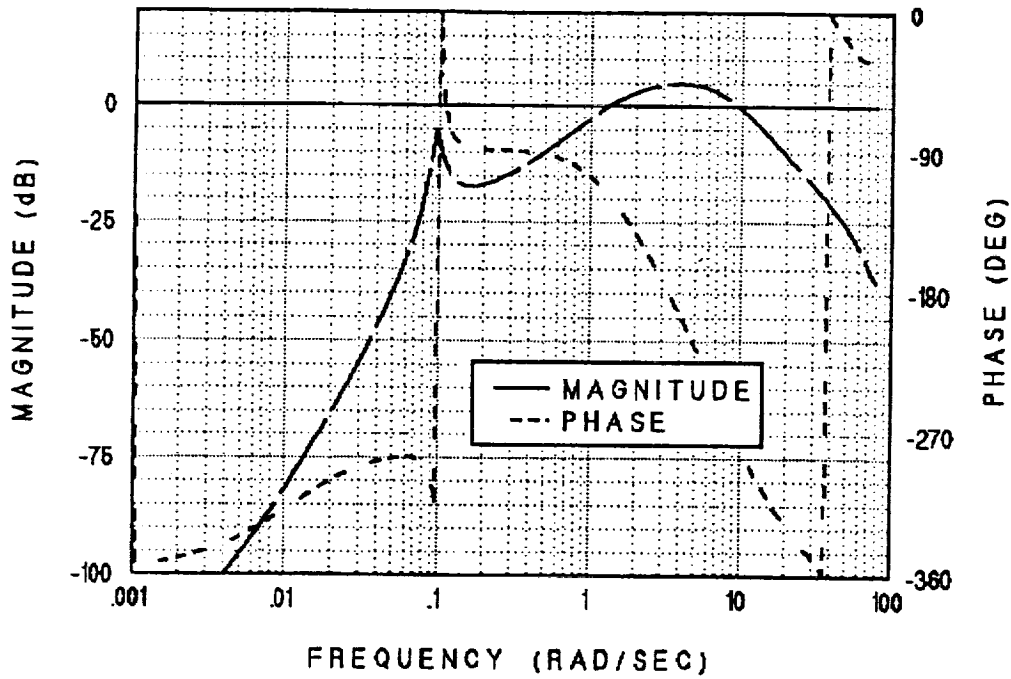


Figure 22a. Effect of plant disturbance (at input) on pitch rate ( $q$ ) for Model 1.

ACET™ FREQUENCY ANALYSIS

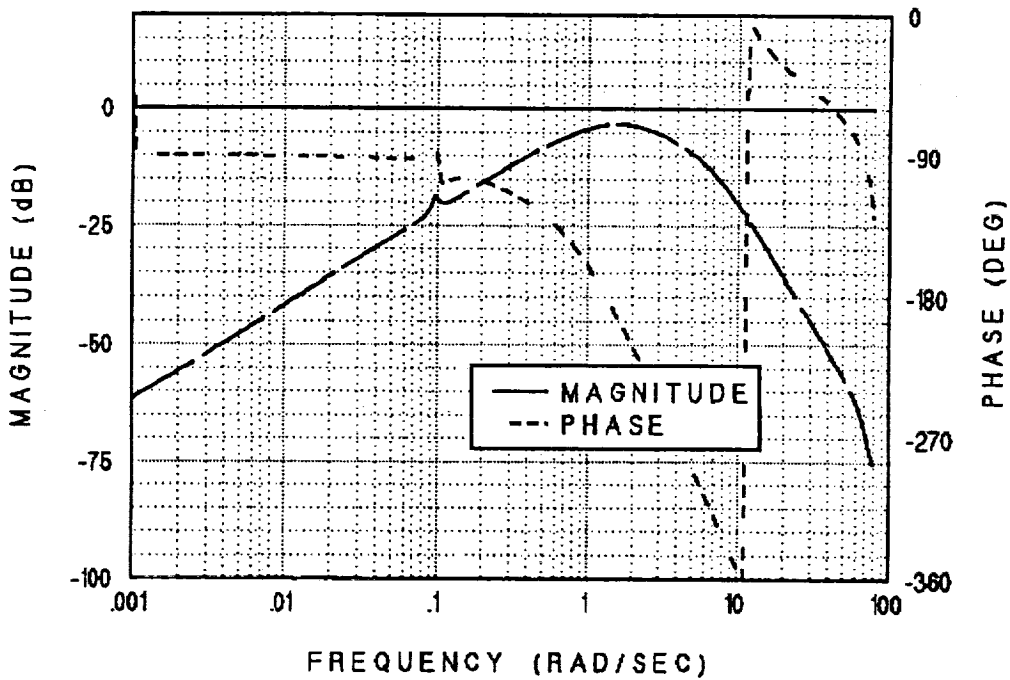


Figure 22b. Effect of plant disturbance (at input) on angle-of-attack ( $\alpha$ ) for Model 1.

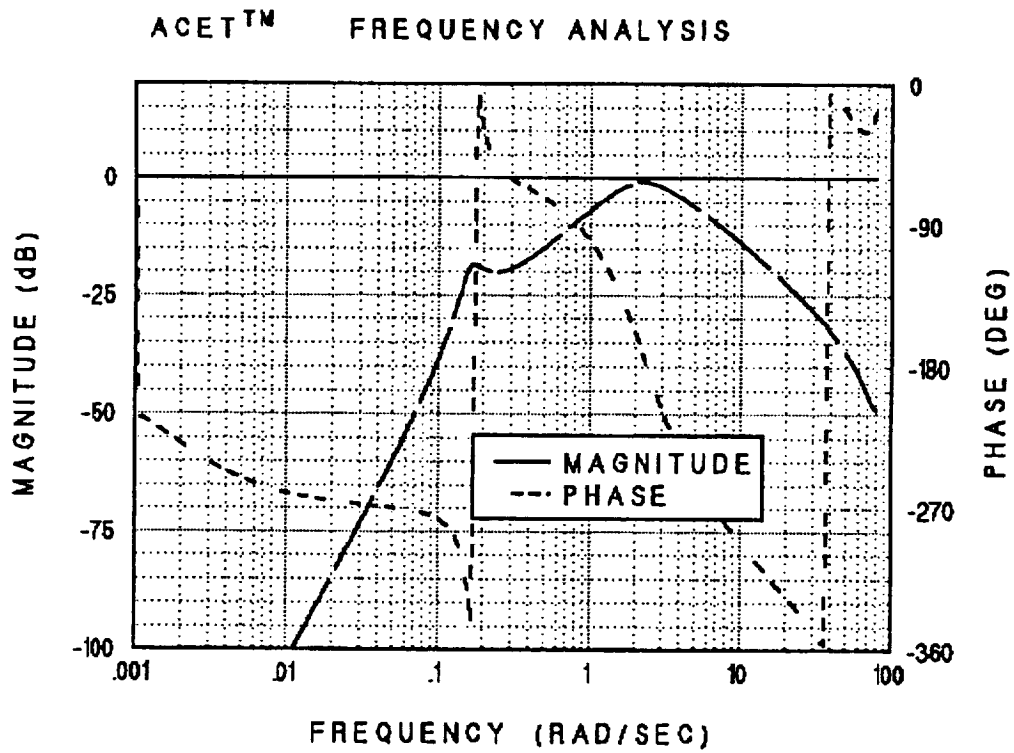


Figure 23a. Effect of plant disturbance (at input) on pitch rate ( $q$ ) for Model 2.

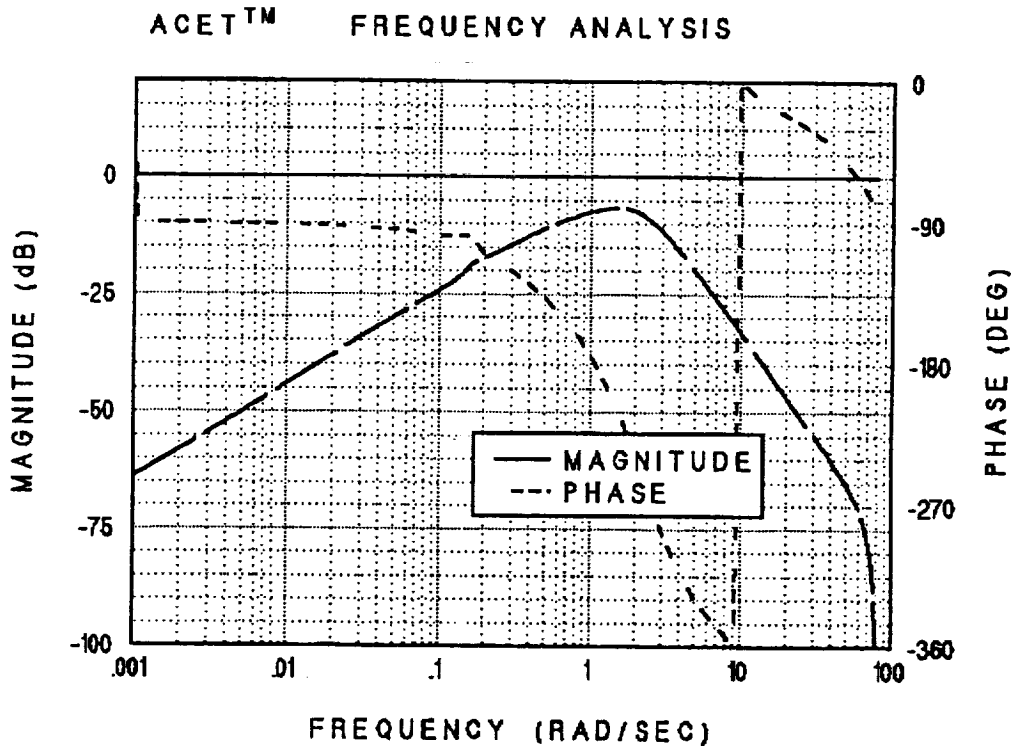


Figure 23b. Effect of plant disturbance (at input) on angle-of-attack ( $\alpha$ ) for Model 2.

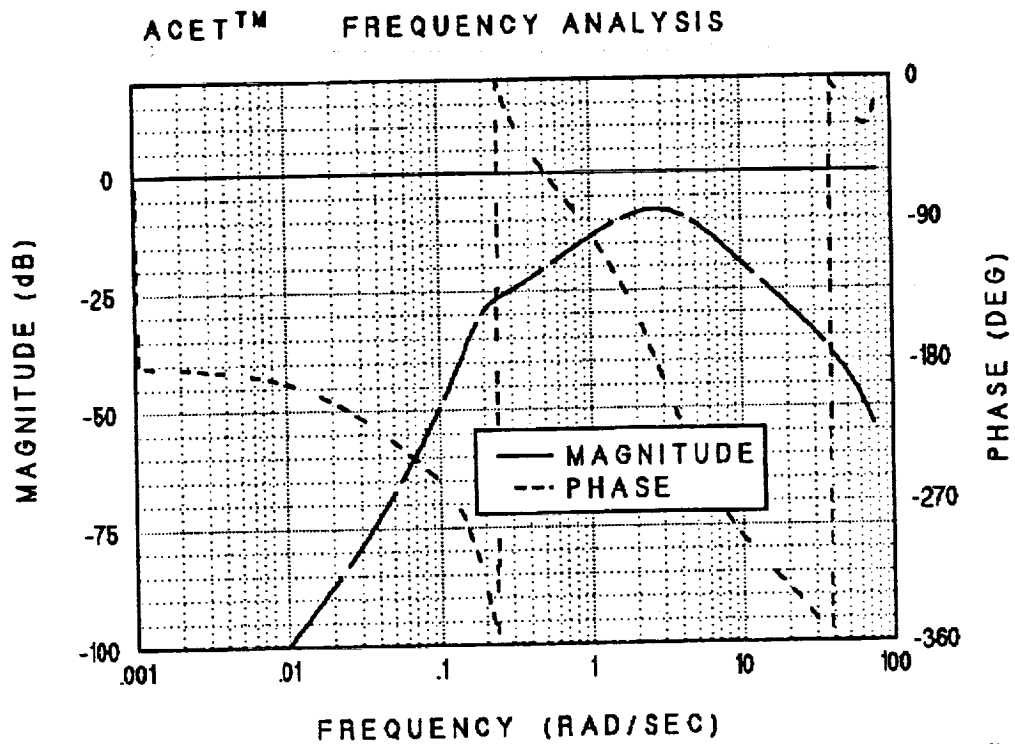


Figure 24a. Effect of plant disturbance (at input) on pitch rate ( $q$ ) for Model 3.

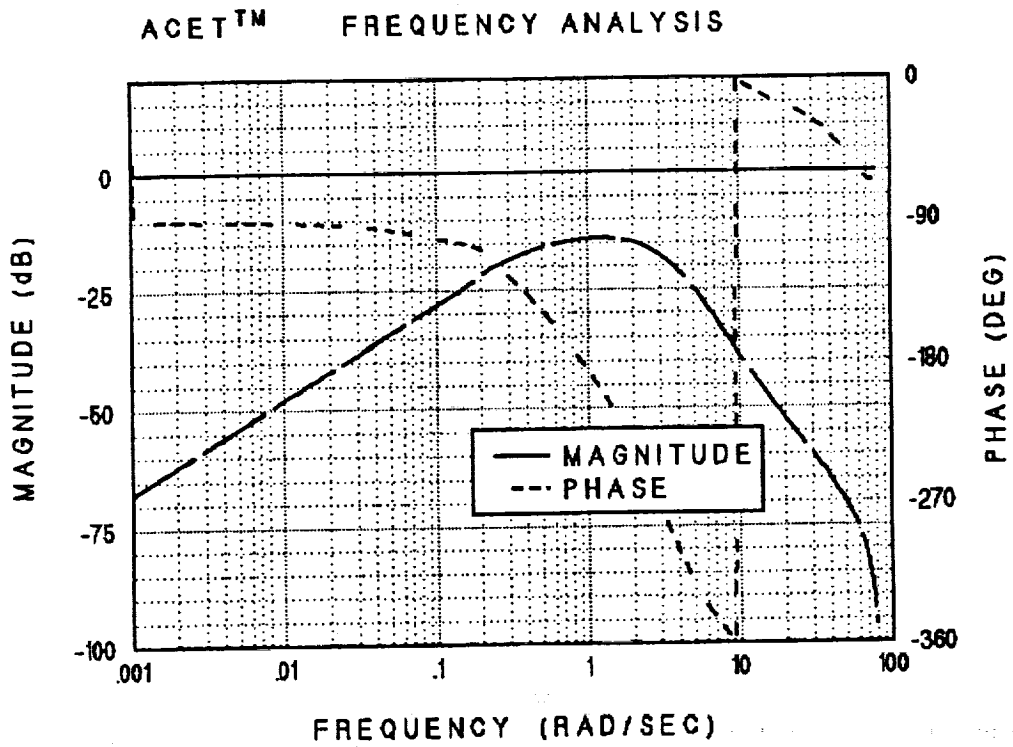


Figure 24b. Effect of plant disturbance (at input) on angle-of-attack ( $\alpha$ ) for Model 3.

anti-symmetric operation of the right and left ailerons surfaces  $\delta A_R$  and  $\delta A_L$ , respectively, whereas  $\delta R$  corresponds to the symmetric operation of the right and left rudder surfaces,  $\delta R_R$  and  $\delta R_L$ , respectively. Thus,

$$\delta A_L = \delta A \quad , \quad \delta A_R = -\delta A \quad (164)$$

$$\delta R_L = \delta R \quad , \quad \delta R_R = \delta R \quad (165)$$

The leading edge and trailing edge flap positions were set by an automatic program as a function of Mach number and angle-of-attack.

### Feedback

While the simulation incorporates actuator dynamics models for the aileron and rudder surfaces, these actuators are very fast. For the design of the lateral control law, the actuator dynamics were neglected. For the feedback design model, the flight condition corresponding to 20° angle-of-attack was used.

Using a 0.04 sec sampling period, the plant was discretized with the standard sampled-data discretization method.

The lateral output or feedback vector  $y_x$  was

$$y_x = \begin{pmatrix} \beta \\ p \\ r \end{pmatrix} + \nu_x + b_x \quad (166)$$

Thus, a sideslip or  $\beta$ -vane and lateral rate gyros were used as the sensor configuration.

A Proportional-Integral-Filter (PIF) structure was used for the feedback control law. For the current problem, the PIF structure adds 4 more states to the lateral dynamics model. The additional 4 states correspond to the aileron and rudder surface position commands, one roll rate ( $p$ ) integrator and one sideslip ( $\beta$ ) integrator. Thus, the lateral

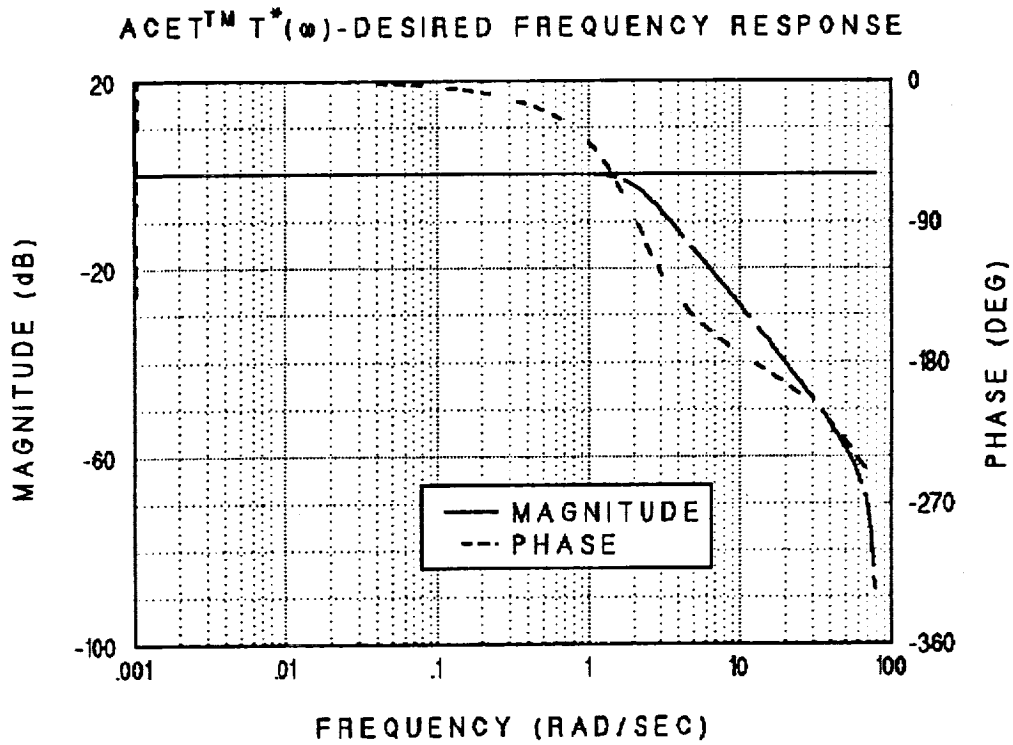


Figure 25a. Desired frequency response of angle-of-attack ( $\alpha$ ) to pilot inputs.

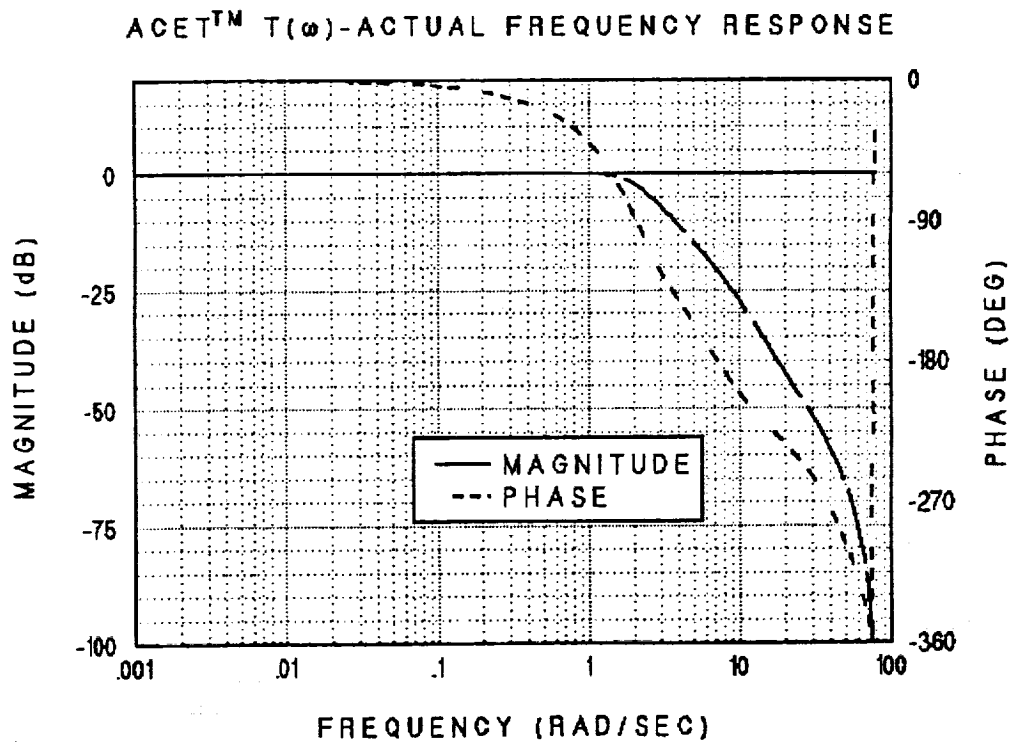


Figure 25b. Actual frequency response of angle-of-attack ( $\alpha$ ) to pilot inputs for Model 1.



ACET™ T( $\omega$ )-ACTUAL FREQUENCY RESPONSE

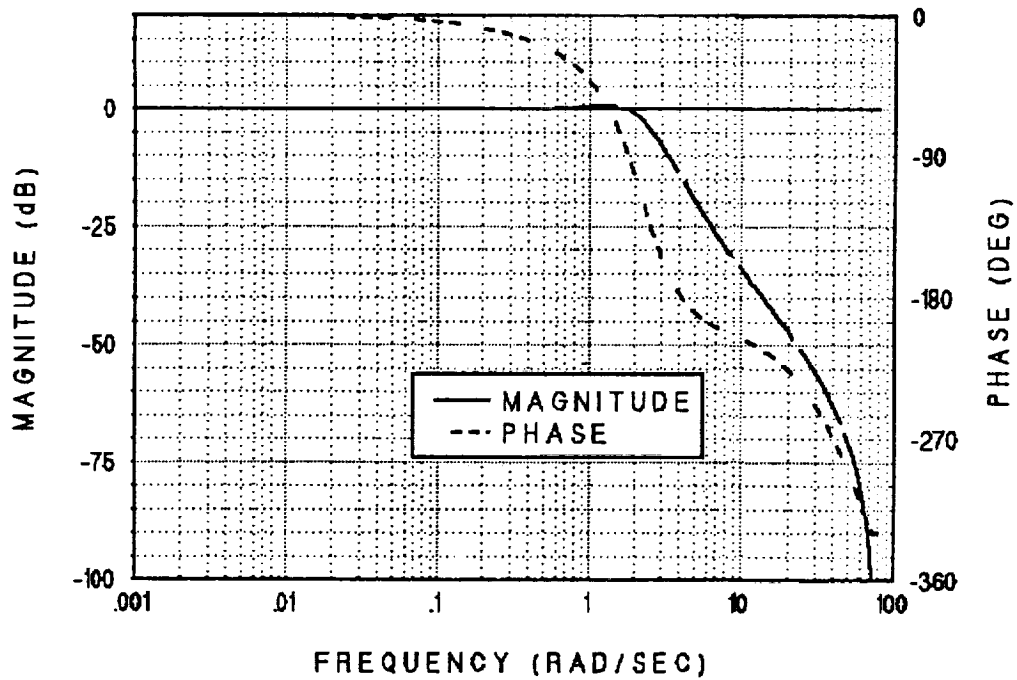


Figure 25c. Actual frequency response of angle-of-attack ( $\alpha$ ) to pilot inputs for Model 2.

ACET™ T( $\omega$ )-ACTUAL FREQUENCY RESPONSE

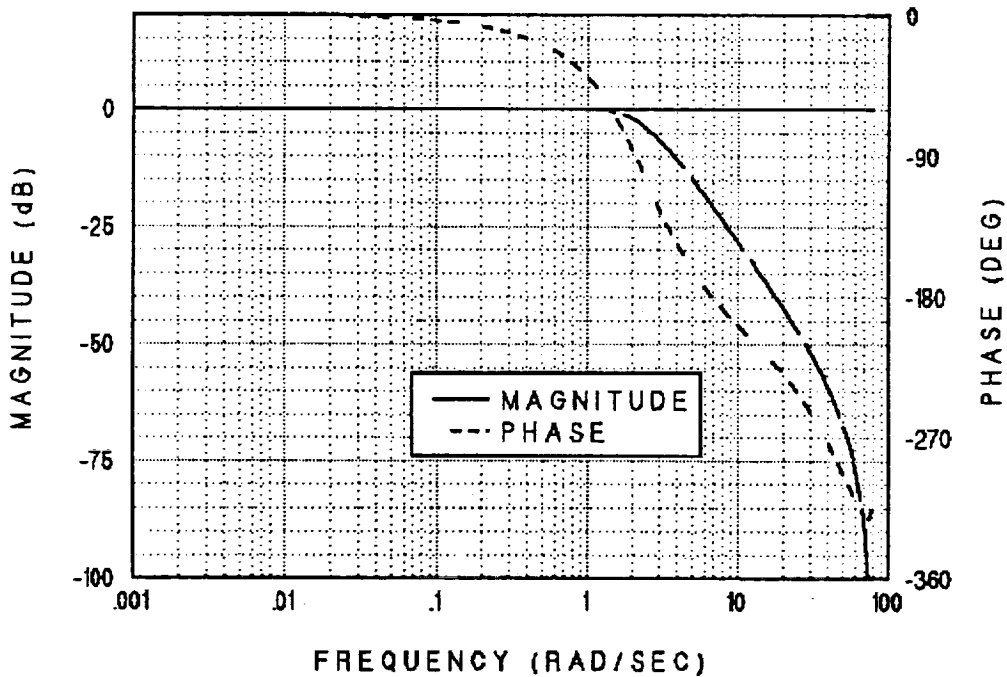


Figure 25d. Actual frequency response of angle-of-attack ( $\alpha$ ) to pilot inputs for Model 3.

feedback design model has a total of 8 states. The digital Stochastic Output Feedback [1], [2] technique was used to design the lateral feedback law.

### Feedforward

The 4<sup>th</sup>-order dynamics model used in the feedback design model was also used to design the feedforward control law. Thus, the feedforward design also neglected inclusion of actuator dynamics for the simplicity of the control law.

The command model for the lateral feedforward used a 2<sup>nd</sup>-order system for the roll rate command and a 1<sup>st</sup>-order model for the sideslip command. For the roll rate, the command model is the discretized version of

$$\frac{p^*(s)}{u_{z1}(s)} = \frac{y_{z1}(s)}{u_{z1}(s)} = \frac{w_n^2}{s^2 + 2\zeta w_n s + w_n^2}, \quad \zeta = .7, \quad w_n = 3. \quad (167)$$

For a unit step input, this model reaches the  $e^{-1}$  level in less than 0.9 sec and reaches the commanded level of unity in about 1.5 sec, as it produces a small overshoot. Thus, it may be compared to a time constant between .5 sec and .9 sec. Pilot ratings of the open-loop roll mode are found satisfactory for time constants  $T_R$  under 2 sec with corresponding values of initial roll acceleration (e.g., see [21] pp. 520-523). Thus, the command model seems appropriate to achieve the desired response. For the sideslip command model, a 1<sup>st</sup>-order model with a time constant of 4 sec was used. Thus, the complete lateral command model was of 3<sup>rd</sup>-order, and was obtained by augmenting the roll rate and sideslip models described above.

Using the method described in section IV, a perfect tracking feedforward control law was obtained. The incremental digital implementation of the lateral control law was used in the simulation runs shown later.

**TABLE 1**  
**EIGENVALUE ANALYSIS: MODEL 1**  
**OPEN-LOOP EQUIVALENT s-PLANE EIGENVALUES**

REAL	IMAGINARY	DAMPING RATIO	NATURAL FREQUENCY	
0.000000	0.000000	0.000000	0.000000	} CRC
0.000000	0.000000	0.000000	0.000000	
- 0.002215	-0.068608	0.032264	0.068644	} PHUGOID
- 0.002215	0.068608	0.032264	0.068644	
- 0.547966	-1.344528	0.377412	1.451903	} SHORT PERIOD
- 0.547966	1.344528	0.377412	1.451903	
-30.000000	0.000000	1.000000	30.000000	} STAB. ACTUATOR

**TABLE 2**  
**EIGENVALUE ANALYSIS: MODEL 1**  
**CLOSED-LOOP EQUIVALENT s-PLANE EIGENVALUES**

REAL	IMAGINARY	DAMPING RATIO	NATURAL FREQUENCY	
- 0.004555	-0.096194	0.047297	0.096302	} PHUGOID
- 0.004555	0.096194	0.047297	0.096302	
- 1.547369	-0.449355	0.960326	1.611295	} SHORT PERIOD
- 1.547369	0.449355	0.960326	1.611295	
- 5.583268	-4.599254	0.771844	7.233672	
- 5.583268	4.599254	0.771844	7.233672	
-61.775017	0.000000	1.000000	61.775017	

**TABLE 3**

**EIGENVALUE ANALYSIS: MODEL 2**

**OPEN-LOOP EQUIVALENT s-PLANE EIGENVALUES**

REAL	IMAGINARY	DAMPING RATIO	NATURAL FREQUENCY	
0.000000	0.000000	0.000000	0.000000	} CRC INTEGRATOR
0.000000	0.000000	0.000000	0.000000	
- 0.009877	-0.148653	0.066297	0.148981	} PHUGOID
- 0.009877	0.148653	0.066297	0.148981	
- 0.251082	-0.637923	0.366245	0.685557	} SHORT PERIOD
- 0.251082	0.637923	0.366245	0.685557	
-30.000000	0.000000	1.000000	30.000000	} STAB. ACTUATOR

**TABLE 4**

**EIGENVALUE ANALYSIS: MODEL 2**

**CLOSED-LOOP EQUIVALENT s-PLANE EIGENVALUES**

REAL	IMAGINARY	DAMPING RATIO	NATURAL FREQUENCY	
- 0.025907	-0.160355	0.159491	0.162434	} PHUGOID
- 0.025907	0.160355	0.159491	0.162434	
- 0.820359	0.000000	1.000000	0.820359	} SHORT PERIOD
- 1.342804	-1.750519	0.608642	2.206288	
- 1.342804	1.750519	0.608642	2.206288	
-10.839646	0.000000	1.000000	10.839646	
-41.800201	0.000000	1.000000	41.800201	

TABLE 5

EIGENVALUE ANALYSIS: MODEL 3

OPEN-LOOP EQUIVALENT s-PLANE EIGENVALUES

REAL	IMAGINARY	DAMPING RATIO	NATURAL FREQUENCY	
0.000000	0.000000	0.000000	0.000000	} CRC
0.000000	0.000000	0.000000	0.000000	
- 0.028034	-0.183087	0.151357	0.185221	} PHUGOID
- 0.028034	0.183087	0.151357	0.185221	
- 0.279930	-0.665594	0.387681	0.722064	} SHORT PERIOD
- 0.279930	0.665594	0.387681	0.722064	
-30.000000	0.000000	1.000000	30.000000	} STAB. ACTUATOR

TABLE 6

EIGENVALUE ANALYSIS: MODEL 3

CLOSED-LOOP EQUIVALENT s-PLANE EIGENVALUES

REAL	IMAGINARY	DAMPING RATIO	NATURAL FREQUENCY	
- 0.067430	-0.181984	0.347443	0.194074	} PHUGOID
- 0.067430	0.181984	0.347443	0.194074	
- 0.530053	0.000000	1.000000	0.530053	
- 2.460401	-2.044951	0.769048	3.199281	} SHORT PERIOD
- 2.460401	0.044951	0.769048	3.199281	
- 4.119399	0.000000	1.000000	4.119399	
-36.188185	0.000000	1.000000	36.188185	

### 3. Analysis and Simulation

The Variable-Gain SOFFT control law designed for the longitudinal/vertical dynamics of the F/A-18 was evaluated in detail. The evaluation of this  $\alpha$ -command FCS included both analysis and simulation. Note that both the feedforward and feedback control laws are direct digital designs whereas the nonlinear aircraft dynamics and actuation systems are continuous. So that the closed-loop or, more precisely, the compensated system is a sampled-data system. The frequency response analyses are computed directly in the  $z$ -plane and shown as a function of the frequency  $\omega$ , where  $z = e^{-\omega\Delta t}$ . Thus, no approximation back into the  $w$ -plane is made in order to analyze the compensated system. Thus, the exact sampled-data system is analyzed and then displayed in the format of an analog system which is familiar to most designers.

#### Eigenvalues

The eigenvalues of the open-loop plant and the plant with the loop closed by the feedback control law are shown in Tables 1, 2 and 3 for each of the models used. These eigenvalues determine the stability of the system at the given models. They also show the damping ratio of each mode.

The main objective here is to provide adequate damping for the short period mode and the other modes in the feedback compensator. As discussed earlier, while some improvement in the phugoid damping is achieved in each model, sufficient damping is not expected from this feedback law as it does not feed back the phugoid variables: pitch and airspeed.

The short period mode has been brought to comfortable levels of damping for  $\alpha = 5^\circ, 20^\circ$  and  $40^\circ$ .

#### Feedback Loop Analysis

The loop gains at stabilator input are shown in Figures 16 - 18 for each model. The

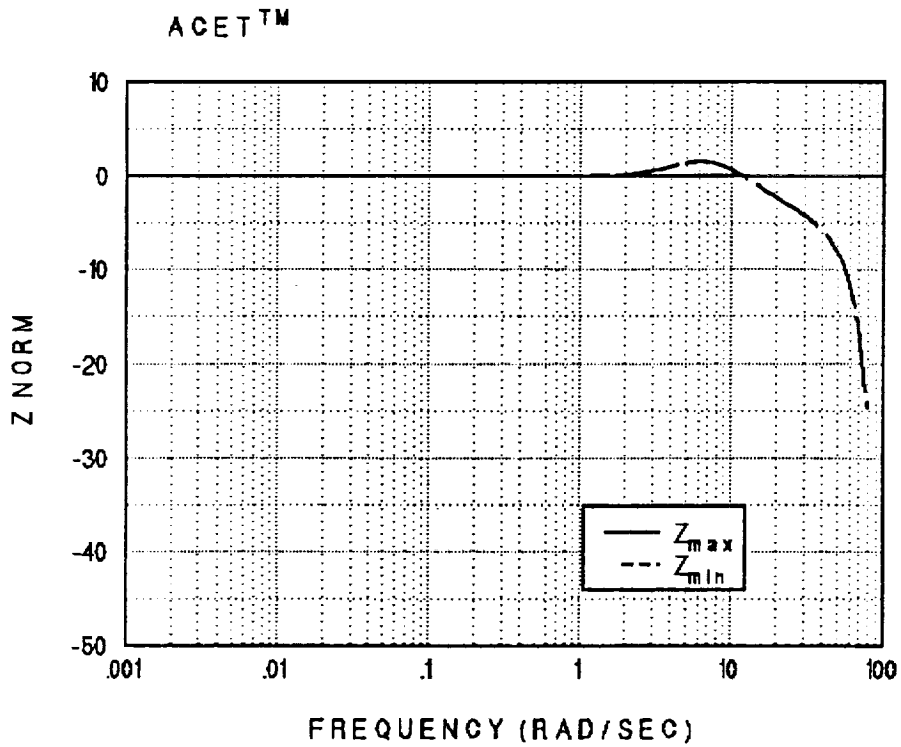


Figure 26a. Command tracking performance for Model 1:  $Z$ -norm (unweighted).

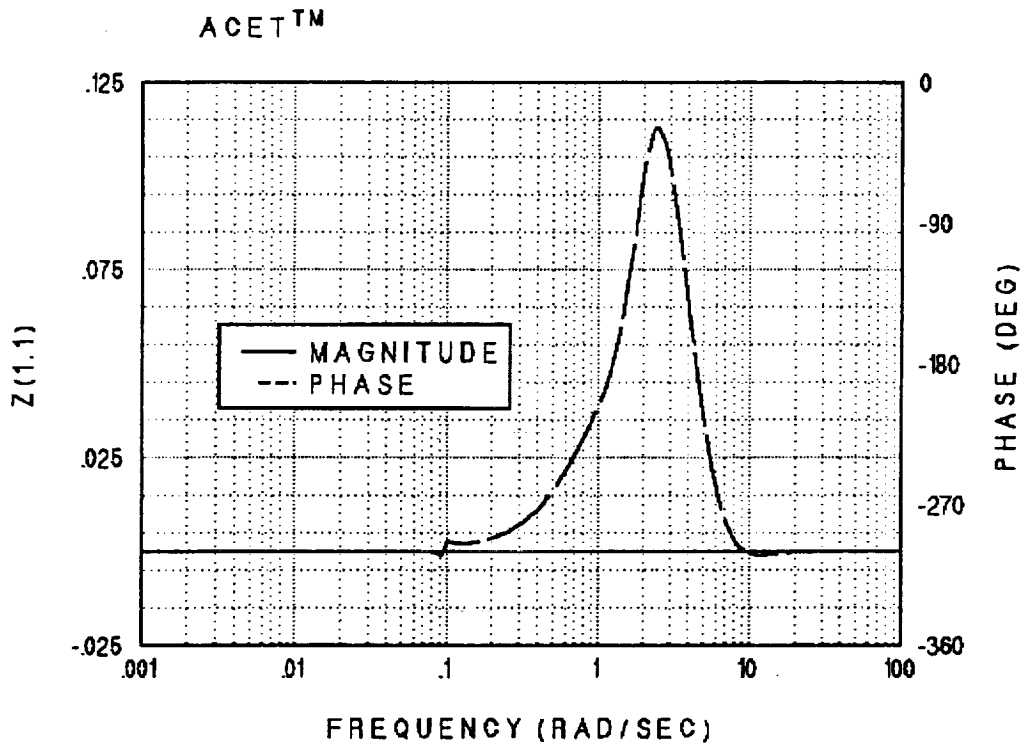


Figure 26b. Command tracking performance for Model 1: weighted  $Z$ -norm.

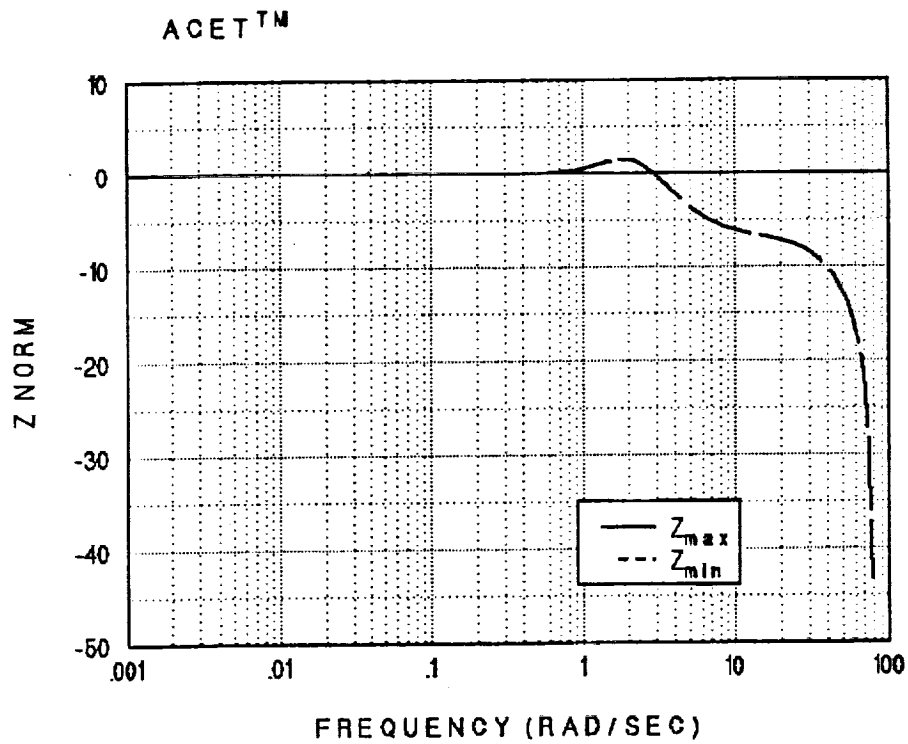


Figure 27a. Command tracking performance for Model 2:  $Z$ -norm (unweighted).

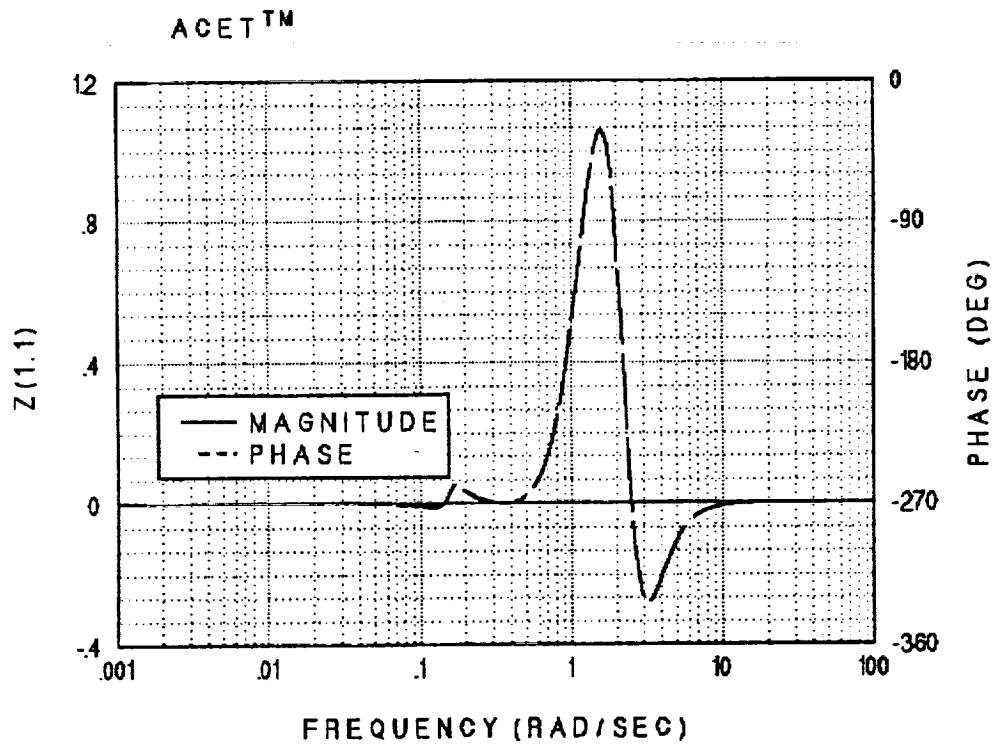


Figure 27b. Command tracking performance for Model 2: weighted  $Z$ -norm.



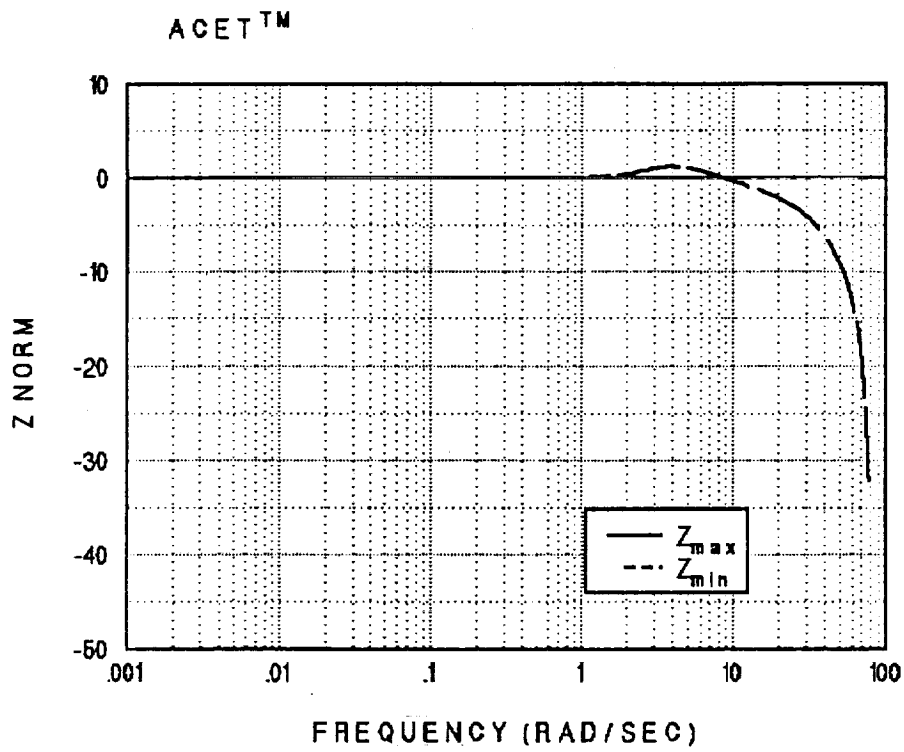


Figure 28a. Command tracking performance for Model 3:  $Z$ -norm (unweighted).

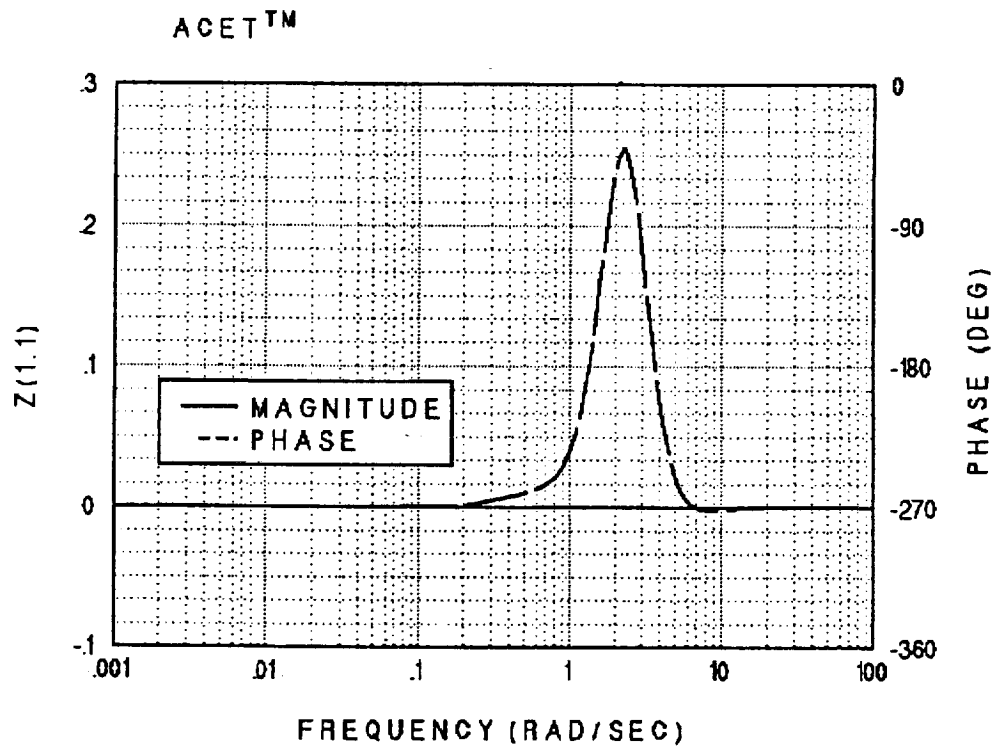


Figure 28b. Command tracking performance for Model 3: weighted  $Z$ -norm.

Bode plots show that the closed-loop system is in fact a type-1 system and will produce zero error in steady-state for constant commands. For model 1 at  $\alpha = 5^\circ$ , the Bode plots also show a significant drop in the loop gain near .1 rad/sec. This is clearly due to the phugoid mode.

The stability margins can be seen from both the Nyquist and Bode plots. The phase margins are greater than  $44^\circ$  for each model. The gain margins are below -10 db for all models.

The  $\sigma$ -plots or the return difference are positive except over a narrow bandwidth with the lowest value being above -4 db.

### Sensor Noise/Error Suppression

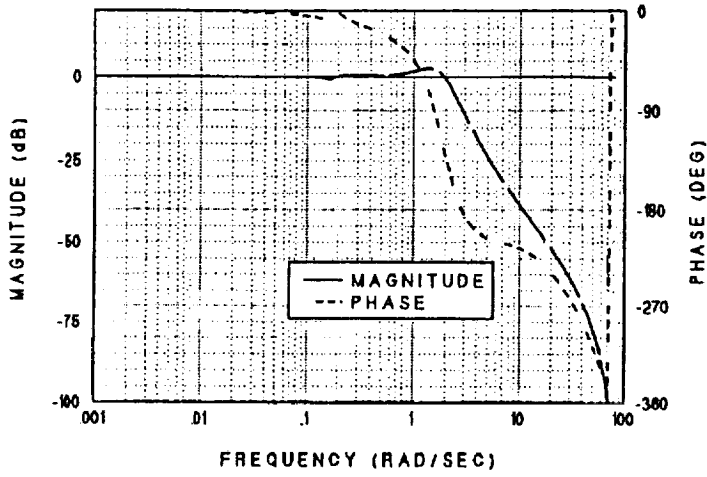
One of the objectives allocated to the feedback law by the SOFFT approach is to suppress measurement errors. Or at least not to amplify these noises except when necessitated by a more important objective.

To analyze the impact of sensor errors on the aircraft response, we show the frequency response of the angle-of-attack to measurement noises introduced by the pitch rate gyro and the  $\alpha$ -vane. These plots are shown in Figures 19 - 21 for  $\alpha = 5^\circ, 20^\circ, 40^\circ$ .

The pitch rate gyro errors are significantly attenuated throughout the spectrum for all three models. It is important to note that any bias errors present in the rate gyro will have no impact on the angle-of-attack.

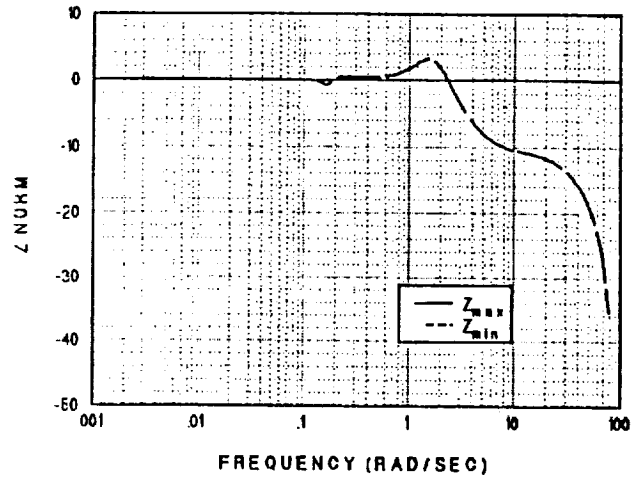
Errors and noises in the  $\alpha$ -vane are also suppressed. However, the attenuation comes largely in the higher frequencies. Within the command bandwidth which we consider to be the low-pass band below 2 rad/sec,  $\alpha$ -vane errors are essentially passed through. Thus,  $\alpha$ -vane noise is suppressed through a low-pass filter. This, of course, is necessary if we are to pass through the largest part of the sensor signal or the true value of the angle-of-attack. Thus, a bias error in the  $\alpha$ -vane will result in the angle-of-attack being off by the same amount.

ACET™ T( $\omega$ )-ACTUAL FREQUENCY RESPONSE



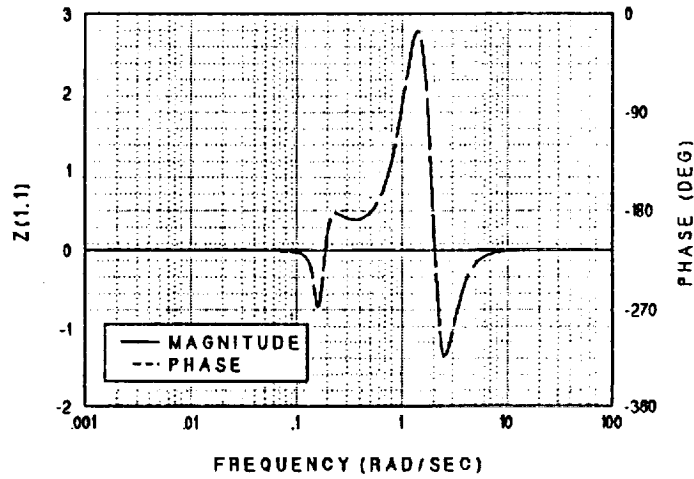
(a) Frequency response

ACET™



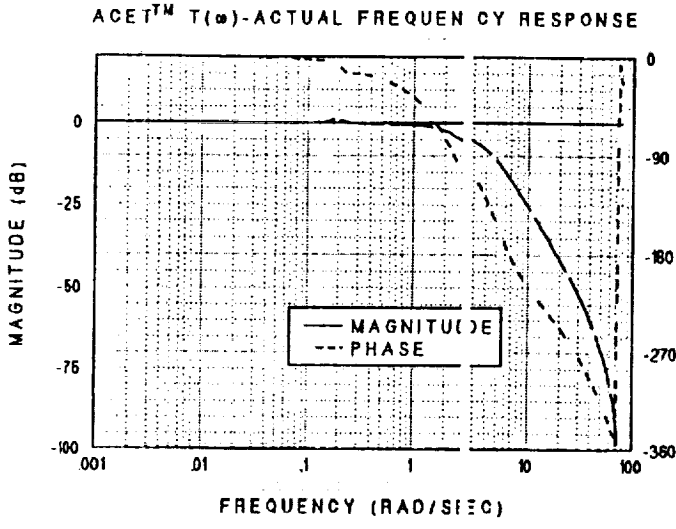
(b) Z-norm

ACET™

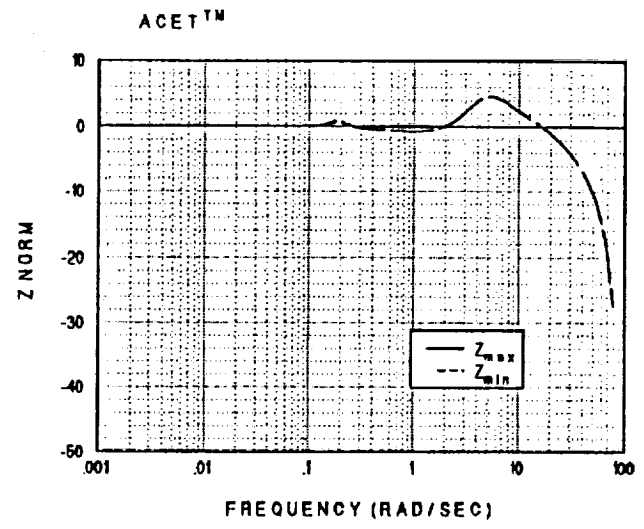


(c) Weighted Z-norm

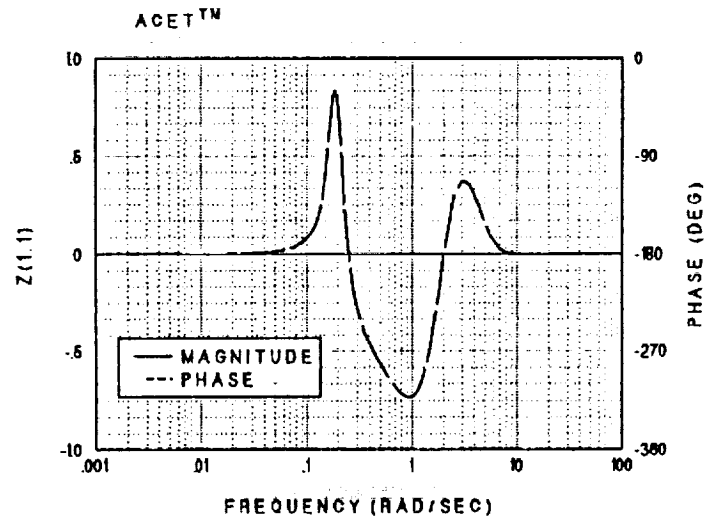
Figure 29. Command Tracking Performance Sensitivity:  $p_{true} = 30^\circ$ ,  $p_{est} = 20^\circ$ .



(a) Frequency response



(b) Z-norm



(c) Weighted Z-norm

Figure 30. Command Tracking Performance Sensitivity:  $p_{true} = 30^\circ, p_{est} = 40^\circ$ .

## Plant Disturbance Accommodation

Another important objective allocated to the feedback law by the SOFFT approach is to accommodate or suppress plant disturbances. For example from the linearization equations in section II (e.g., (10), (11)), we see that when the aircraft moves from one flight condition to another, the second order terms may start from zero, but they get larger and settle at a non-zero constant value which acts as a plant disturbance. For example, the 2<sup>nd</sup> order term  $o_x^2(t)$  in (10) is zero when the initial condition is  $(x_0, u_{x0})$  because  $o_x^2(t)$  is a function of the perturbation in  $x$  and  $u$ . As the perturbations  $(x - x_0)$  and  $(u_x - u_{x0})$  get larger,  $o_x^2(t)$  will act as a disturbance.

Here we have analyzed a plant disturbance acting at the stabilator input such as a nonlinearity in the actuator system or the aerodynamic load on the horizontal tail. Figures 22 - 24 show the effect of such a disturbance on the pitch rate and angle-of-attack responses at  $\alpha = 5^\circ, 20^\circ, 40^\circ$ .

Note that significant suppression of the disturbance is being achieved at all models. Thus, the impact of most nonlinear effects or other disturbances such as winds is likely to be small according to the plots. Note that at  $\alpha = 5^\circ$  high frequency artifacts mainly outside the command bandwidth will be slightly amplified. This is not present at the other  $\alpha$  values. A small modification of the feedback law should cure this effect. In general, the system appears to accommodate most disturbances.

## Command Tracking Performance

The preceding considerations such as stability, damping, sensor noise suppression and plant disturbance accommodation are the objectives allocated to the feedback control law. However, they do not guarantee satisfactory flying qualities without an appropriate feedforward design.

Here we analyze the impact of the feedforward control law on the closed-loop system.

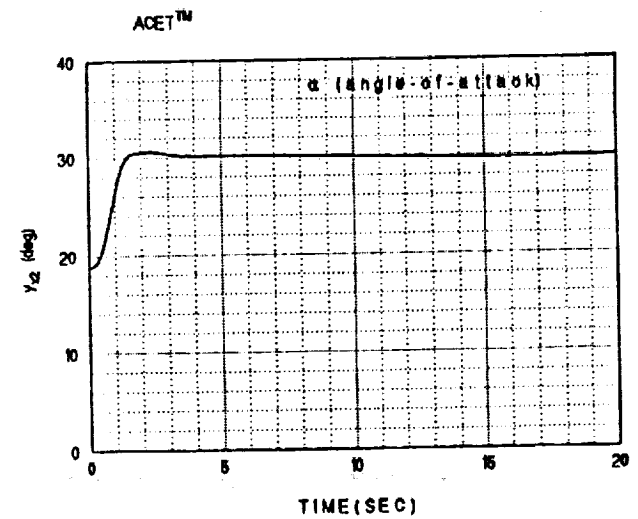
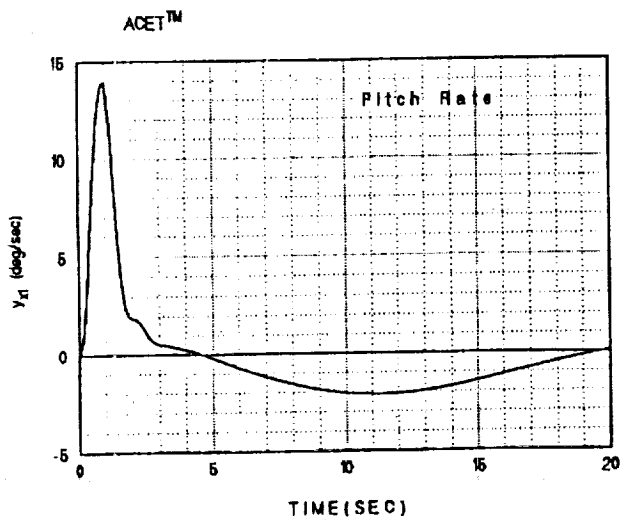
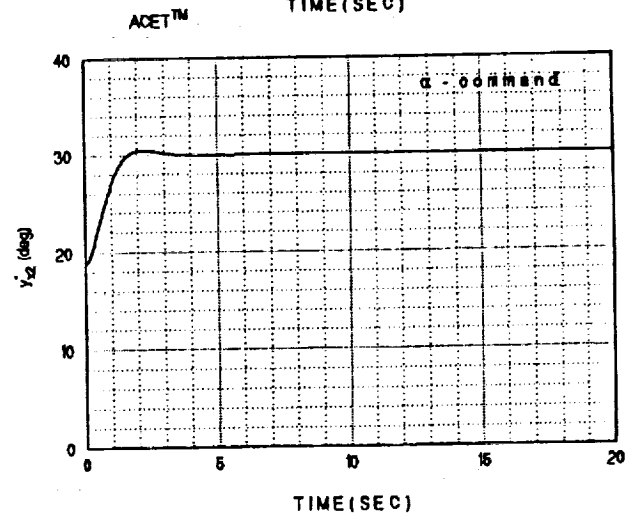
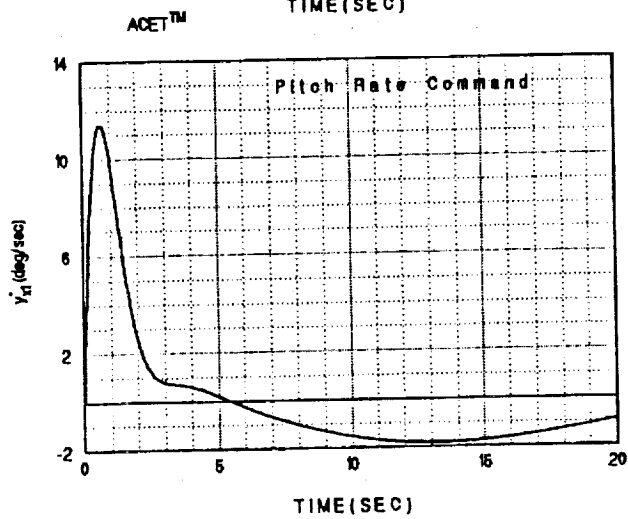
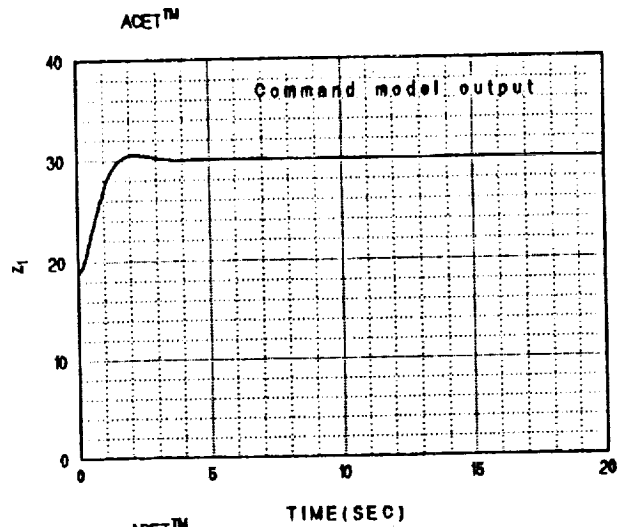
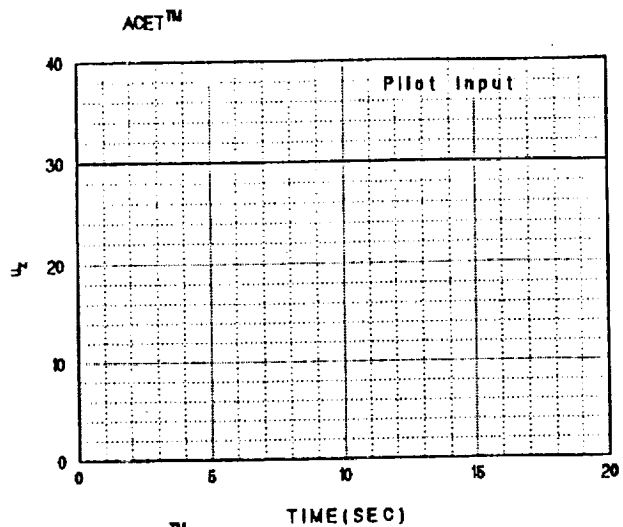


Figure 31a. F/A-18 SOFFT control law simulation:  $\alpha$ -command =  $30^\circ$ .

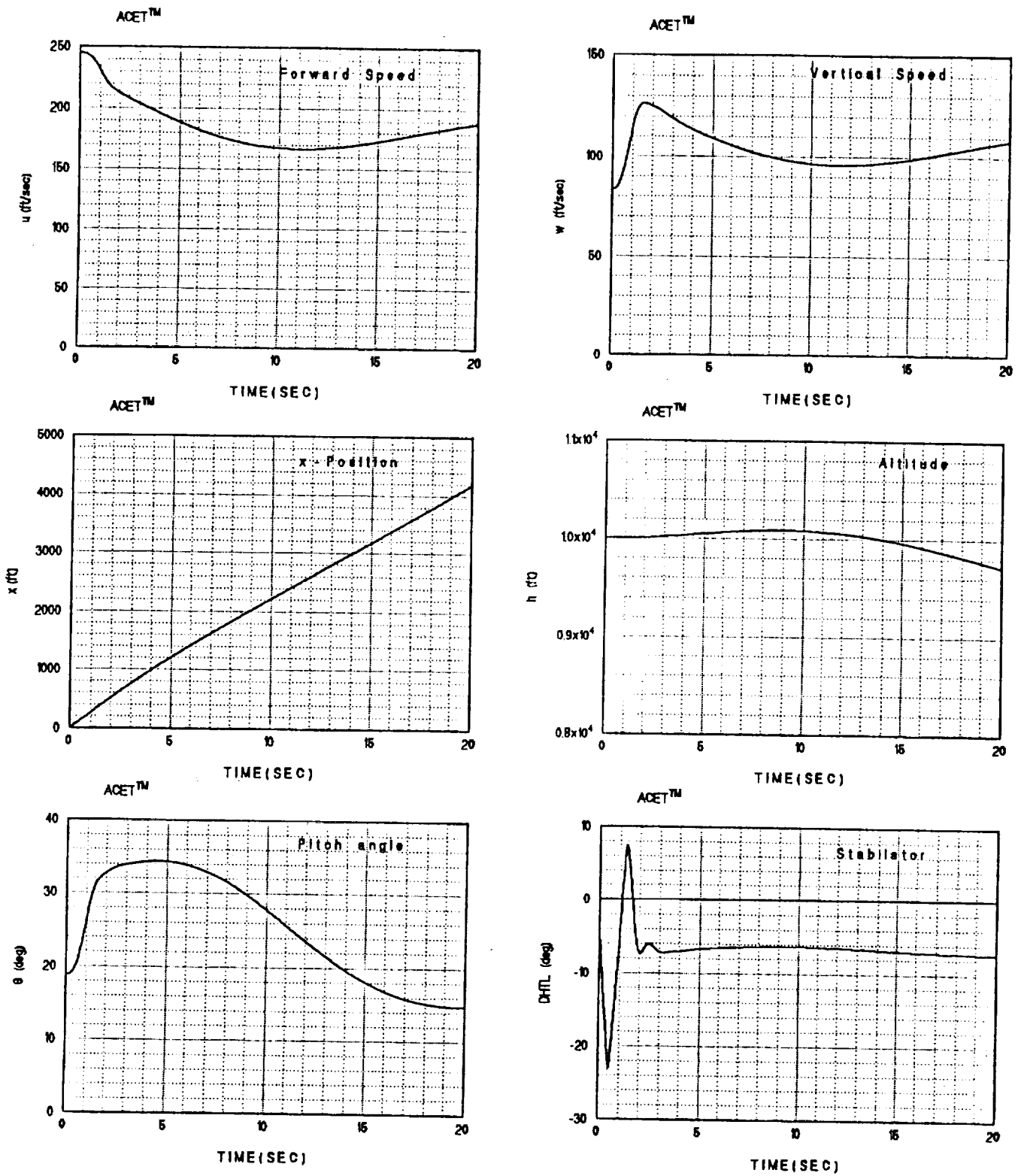


Figure 31b. F/A-18 SOFFT control law simulation:  $\alpha$ -command =  $30^\circ$ .

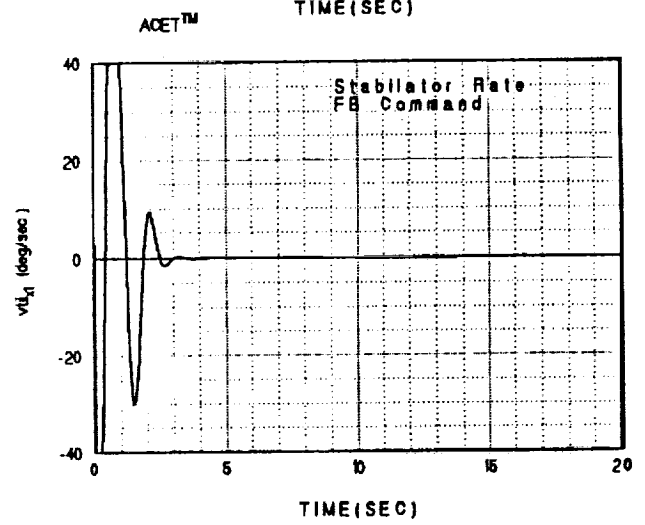
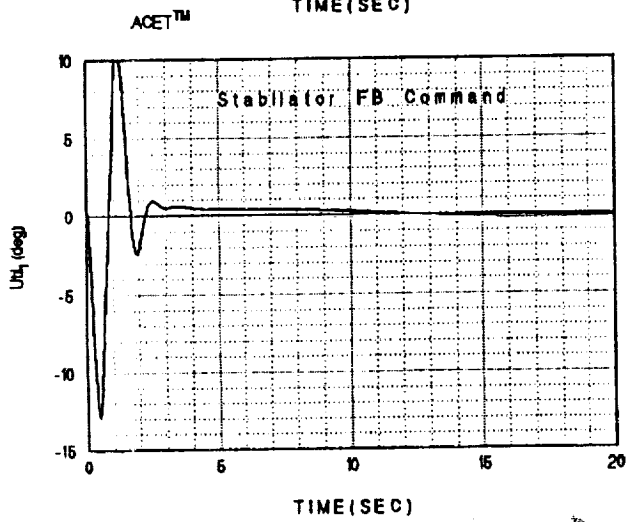
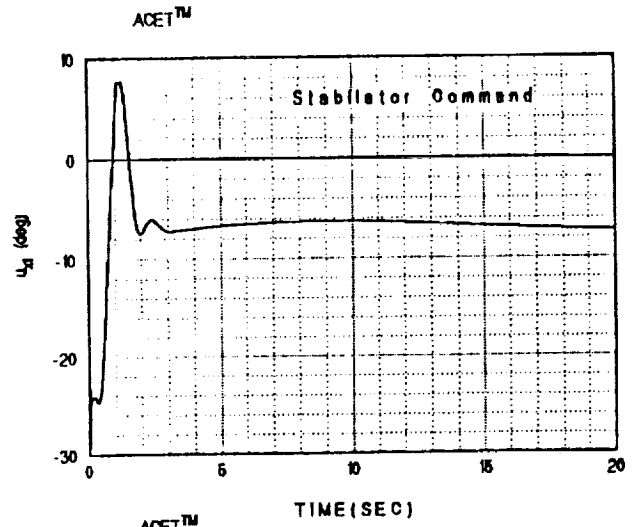
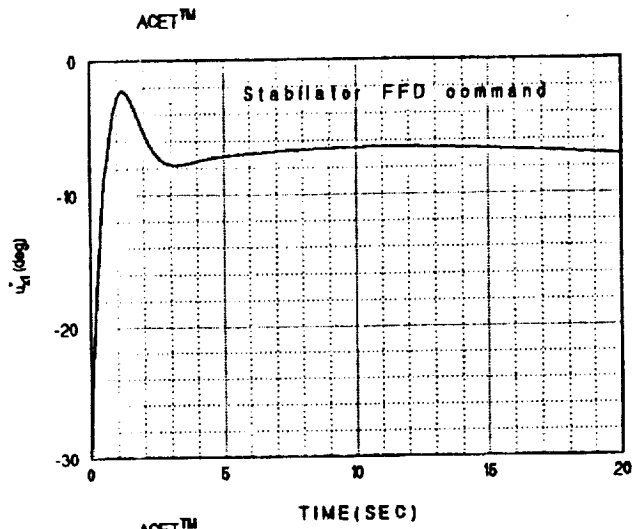


Figure 31c. F/A-18 SOFFT control law simulation:  $\alpha$ -command =  $30^\circ$ .



Thus, we shall look at the response of the angle-of-attack to a command input by the pilot.

Figure 25a shows the desired frequency response,  $T^*(\omega)$ , of the angle-of-attack to a pilot input. Thus, this is the frequency response of the command model which has been selected to produce flying qualities deemed satisfactory by the pilot. Observing  $T^*(\omega)$ , we note that it is essentially flat until 1 rad/sec at which point it starts to move down at 40 db/decade. We may consider the command bandwidth to extend from 0 rad/sec till 2 rad/sec. Thus, we would like to pass through commands within this bandwidth and attenuate signals outside. This is why the feedback law can attenuate high-frequency noise signals.

The actual frequency response of the combined feedforward and feedback control laws is shown in Figures 25b, c and d for models 1, 2 and 3, respectively. Note the high accuracy of these response. In large part, this is due to the fact that we are using a variable-gain SOFFT control law rather than a single-model SOFFT control law. Clearly, for small pilot inputs, the response of the angle-of-attack will be nearly perfect producing high pilot ratings.

We can assess the command tracking performance more clearly by looking at the system's  $Z$ -plots, defined in section III. Figures 26 - 28 show the  $Z$ -plots for the SOFFT control law at each model. Since there is one control,  $Z_I = Z_0$ . Furthermore,  $Z_{max}(\omega) = Z_{min}(\omega) = \|Z(\omega)\|_2 = Z\text{-norm}$  and  $Z_c(\omega) = 0$ . Figures 26b, 27b and 28b show the weighted  $Z$ -norm which weights the  $Z$ -norm by the square magnitude of the desired response. The intent here is to weigh the command bandwidth more than points outside the bandwidth. Note that the  $Z$ -norms for each model are within 2 db inside the command bandwidth. The weighted norms show good performance throughout.

### Tracking Performance Sensitivity

The adaptive nature of the variable-gain SOFFT controller makes it highly robust, simply because the control gains are constantly adapting to the current conditions. To

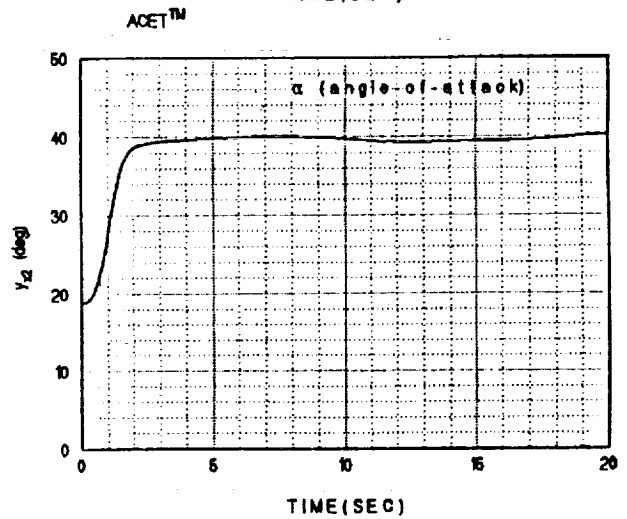
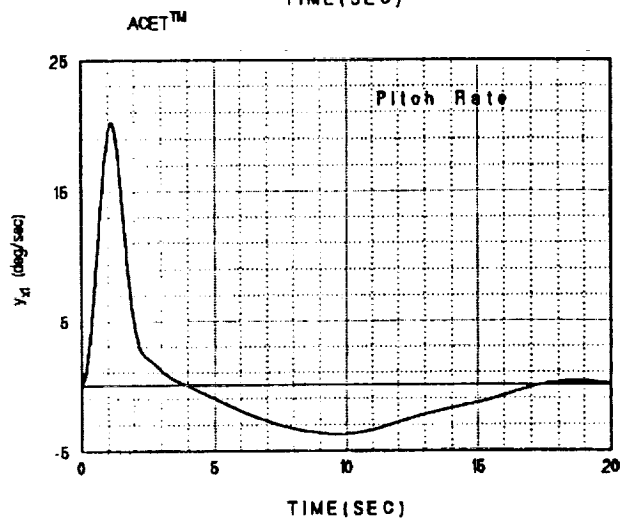
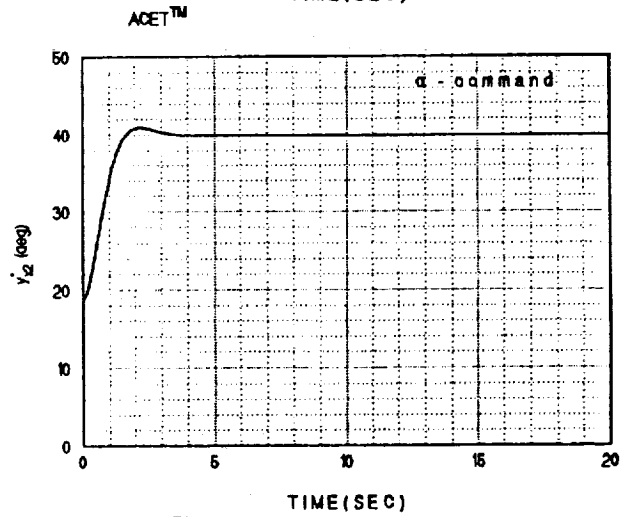
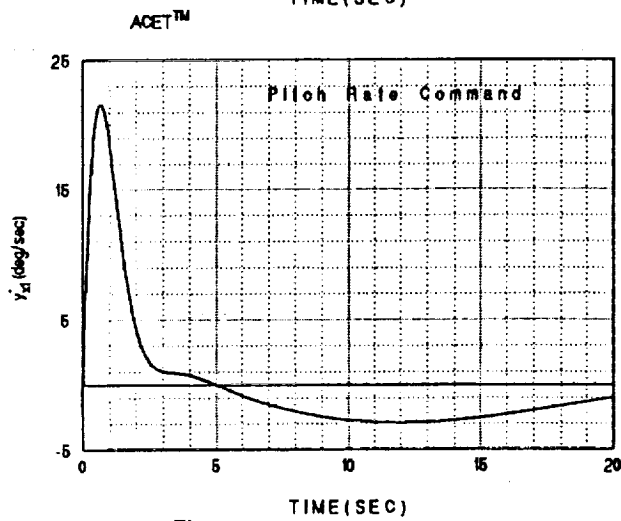
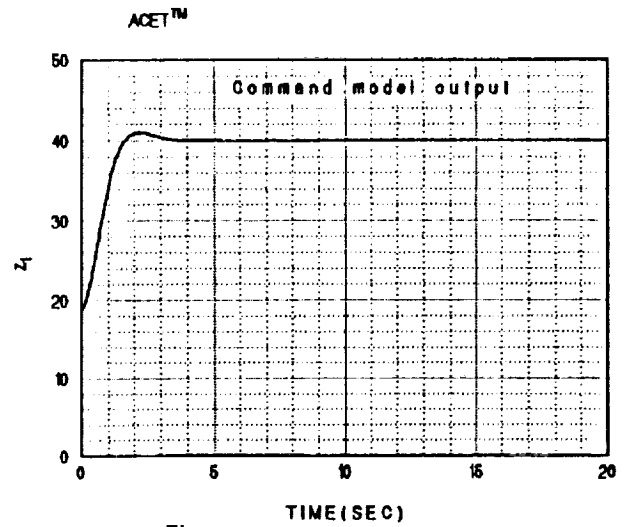
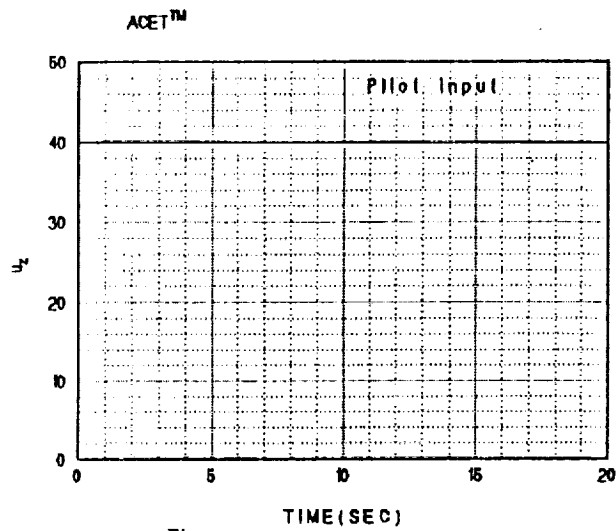


Figure 32a. F/A-18 SOFFT control law simulation:  $\alpha$ -command =  $40^\circ$ .

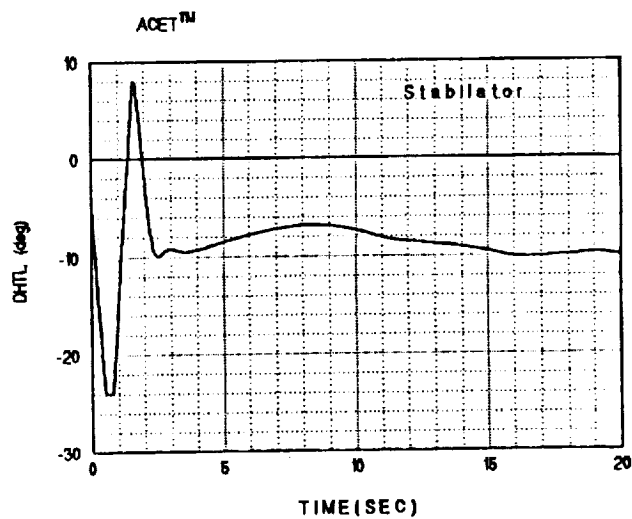
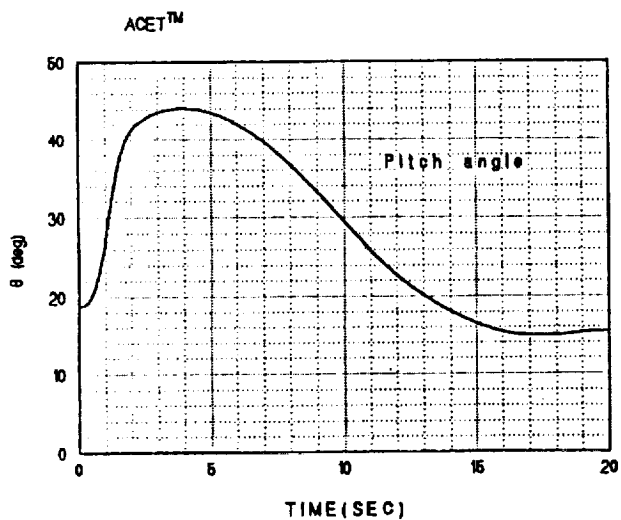
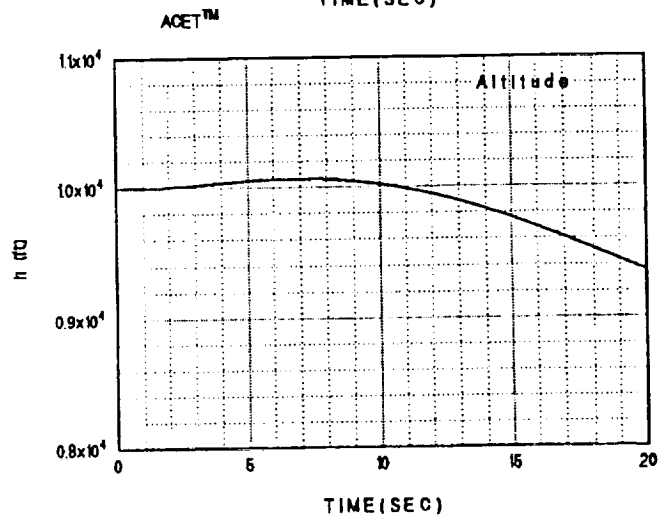
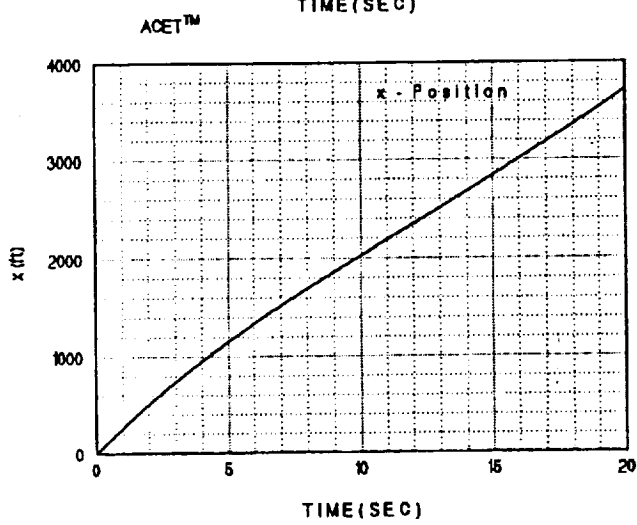
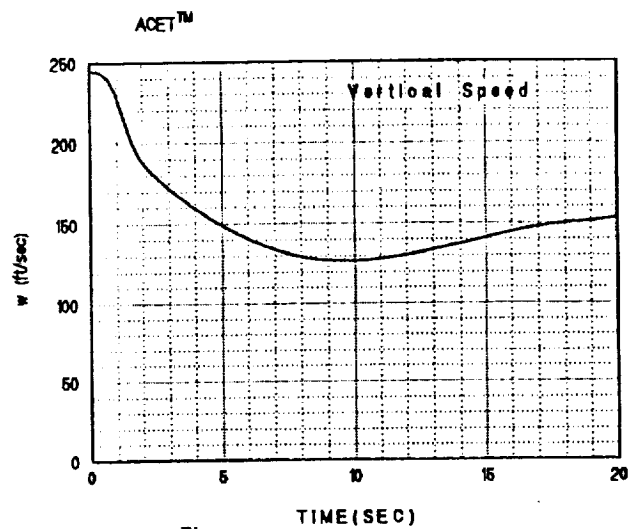
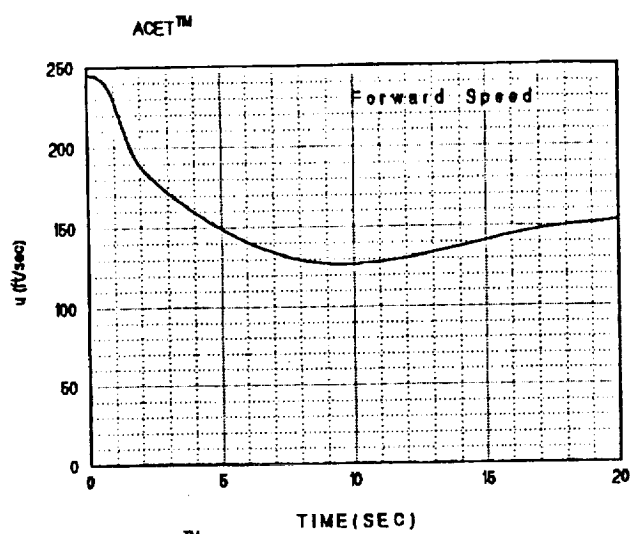


Figure 32b. F/A-18 SOFFT control law simulation:  $\alpha$ -command =  $40^\circ$ .

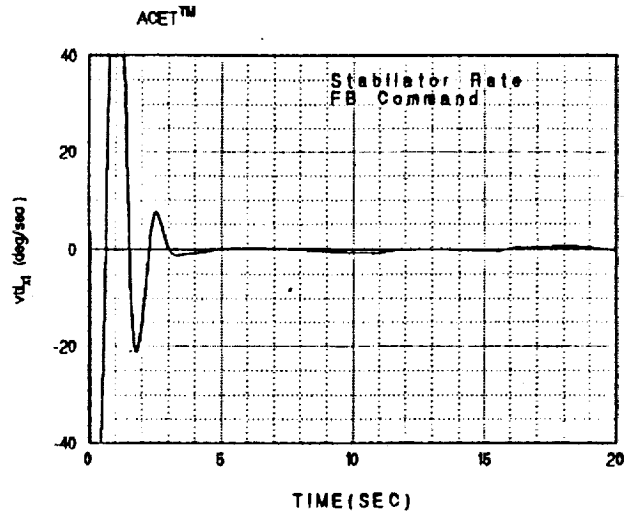
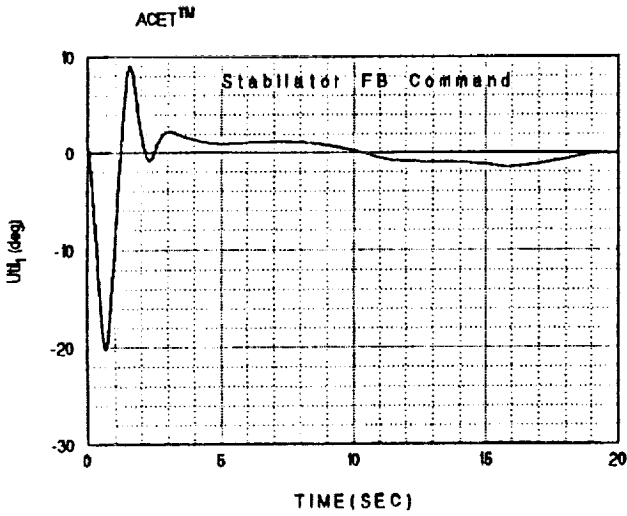
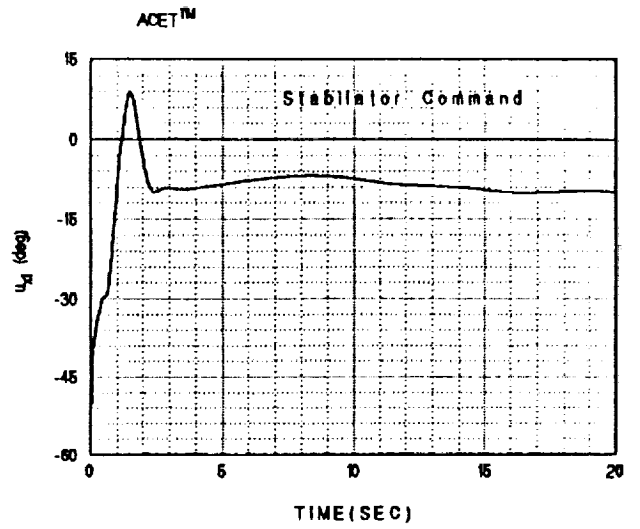
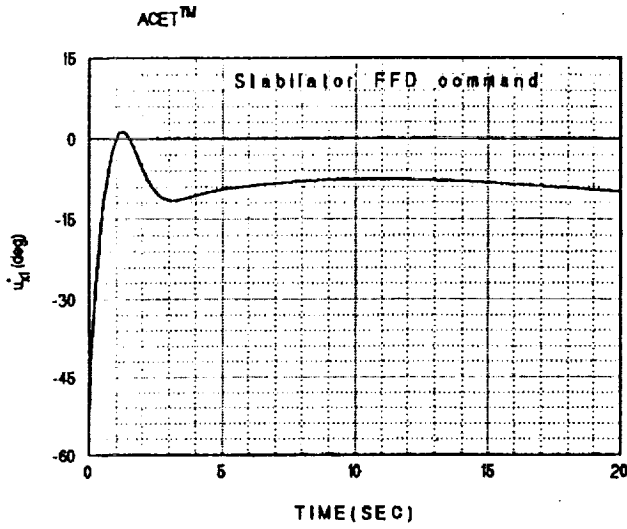


Figure 32c. F/A-18 SOFFT control law simulation:  $\alpha$ -command =  $40^{\circ}$ .

assess the robustness of the command tracking performance, we must introduce uncertainties.

Now suppose that the operating point parameter vector  $p$  used by the control laws has a value of  $20^\circ$  while the true value is  $30^\circ$ . Clearly such large discrepancies are not likely to occur, even though small errors in the sensor are generally present. However, it illustrates the robustness of the variable-gain SOFFT control law.

Thus, Figure 29 shows the frequency response, the  $Z$ -norm and the weighted  $Z$ -norm for this situation. Note that the  $Z$ -norm is within 3.5 db throughout the command bandwidth, but shows higher departures outside the bandwidth.

Figure 30 shows the scenario when the control law is configured for  $p = 40^\circ$  while the true value is  $30^\circ$ . Within the command bandwidth, the  $Z$ -norm is within 1 db of perfect tracking.

### Simulations

The variable-gain SOFFT  $\alpha$ -command control law and the lateral  $p/\beta$ -command system were used to compensate a highly accurate nonlinear simulation of the F/A-18 aircraft. The simulation is described in section V. In all the runs shown, the aircraft is initially at trim in level flight, with wings level and at  $18.8^\circ$  of angle-of-attack. The throttle (PLAC) is set at  $60.8^\circ$  and remains at this level throughout the simulation.

Figure 31 shows the response to a pilot step input commanding  $30^\circ$  angle-of-attack at time 0. The command model produces the desired response for  $z_1$ . The SOFFT feedforward control generates the desired or  $*$ -trajectory  $y_x^*$ ;  $y_{x1}^*$  is the pitch rate,  $y_{x2}^*$  the angle-of-attack. Now  $y_x^*$  is fed into the feedback loop to form the error signal,  $\tilde{y}_x$ . Simultaneously, the feedforward generates the command  $u_x^*$  shown in Figure 31c which goes directly to the stabilator actuator. The feedback control law uses the output error  $\tilde{y}_x$  to generate the feedback portion of the control  $\tilde{u}_x$  which added to the feedforward command  $u_x^*$  to produce the total command to the stabilator actuator system.

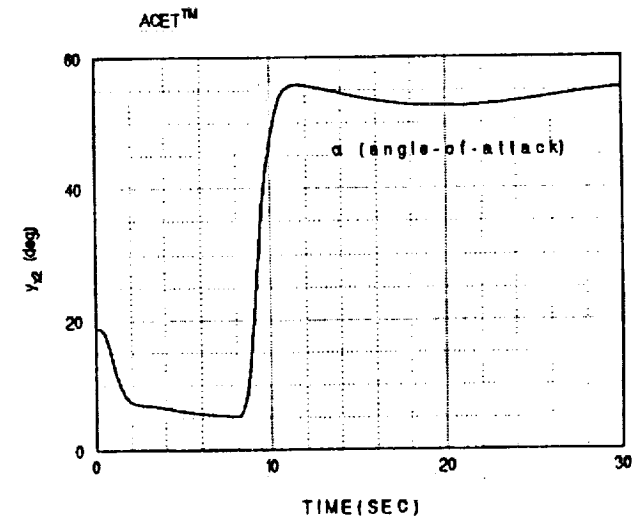
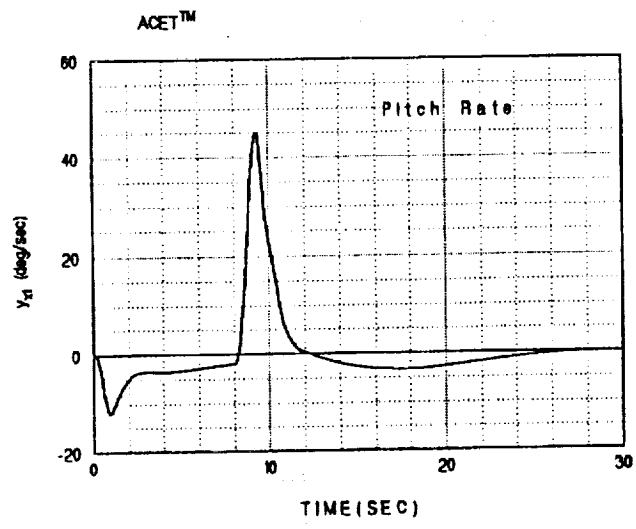
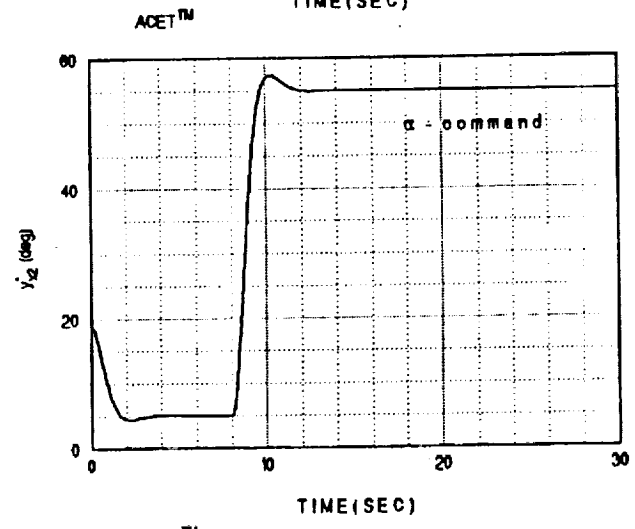
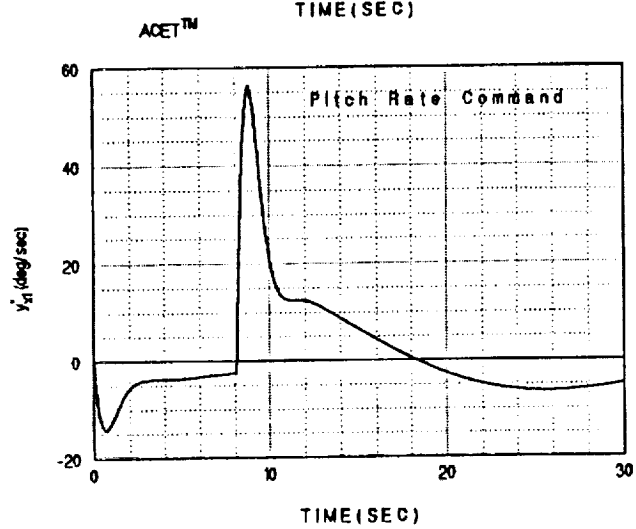
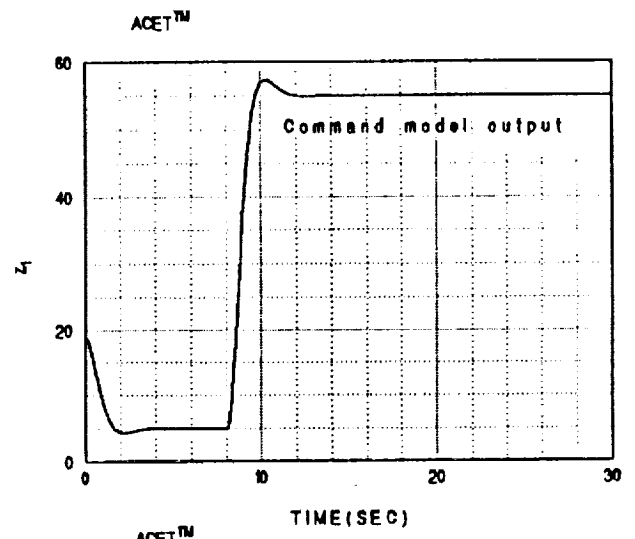
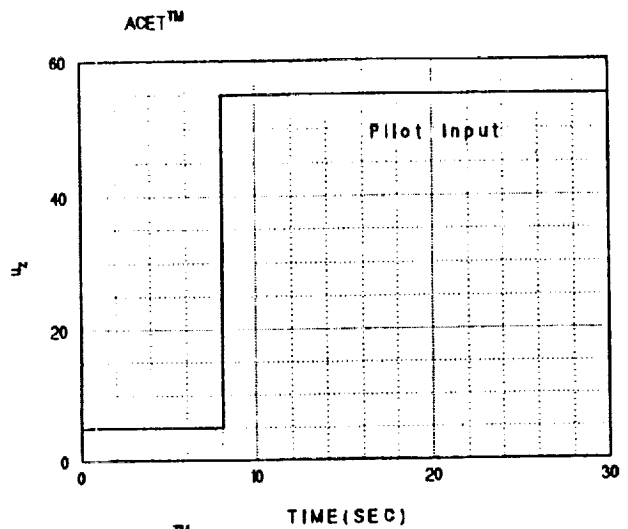


Figure 33a. F/A-18 SOFFT control law simulation:  $\alpha$ -command =  $5^\circ, 55^\circ$ .

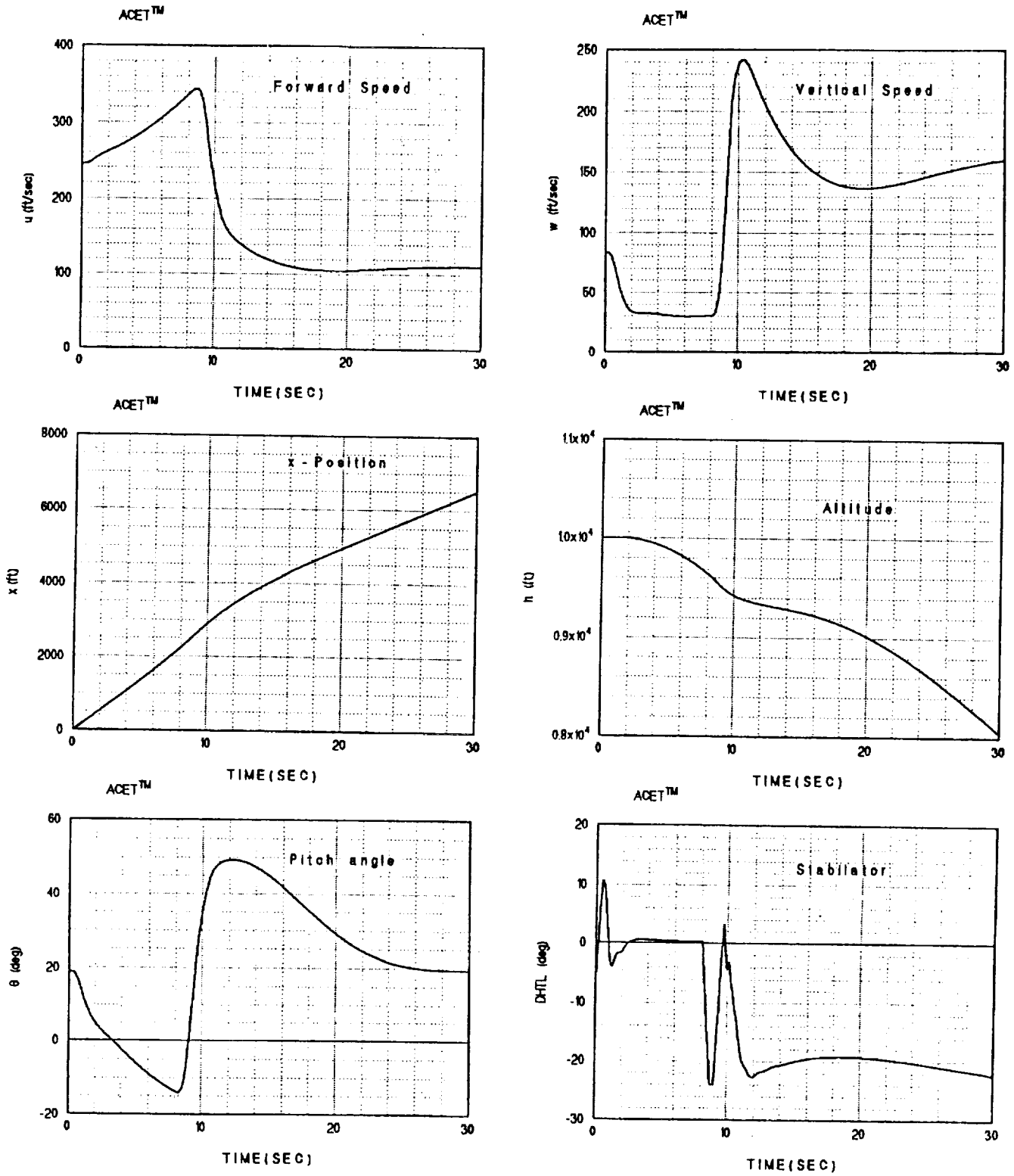


Figure 33b. F/A-18 SOFT control law simulation:  $\alpha$ -command =  $5^\circ, 55^\circ$ .

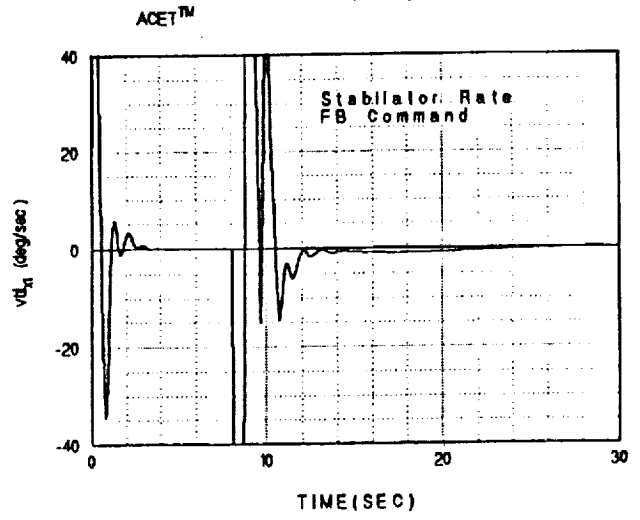
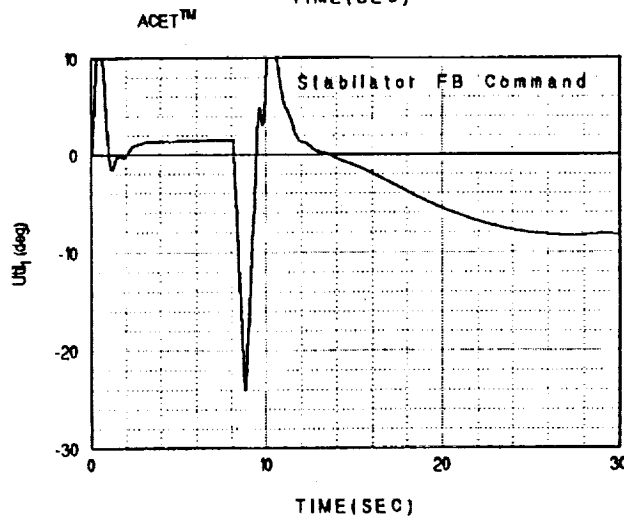
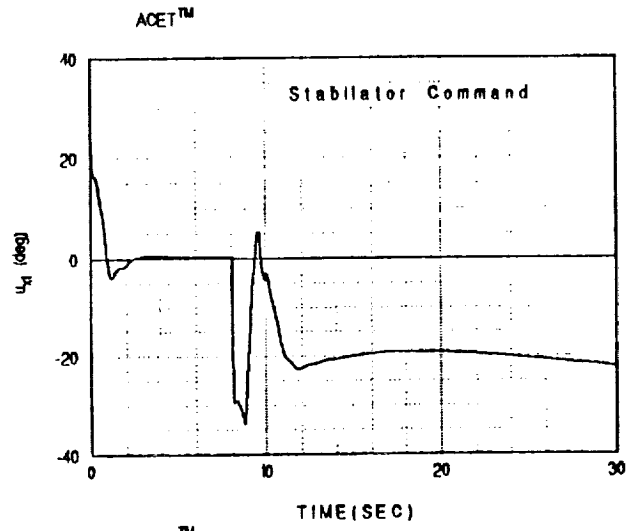
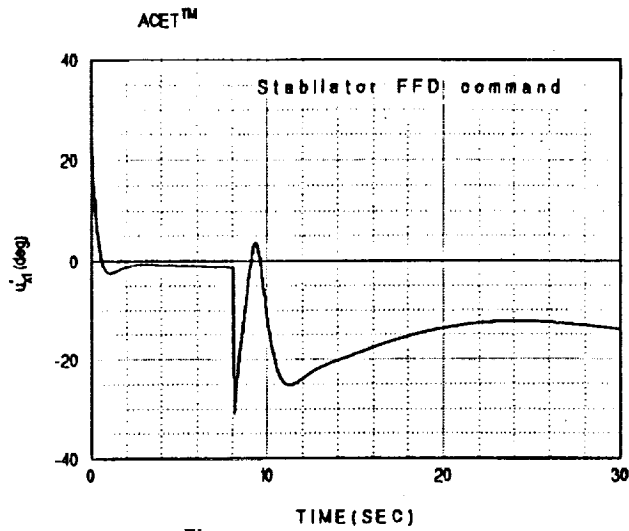


Figure 33c. F/A-18 SOFFT control law simulation:  $\alpha$ -command =  $5^\circ, 55^\circ$ .



Comparison of the  $\alpha$  response ( $y_{x2}$ ) and the command  $y_{x2}^*$  shows that they are practically the same! The pitch rate response is also very accurate. From the stabilator (DHTL) response, note that the actuator has reached its rate limit and the aircraft is pitching up at the maximum rate possible for this condition.

Figure 32 shows the simulated responses to a pilot step input of  $40^\circ$  of angle-of-attack. The  $\alpha$  response is just as fast; however it has a sharp break point at  $39^\circ$  at 2 sec and levels off, reaching  $40^\circ$  at 5 sec. The underdamped phugoid mode is noticeable.

Figure 33 shows the simulated responses to a pilot step into of  $5^\circ$  at time zero. At 8 sec, the pilot commands  $55^\circ$  of angle-of-attack. The  $\alpha$  response slightly undershoots with a breakpoint at  $7.5^\circ$  in under 1 sec. From  $5^\circ$  the angle-of-attack reaches  $55^\circ$  in less than 3 sec, displaying an excellent overall response. The pitch rate reaches a peak of 45 deg/sec in less than 1.5 sec.

It should be noted that the response is obtained without the benefit of any throttle action helping in the pitching moment. Also note that the aircraft physical limit for sustained angle-of-attack is about  $57^\circ$ ; so that after  $45^\circ$  the aircraft may be considered in the stall region.

Figure 34 shows the simulated responses for a pilot command of  $18.8^\circ$  of  $\alpha$ . However, the lateral pilot input commands a 10 deg/sec roll rate at 2 sec for 2 sec, then a -10 deg/sec roll rate at 10 sec for 2 sec, while a sideslip of 0.0 deg is commanded throughout. The roll rate follows the command model output with accuracy. The angle-of-attack is maintained very near its commanded value of  $18.8^\circ$  despite the roll maneuver. Also note the yaw rate command and response to produce zero sideslip, and the corresponding drop in the pitch angle while  $\alpha$  remains constant.

Figures 35 and 36 show the simulated responses for a constant-gain SOFFT control law designed for  $\alpha = 20^\circ$ . While the robust behavior is impressive, the variable-gain control performs better.

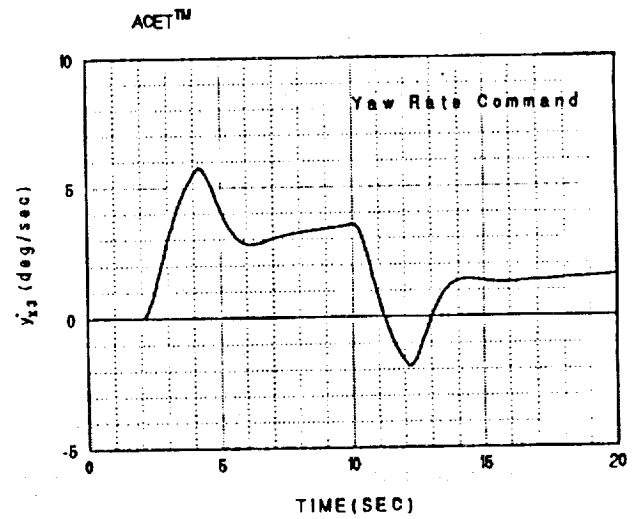
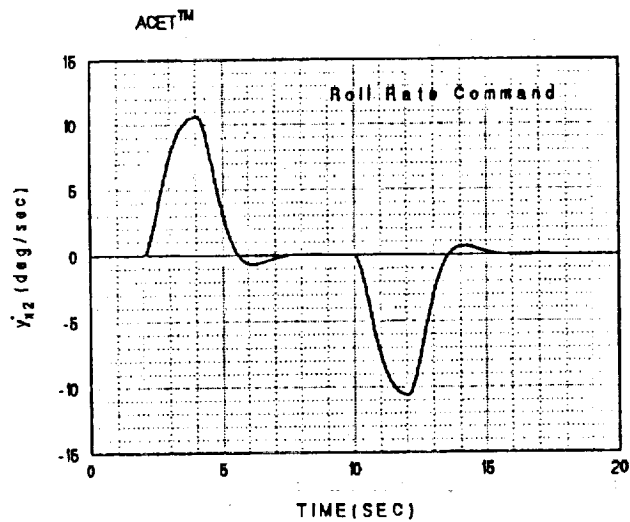
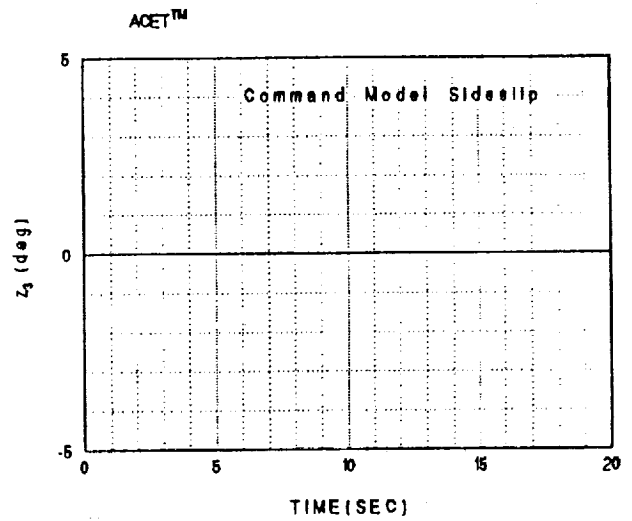
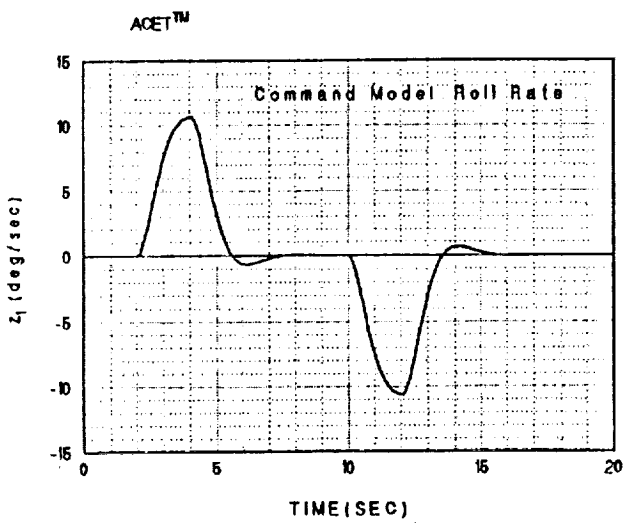
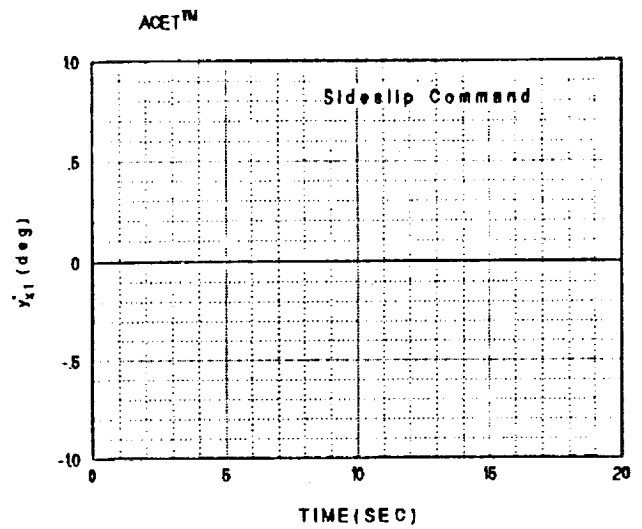
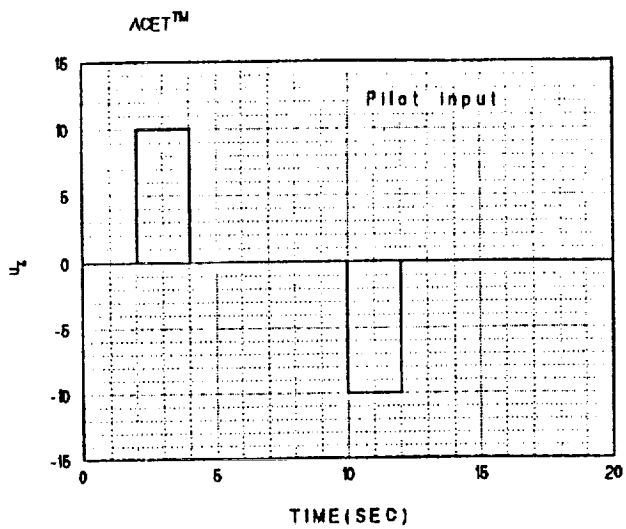


Figure 34a. F/A-18 SOFT control law simulation:  $\alpha$ -command =  $18.8^\circ$ ;  $p$ -command = doublet;  $\beta$  command =  $0^\circ$ .

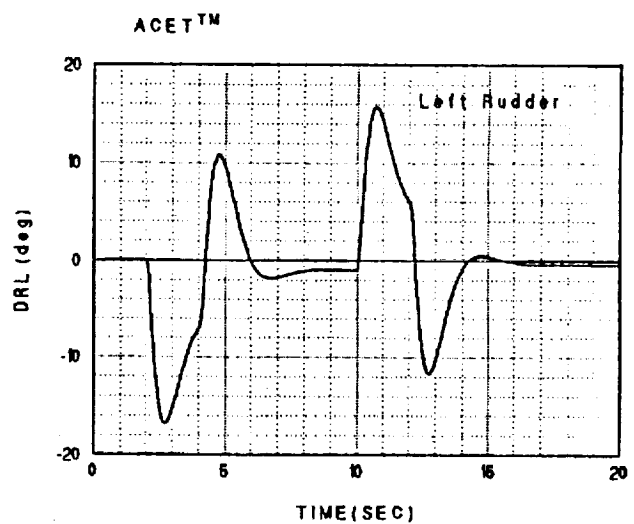
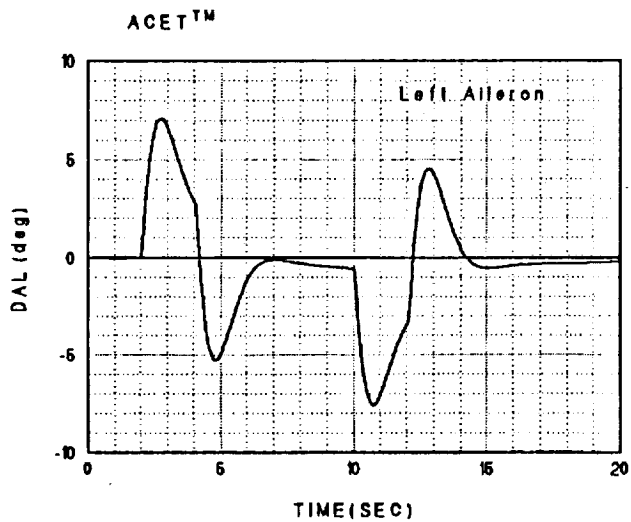
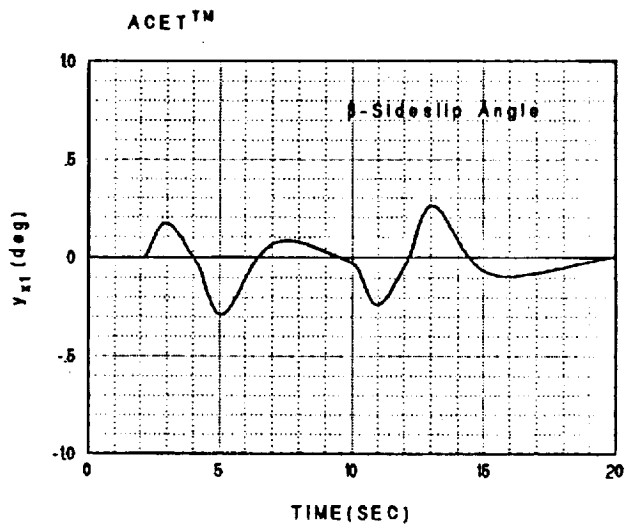
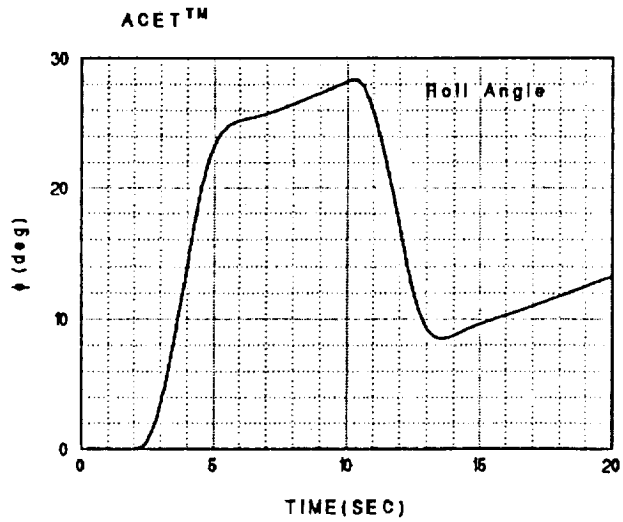
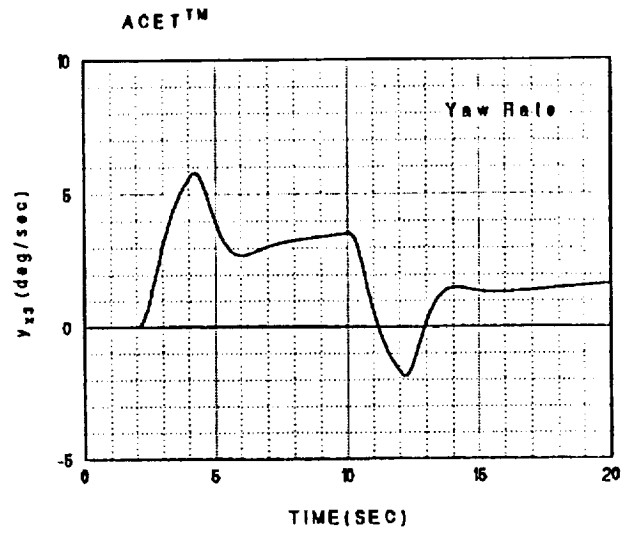
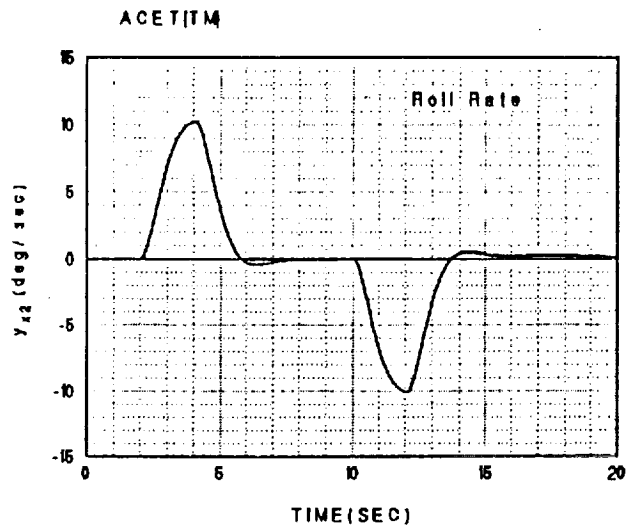


Figure 34b. F/A-18 SOFFT control law simulation:  $\alpha$ -command =  $18.8^\circ$ ;  
 $p$ -command = doublet;  $\beta$  command =  $0^\circ$ .

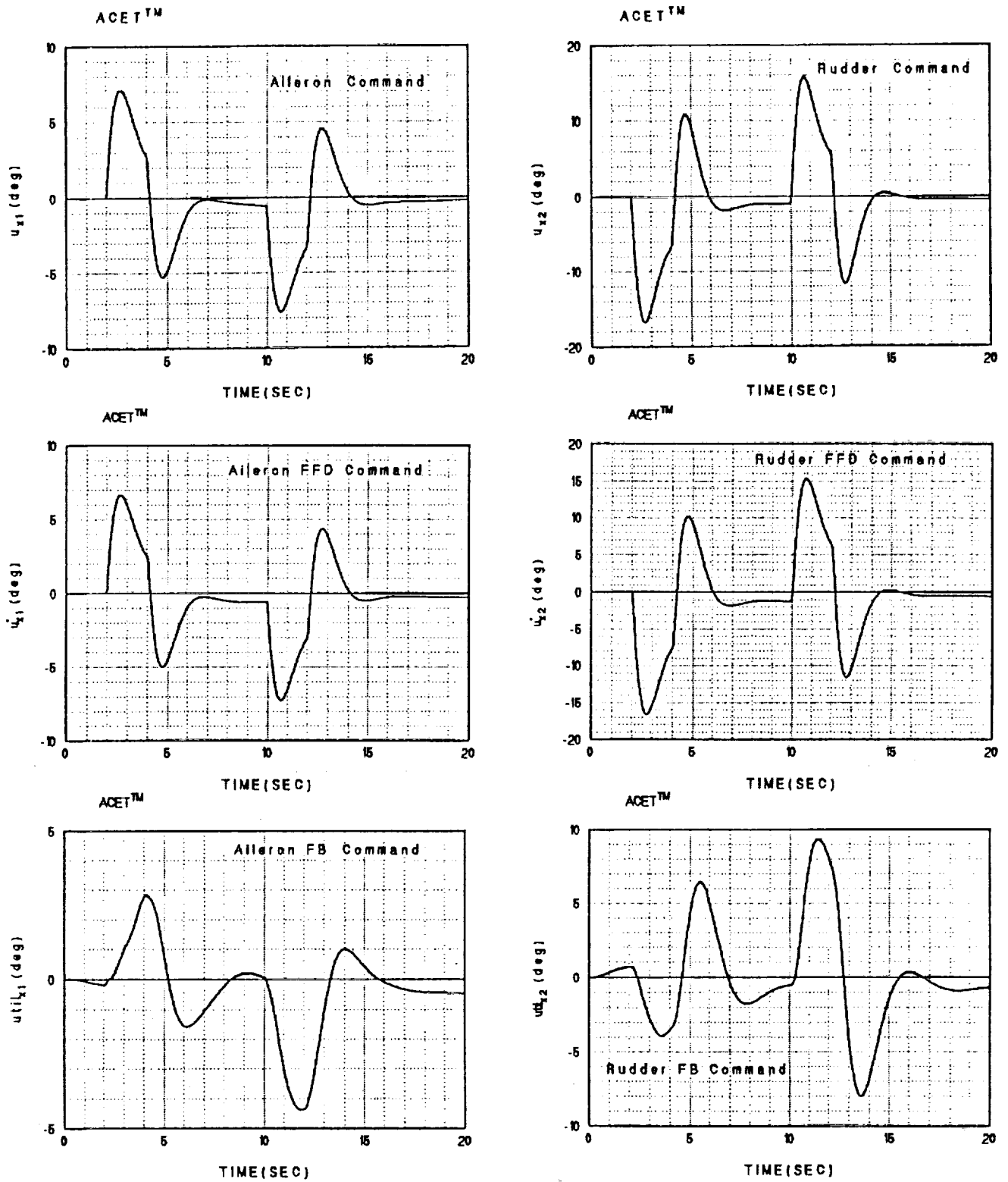


Figure 34c. F/A-18 SOFT control law simulation:  $\alpha$ -command =  $18.8^\circ$ ;  $p$ -command = doublet;  $\beta$  command =  $0^\circ$ .

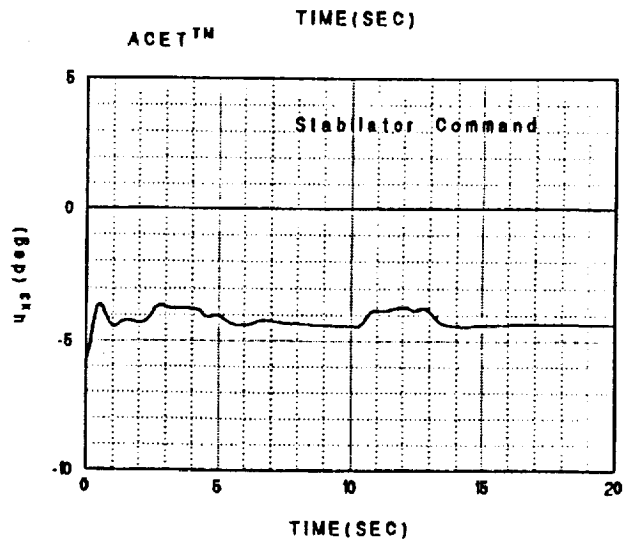
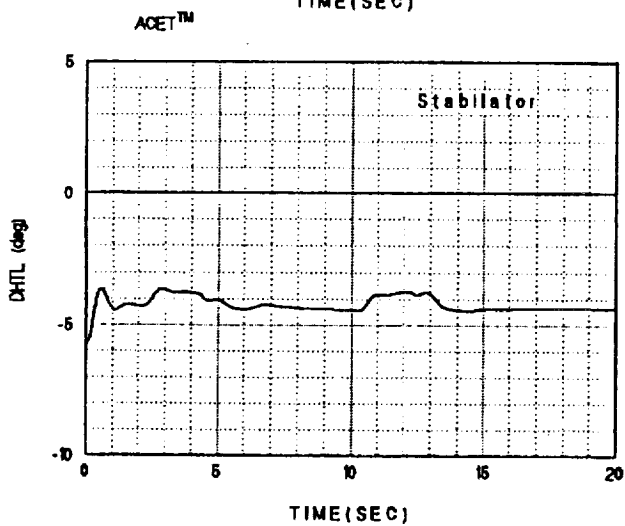
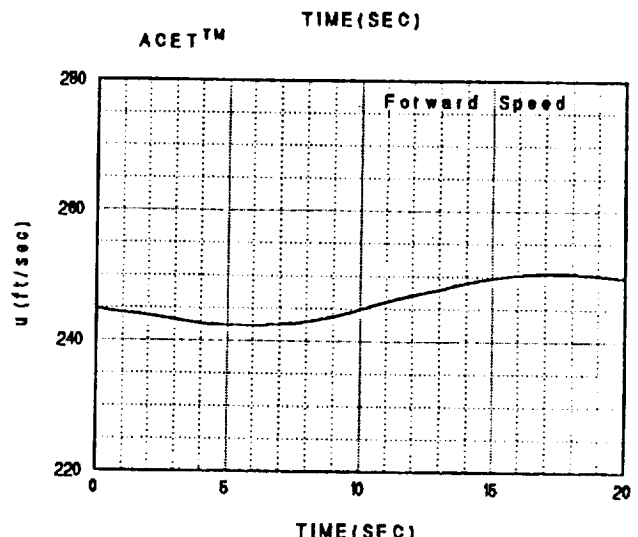
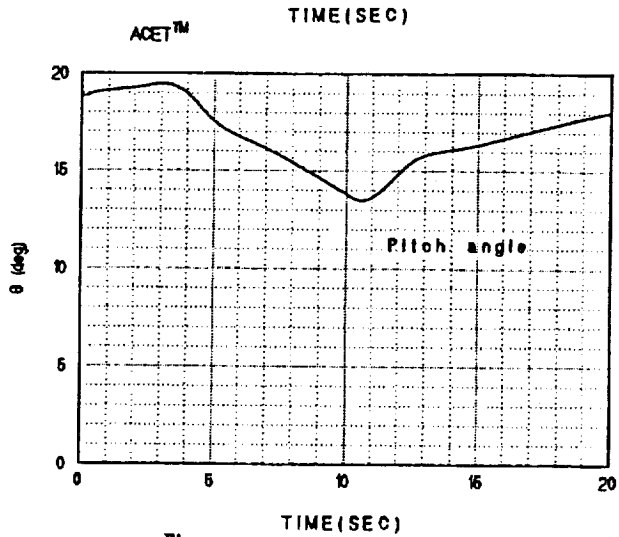
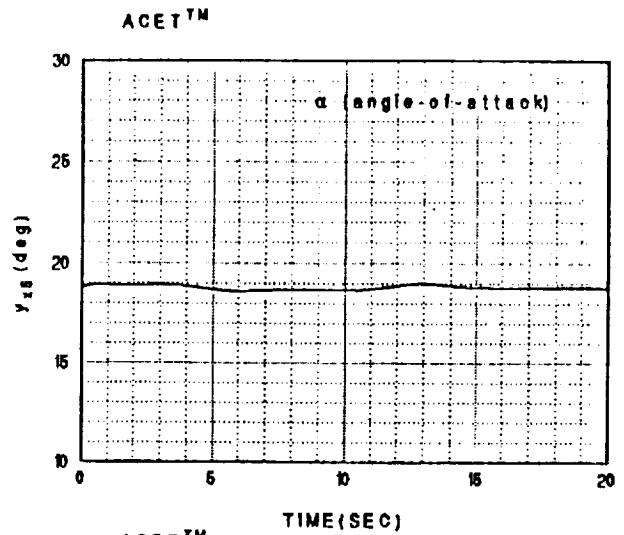
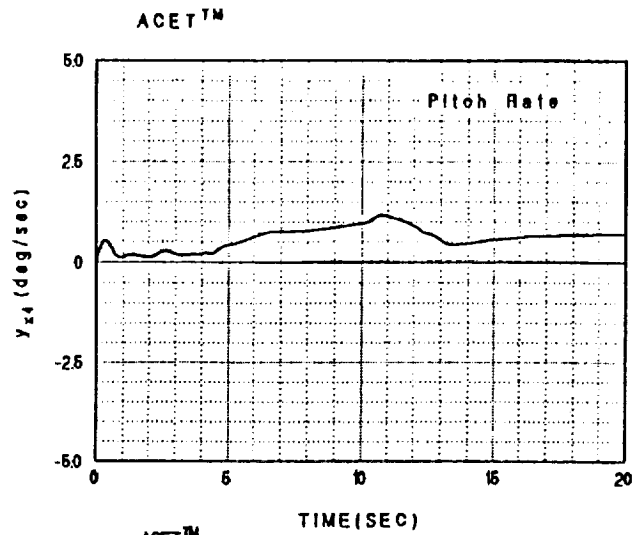


Figure 34d. F/A-18 SOFT control law simulation:  $\alpha$ -command =  $18.8^\circ$ ;  $p$ -command = doublet;  $\beta$  command =  $0^\circ$ .

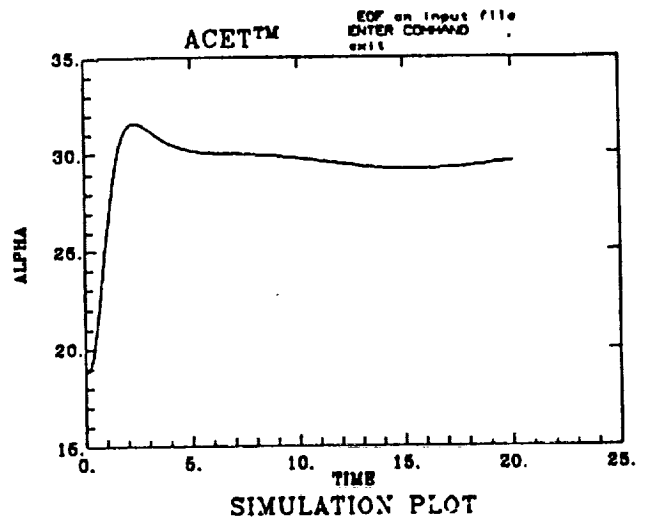
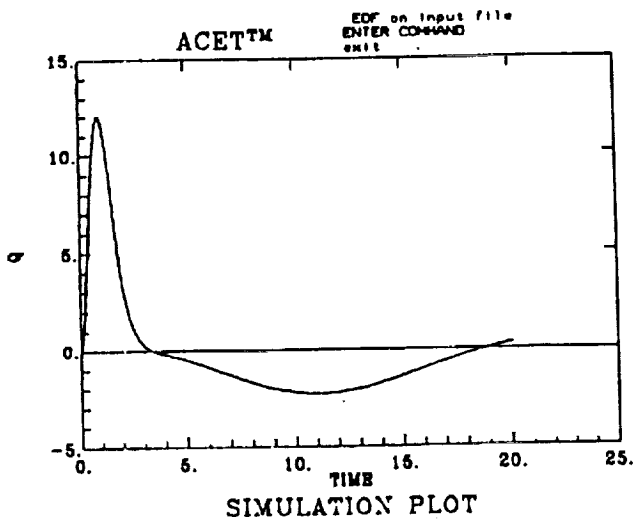
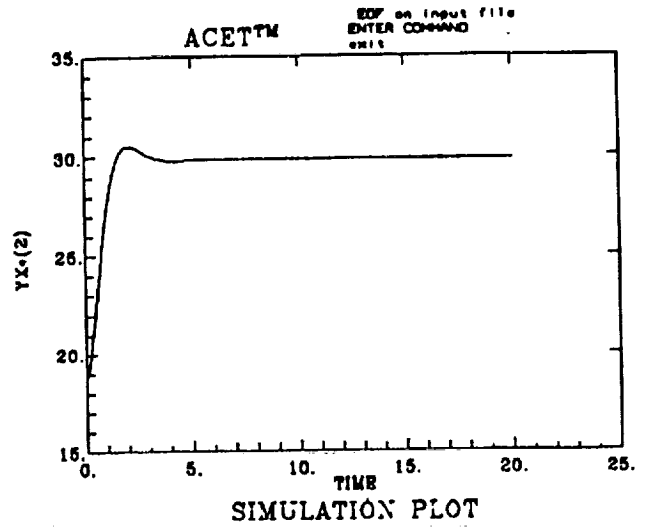
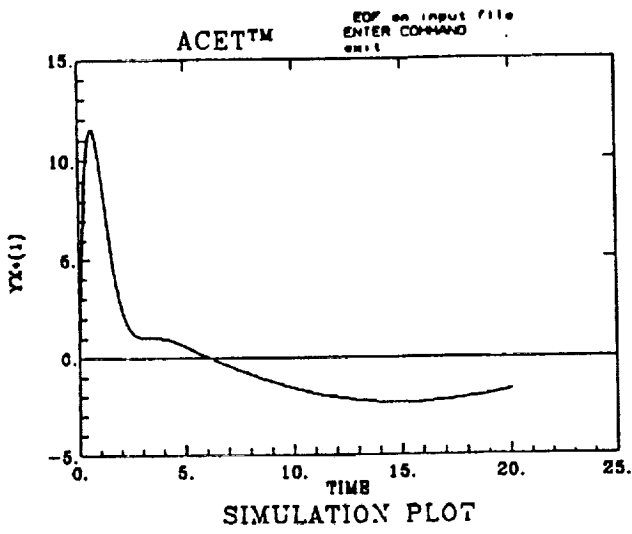


Figure 35a. F/A-18 Single-Model SOFT Control Law Simulation:  $\alpha$ -command =  $30^\circ$ .

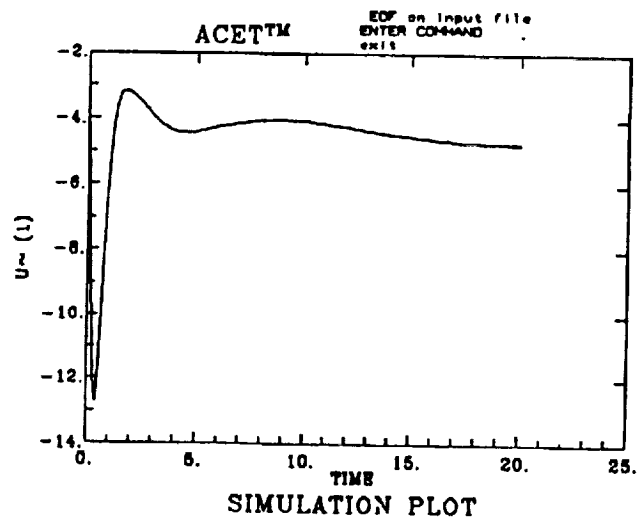
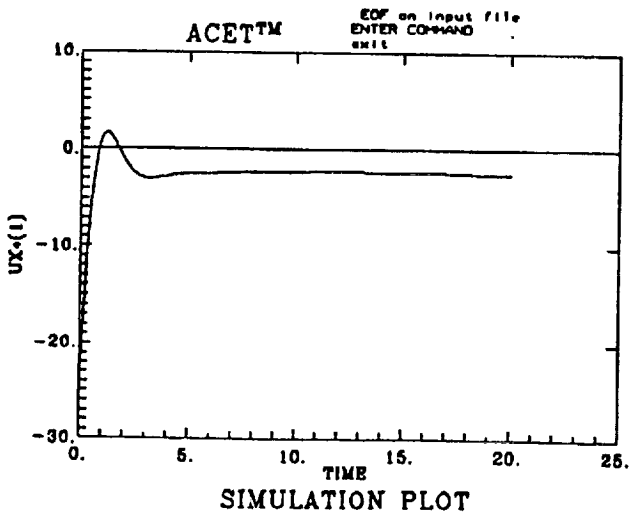
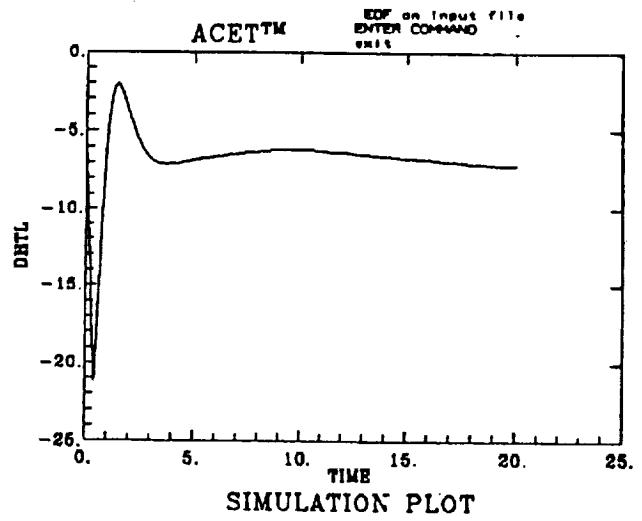
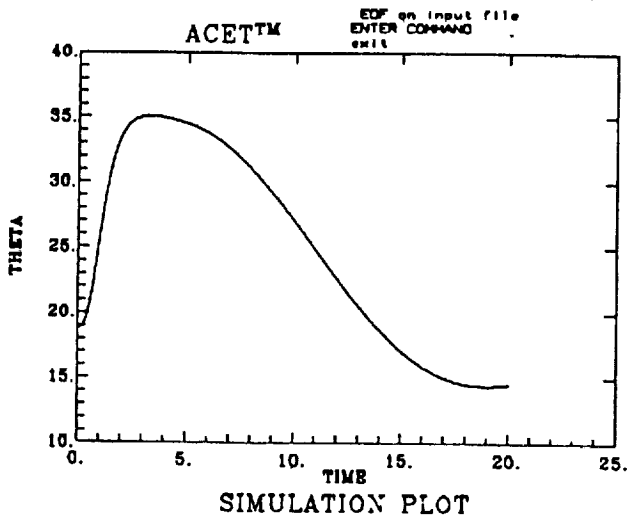
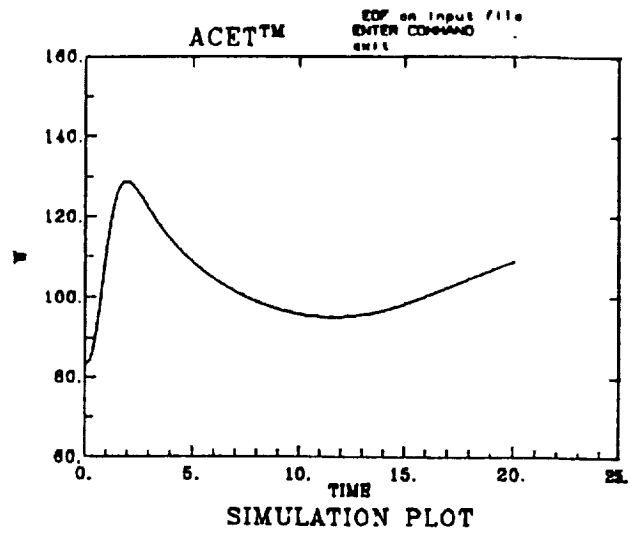
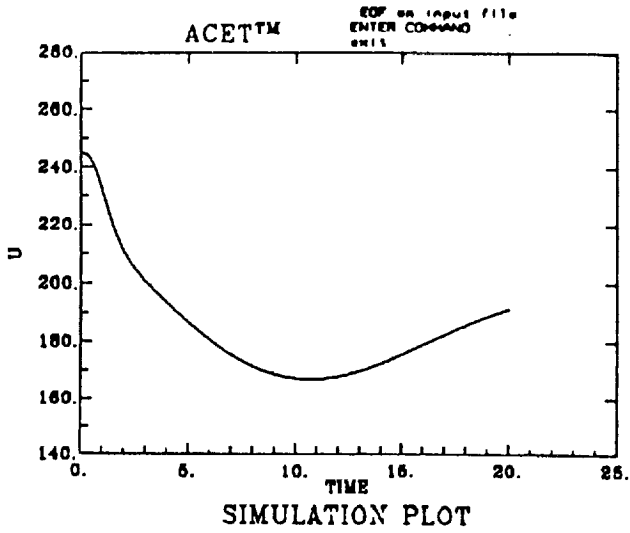


Figure 35b. F/A-18 Single-Model SOFFT Control Law Simulation:  $\alpha$ -command =  $30^\circ$ .

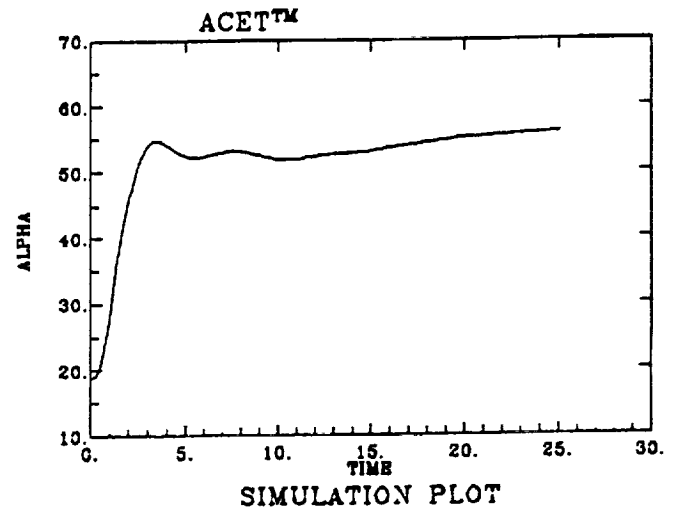
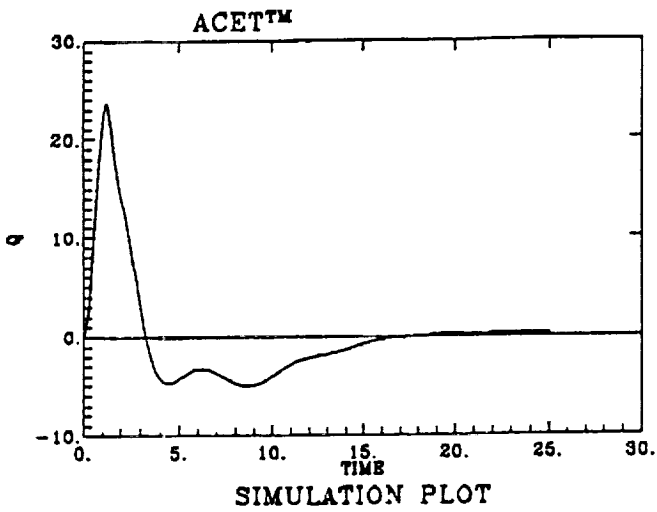
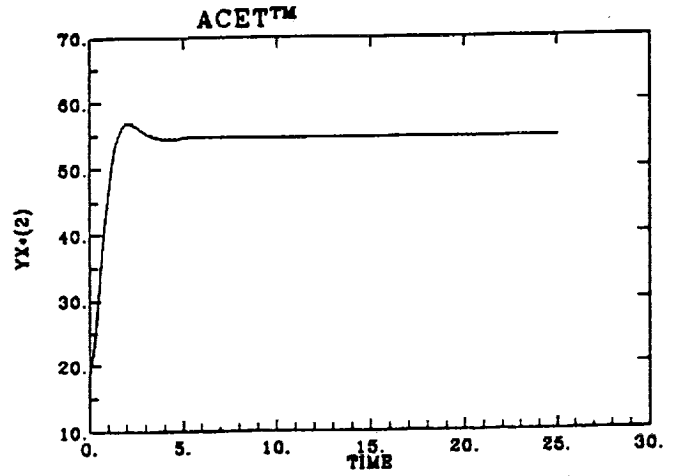
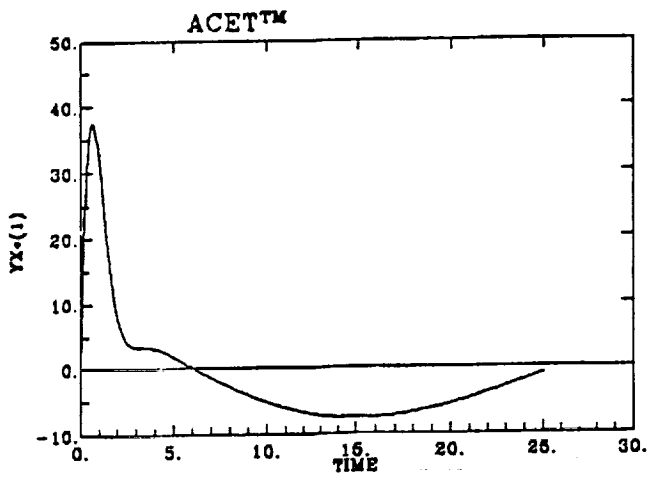


Figure 36a. F/A-18 Single-Model SOFT Control Law Simulation:  $\alpha$ -command =  $55^\circ$ .



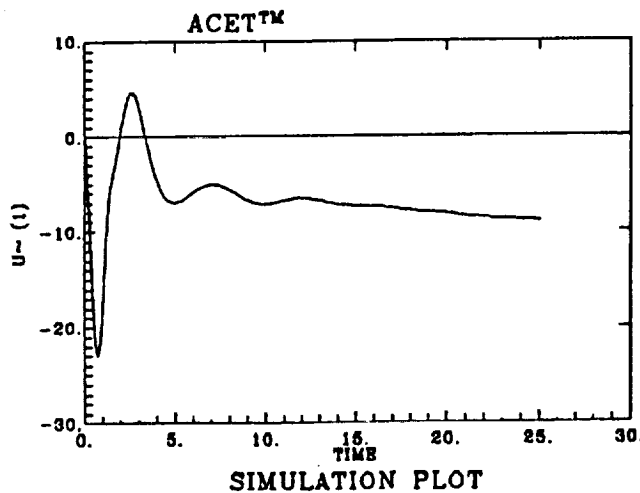
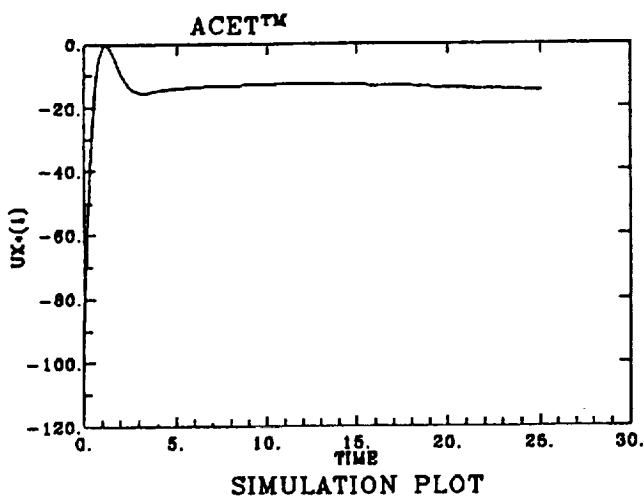
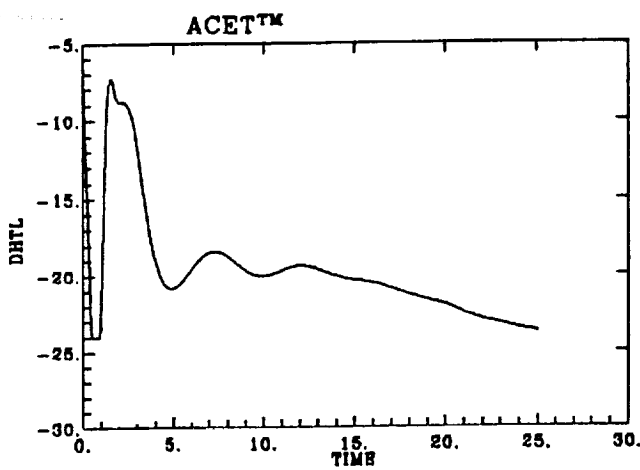
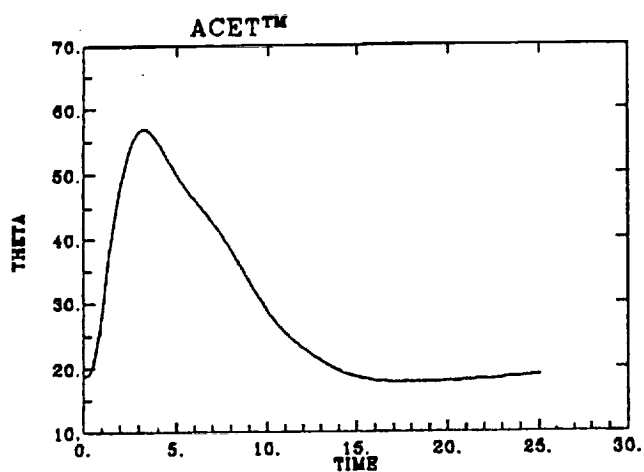
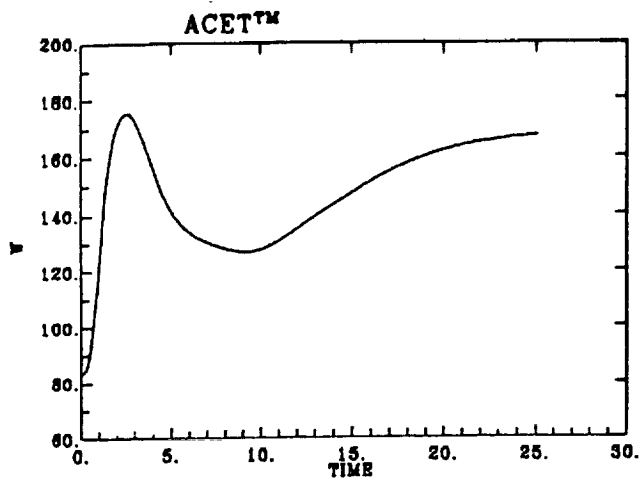
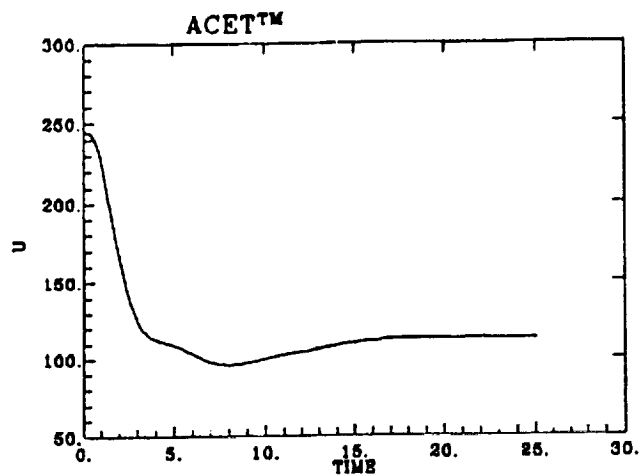


Figure 36b. F/A-18 Single-Model SOFFT Control Law Simulation:  $\alpha$ -command =  $55^\circ$ .

## CONCLUSIONS

The Stochastic Optimal Feedforward and Feedback Technique (SOFFT) is a new control system design methodology in which the feedforward and feedback control systems are designed separately and then combined so as to cooperate with each other. Traditional design techniques optimize a single cost function (which expresses the design objectives) to obtain both the feedforward and feedback control laws. In the SOFFT approach, two cost functions are defined. The feedforward control law is designed to optimize one cost function, the feedback optimizes the other.

The main feedforward design objective is to produce a desirable response in tracking input commands when no random noises and disturbances are present. In particular, a fast and smooth tracking response during the transient phase when difficult maneuvers are being performed is the goal of the feedforward law.

The main feedback design objectives are to suppress sensor noise, accommodate plant disturbances and provide stability in the presence of plant modeling uncertainties.

Since the feedforward response must be fast while the feedback response must be relatively slow (to attenuate noise), combining these objectives into a single cost function produces conflicting demands. In this case, neither of the objectives is fully achieved. By separating the design objectives and decoupling the feedforward and feedback design processes, we are able to achieve both objectives fully.

An important by-product of the SOFFT approach is that by removing the conflicting demands on the control system, we can design both feedforward and feedback control laws with less effort and in less time. The difficult and long process of fixing one problem only to find that another problem has popped up somewhere else is characteristic of conflicting demands. This effort seems to be mostly eliminated in the SOFFT approach.

Our main conclusion is that the concept of separating the feedforward and feedback objectives and decoupling the two designs as embodied in SOFFT works well. It produces both fast and smooth command tracking as well as noise attenuation, stability and robustness. The design process also takes less effort.

The SOFFT methodology can be used to design constant-gain feedforward and feedback systems as well as variable-gain control systems. Our experience with constant-gain design shows that we can achieve perfect tracking when the plant matches the model used in the feedforward design. When the plant moves to a non-matching operating point, the response seems highly robust.

A new measure of command tracking performance was developed. By analyzing these  $Z$ -plots at off-nominal operating points, we can predict the sensitivity or robustness of the total system in tracking commands.  $Z$ -plots provide an important tool for designing robust control systems.

The Variable-Gain SOFFT methodology was used to design a flight control system for the F/A-18 aircraft. The purpose of using a Variable-Gain SOFFT controller was to extend the operating regime of the aircraft and to provide greater performance (flying/handling qualities) throughout the extended regime. The angle-of-attack ( $\alpha$ ) command system designed brings the aircraft to within 3 degrees of its physical (actuator) limit. A detailed nonlinear simulation of the aircraft and control system displays excellent command tracking performance.

Finally, all the gain computation algorithms, and the analysis tools shown in this report were obtained using our Computer-Aided Control System Design (CACSD) software tool ACET<sup>TM</sup>. A new module to ACET has been developed in conjunction with the theoretical methodology development. ICS plans to market this new SOFFT design module in the coming months.

In conclusion, the high degree of success of the SOFFT design methodology has been rewarding. We recommend testing a Variable-Gain SOFFT flight control system in flight as a demonstration of this new technology.

## REFERENCES

1. Halyo, N. and J. R. Broussard, "Investigation, Development, and Application of Optimal Output Feedback Theory. Volume I — A Convergent Algorithm for the Stochastic Infinite-Time Discrete Optimal Output Feedback Problem", NASA CR-3828, August 1984.
2. Halyo, N. and J. R. Broussard, "A Convergent Algorithm for the Stochastic Infinite-Time Discrete Optimal Output Feedback Problem", *Proc. of the 1981 Joint Auto. Control Conf.* Volume 1., Amer. Auto. Control Council, c. 1981, paper WA-1E. Charlottesville, VA.
3. Halyo, N., "Development of a Digital Automatic Control Law for Steep Glideslope Capture and Flare", NASA CR-2834, June 1977.
4. Halyo, N., "Terminal Area Automatic Navigation, Guidance, and Control Research Using the Microwave Landing System (MLS), Part 5 — Design and Development of a Digital Integrated Automatic Landing System (DIALS) for Steep Final Approach Using Modern Control Techniques", NASA CR-3681, April 1983.
5. Halyo, N. and R. E. Foulkes, "On the Quadratic Sampled-Data Regulator with Unstable Random Disturbances", *IEEE SMC Cos. Proc. 1974 Int. Conf. on Syst., Man and Cybern.*, October 1974.
6. Halyo, N., "Flight Tests of the Digital Integrated Automatic Landing System (DIALS)", NASA CR-3859, December 1984.
7. Halyo, N. and J. R. Broussard, "Algorithms for Output Feedback, Multiple Model and Decentralized Control Problems", NASA Aircraft Controls Research — 1983, NASA CP-2296, October 25-27, 1983.
8. Halyo, N., "A Combined Stochastic Feedforward and Feedback Control Design Methodology With Application to Autoland Design", NASA CR-4078, July 1987.

9. Halyo, N., "Investigation, Development, and Application of Optimal Output Feedback Theory. Volume IV — Measures of Eigenvalue/Eigenvector Sensitivity to System Parameters and Unmodeled Dynamics", NASA CR-4108, December 1987.
10. Halyo, N. and A. K. Caglayan, "A Separation Theorem for the Stochastic Sampled-Data LQG Problem", *Int. J. Control*. Volume 23, No. 2, pp. 237-244, February 1976.
11. Kwakernaak, H. and R. Sivan, *Linear Optimal Control Systems*, John Wiley & Sons, Inc., New York, 1972.
12. Doyle, J. C. and G. Stein, "Multivariable Feedback Design: Concepts for a Classical/Modern Synthesis", *IEEE Trans. Auto. Control*. Volume AC-26, February 1981.
13. Broussard, J. R. and M. J. O'Brien, "Feedforward Control to Track the Output of a Forced Model", *IEEE Trans. Auto. Control*. Volume AC-25, No. 4, pp. 851-853, August 1980.
14. Broussard, J. R. and N. Halyo, "Investigation, Development, and Application of Optimal Output Feedback Theory. Volume II — Development of an Optimal Limited State Feedback Outer-Loop Digital Flight Control System for 3-D Terminal Area Operation", NASA CR-3829, August 1984.
15. Kirk, D. E., *Optimal Control Theory: An Introduction*, John Wiley & Sons, Inc., New York, 1972.
16. Maybeck, P. S., *Stochastic Models, Estimation and Control*. Volume 3, Academic Press, New York, 1982.
17. Halyo, N., "A Variable-Gain Output Feedback Control Design Approach", *Proc. AIAA Guidance Navigation, and Control Conf.*, Boston, MA, August 1989.
18. Halyo, N., Moerder, D. D., Broussard, J. R. and D. B. Taylor, "A Variable-Gain Output Feedback Control Design Methodology", NASA CR-4226, March 1989.
19. Astrom, K. J., *Introduction to Stochastic Control Theory*, Academic Press, New York, 1970.

20. Kushner, H. J., *Introduction to Stochastic Control*, Holt, Rinehart, and Winston, New York, 1971.
21. Etkin, B., *Dynamics of Atmospheric Flight*, John Wiley & Sons, Inc., New York, 1972.
22. Roskam, J., *Flight Dynamics of Rigid and Elastic Airplanes*, Parts I & II, Roskam Aviation and Engineering Corp., 519 Boulder, Lawrence, KS, 1972.
23. Ostroff, A. J., "Application of Variable-Gain Output Feedback for High-Alpha Control", *Proc. AIAA Guidance Navigation, and Control Conf.*, Boston, MA, August 1989.
24. Moerder, D. D., Halyo, N., Broussard, J. R. and A. Caglayan, "Application of Precomputed Control Laws in a Reconfigurable Aircraft Flight Control System", *J., Guidance, Control and Dynamics*. Volume 12, No. 3, pp. 325-333, May-June 1989.
25. Ostroff, A. J., "High-Alpha Application of Variable-Gain Output Feedback Control", *J., Guidance, Control and Dynamics*, Vol. 15, No. 2, pp. 491-497, March-April 1992.

## APPENDIX A

### Multi-Model Robust SOFFT

In section II, the SOFFT approach considered the control design problem for a single linear time-invariant (LTI) plant. Since most physical plants are nonlinear, it is more realistic to deal with a collection of LTI plants corresponding to a number of operating points. This collection of LTI plants may be referred as a multi-model plant and may also include plant modeling uncertainties such as uncertainties in parameter values or unmodeled dynamics.

The objective in investigating multi-model plants is to design robust SOFFT controllers which have a satisfactory performance with all of the plant models. Thus, the controller deals with model uncertainties and operating point variations without changing any controller parameter values. It is important to note that the Variable-Gain SOFFT Controller also accommodates variations in operating points; however, the controller parameters themselves vary to adapt to the plant variability.

Consider a multi-model plant with  $M$  LTI models described by the system equations

$$x_{ik+1} = \phi_i x_{ik} + \Gamma_i u_{ik} \quad , \quad 1 \leq i \leq M \quad , \quad (\text{A.1})$$

$$y_{ik} = C_i x_{ik} \quad , \quad 1 \leq i \leq M \quad . \quad (\text{A.2})$$

In the single model case (i.e., when  $M = 1$ ), the SOFFT feedforward controller is obtained by solving an optimal control problem. Note that the SOFFT feedforward control system shown in Figure A.1 is a dynamic compensator, not simply a gain matrix.

Now, let the command model be given by



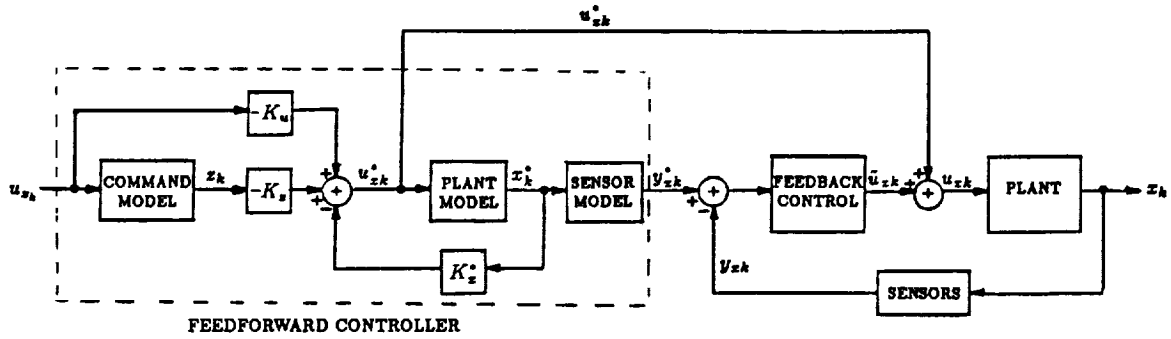


Figure A.1. SOFFT Control Law Structure

$$z_{k+1} = \phi_z z_k + \Gamma_z u_{zk} \quad (\text{A.3})$$

Now, we would like to find a dynamic system of the form

$$x_{k+1}^* = \phi_x^* x_k^* + \Gamma_x^* u_{zk}^* \quad (\text{A.4})$$

$$y_{zk}^* = C_z^* x_k^* \quad (\text{A.5})$$

with an input vector,  $u_{zk}^*$ , of the form

$$u_{zk}^* = -K_x^* x_k^* - K_z z_k - K_u u_{zk} \quad (\text{A.6})$$

so that when  $u_{zk}^*$  is the input of the  $i^{\text{th}}$  plant model in (A.1) - (A.2), the resulting tracking error given by

$$e_{ik} = H_{yi} y_{ik} - H_{zi} z_k = H_{xi} x_{ik} - H_{zi} z_k \quad (\text{A.7})$$

is small for all the models,  $1 \leq i \leq M$ .

In this general formulation, the optimization is not only over the gain matrices  $K_x^*$ ,  $K_z$  and  $K_u$ . We also want to find the dynamic compensator in (A.4); i.e.,  $\phi_x^*$  and  $\Gamma_x^*$  are also

part of the optimization although this was not originally proposed. This is a desirable feature, because a multi-model plant does not always identify (or favor) one particular model over the others.

A second point of importance is that this formulation does not restrict the order (say  $n_{x^*}$ ) of the feedforward dynamic compensator. For example, the multi-model plant order may be 15, whereas we would like to design a feedforward controller of lower order, say 4. This feature was also not originally proposed, but can be very important in practical applications, as has been stressed by Aaron Ostroff, of NASA, Langley Research Center. Finally, the lower order capability also provides a model reduction technique which should be investigated in the future.

The cost function,  $J$ , may be selected as

$$J = \frac{1}{2(N+1)} \sum_{k=0}^N \left\{ \sum_{i=1}^M f_i E \|e_{ik}\|_2^2 + f^* E \|e_k^*\|_2^2 \right\} \quad (\text{A.8})$$

where

$$e_k^* = H_y^* y_{zk}^* - H_z z_k = H_x^* x_k^* - H_z z_k \quad (\text{A.9})$$

The scalar weights  $f_i$  prioritize the multiple models. Note that all the models are included in the cost function so that the design will try to reduce the tracking error for each model. More terms can be added to the cost function to achieve various additional goals. In particular, for order reduction, a slightly different cost is used. Here, we assume that the cost is quadratic.

To develop an algorithm which determines the optimal controller parameters, we will formulate the general problem. We approach the problem in two steps. First, we consider the case in which  $u_{zk} = 0$ . Then, we introduce a non-zero  $u_{zk}$ . Now, consider the following open-loop feedforward model.

$$x_{k+1}^* = \phi_o x_k^* + \Gamma_{oz} u_{zk}^* + \Gamma_{oc} u_{ok}^* \quad (\text{A.10})$$



$$u_k^* = \begin{pmatrix} u_{xk}^* \\ u_{ok}^* \end{pmatrix} = -K^* Y_k^* \quad (\text{A.15})$$

$$K^* = \begin{pmatrix} K_x^* & K_z^* \\ K_{ox}^* & K_{oz}^* \end{pmatrix} \quad (\text{A.16})$$

For the case of the feedforward design, it is reasonable to set the measurement noise covariance to zero. However, we have included these terms for generality.

The augmented system in (A.13) and (A.14), coupled with the control constraint (A.15) and the cost function (A.8) form an optimal output feedback control problem treated by the Principal Investigator previously. Therefore, this algorithm may now be used to obtain the augmented gain matrix,  $K^*$ , in (A.16).

Note that the cost function in (A.8) is of quadratic form and may be computed as follows.

$$H_{xi} = H_{yi} C_i \quad , \quad 1 \leq i \leq M \quad (\text{A.17})$$

$$H_z^* = H_y^* C_x^* \quad (\text{A.18})$$

$$H = \begin{pmatrix} H_{x1} & 0 & \cdots & 0 & -H_{z1} \\ 0 & H_{x2} & & 0 & -H_{z2} \\ \vdots & & \ddots & \vdots & \cdots \\ & & & H_{zM} & 0 & -H_{zM} \\ 0 & & & & H_z^* & -H_z \\ 0 & & & & 0 & 0 \end{pmatrix} \quad (\text{A.19})$$

$$F = \begin{pmatrix} f_1 I & 0 & \cdots & 0 \\ 0 & f_x I & & \\ \vdots & & \ddots & \vdots \\ & & & f_M I & \\ 0 & & & & f^* I & 0 \end{pmatrix} \quad (\text{A.20})$$

$$Q^* = H^T F H + Q_1 \quad (\text{A.21})$$

$$J = \frac{1}{2(N+1)} \left\{ \sum_{k=0}^N X_k^{*T} Q^* X_k^* + u_k^{*T} R^* u_k^* \right\} \quad (\text{A.22})$$

Consider the case in which  $u_{ok}^*$  is not present. When the optimal  $K^*$  is computed, the gains  $K_x^*$  and  $K_z$  determine  $u_{zk}^*$  in the feedforward control law in (A.4) and (A.5) with

$$\phi_x^* = \phi_o \quad , \quad \Gamma_x^* = \Gamma_{ox} \quad . \quad (\text{A.23})$$

In the more general case, solving the optimization problem produces the gain  $K^*$  and its partition in (A.16). In this case, some manipulation yields

$$\phi_x^* = \phi_o - \Gamma_{oc} (K_{ox}^* - \gamma_z K_z^*) \quad (\text{A.24})$$

$$\Gamma_x^* = \Gamma_{ox} + \Gamma_{oc} \gamma_z \quad (\text{A.25})$$

$$\gamma_z = K_{oz} K_z^T [K_z K_z^T]^{-1} \quad (\text{A.26})$$

For (A.24) - (A.26) to be valid, it is sufficient that

$$\Gamma_{oc} K_{oz} \left\{ I - K_z^T [K_z K_z^T]^{-1} K_z \right\} = 0 \quad (\text{A.27})$$

While (A.27) will not hold in general, it will be satisfied when  $K_z$  is non-singular.

To include the effect of  $u_{zk}$ , we augment the system given in (A.13) by

$$u_{zk+1} = 0 u_{zk} + \omega_{u_{zk}} \quad (\text{A.28})$$

and couple it to  $z_k$  through the command model (A.3). Using previously developed results\* to this augmented system, we obtain

---

\*A Combined Stochastic Feedforward and Feedback Control Design Methodology With Application to Autoland Design, NASA CR-4078, July 1987, p. 14.

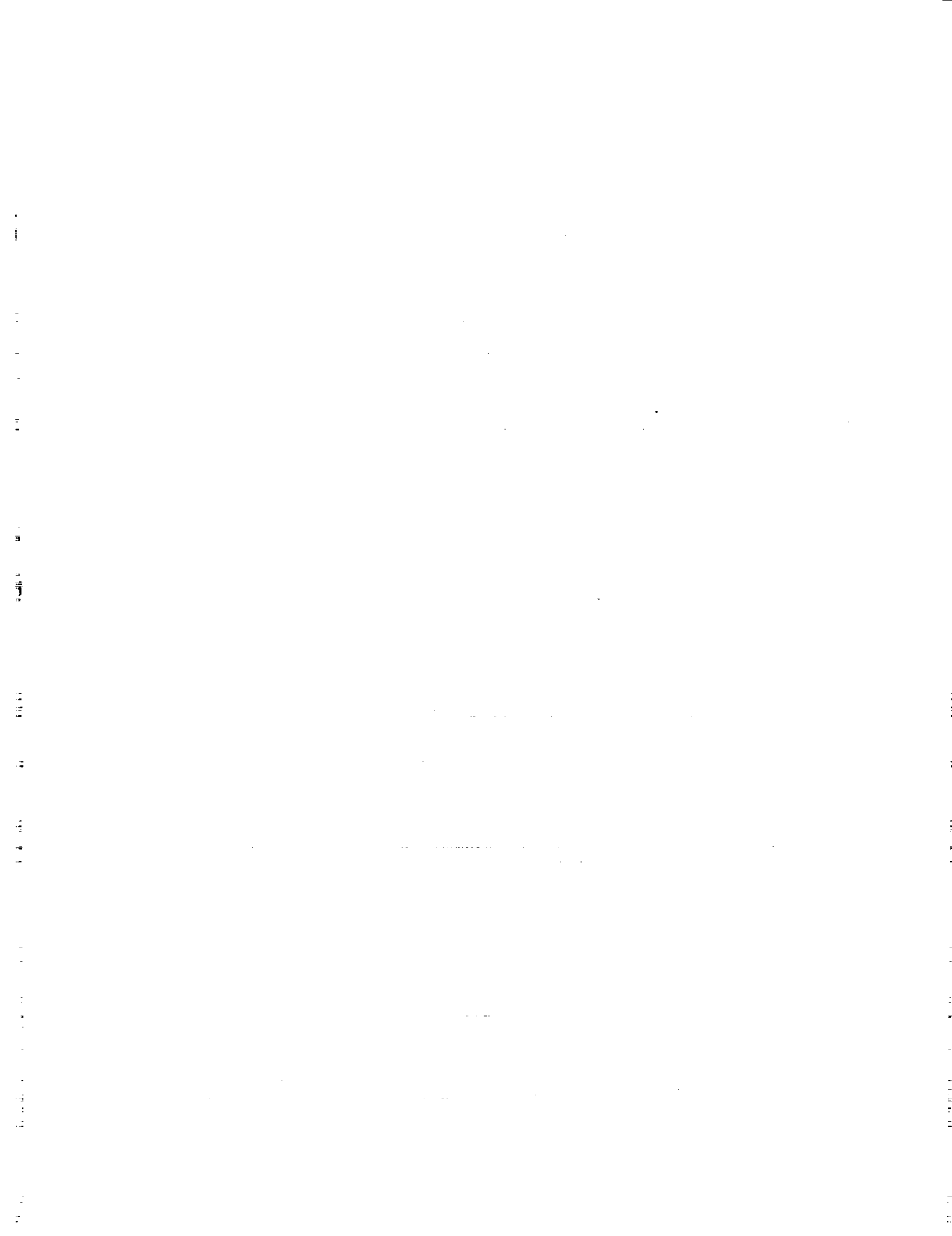
$$K_u = \hat{P}_X^{-1} \Gamma_X^T P_{Xz} \Gamma_z W_u (W_u + V_u)^{-1} \quad (\text{A.29})$$

$$\hat{P}_X = \Gamma_X^T P_X \Gamma_X + R^* \quad (\text{A.30})$$

$$W_u = E(u_{zk} u_{zk}^T) \quad (\text{A.31})$$

$$P = \begin{pmatrix} P_X & P_{Xz} \\ P_{zX} & P_{zz} \end{pmatrix} \quad (\text{A.32})$$

where  $P$  is optimal the cost matrix for the system in (A.13) and  $V_u$  is the covariance of the measurement noise for  $u_{zk}$ . Note that when  $V_u = 0$ , which is usually valid in feedforward control problems,  $W_u$  cancels from (A.29).



REPORT DOCUMENTATION PAGE			Form Approved OMB No 0704-0188	
<small>Public reporting burden for this collection of information is estimated to average 1 hour per response, including the time for reviewing instructions, searching existing data sources, gathering and maintaining the data needed, and completing and reviewing the collection of information. Send comments regarding this burden estimate or any other aspect of this collection of information, including suggestions for reducing this burden, to Washington Headquarters Services, Directorate for Information Operations and Reports, 1215 Jefferson Davis Highway, Suite 1204, Arlington, VA 22202-4302, and to the Office of Management and Budget, Paperwork Reduction Project (0704-0188), Washington, DC 20503.</small>				
1. AGENCY USE ONLY (Leave blank)	2. REPORT DATE November 1992	3. REPORT TYPE AND DATES COVERED		
4. TITLE AND SUBTITLE A Stochastic Optimal Feedforward and Feedback Control Methodology for Superagility			5. FUNDING NUMBERS C NAS1-19091  WU 324-02-01-01	
6. AUTHOR(S) Nesim Halyo Haldun Direskeneli Deborah B. Taylor				
7. PERFORMING ORGANIZATION NAME(S) AND ADDRESS(ES) Information & Control Systems, Incorporated 28 Research Drive Hampton, VA 23666			8. PERFORMING ORGANIZATION REPORT NUMBER FR-692101	
9. SPONSORING / MONITORING AGENCY NAME(S) AND ADDRESS(ES) National Aeronautics and Space Administration Langley Research Center Hampton, VA 23665-5225			10. SPONSORING / MONITORING AGENCY REPORT NUMBER NASA CR-4471	
11. SUPPLEMENTARY NOTES Langley Technical Monitor: Aaron J. Ostroff Final Report				
12a. DISTRIBUTION / AVAILABILITY STATEMENT  Unclassified-Unlimited  Subject Category 63			12b. DISTRIBUTION CODE	
13. ABSTRACT (Maximum 200 words) <p>A new control design methodology is developed: Stochastic Optimal Feedforward and Feedback Technology (SOFFT). Traditional design techniques optimize a single cost function (which expresses the design objectives) to obtain both the feedforward and feedback control laws. This approach places conflicting demands on the control law such as fast tracking versus noise attenuation/disturbance rejection. In the SOFFT approach, two cost functions are defined. The feedforward control law is designed to optimize one cost function, the feedback optimizes the other. By separating the design objectives and decoupling the feedforward and feedback design processes, both objectives can be achieved fully.</p> <p>A new measure of command tracking performance, Z-plots, is also developed. By analyzing these plots at off-nominal conditions, the sensitivity or robustness of the system in tracking commands can be predicted. Z-plots provide an important tool for designing robust control systems.</p> <p>The Variable-Gain SOFFT methodology was used to design a flight control system for the F/A-18 aircraft. It is shown that SOFFT can be used to expand the operating regime and provide greater performance (flying/handling qualities) throughout the extended flight regime.</p> <p>This work was performed under the NASA SBIR program. ICS plans to market the software developed as a new module in its commercial CACSD software package: ACET.</p>				
14. SUBJECT TERMS Feedforward, Feedback, Stochastic optimal control, SOFFT, Sensitivity, Tracking error, Command tracking, Robustness, Z-plots, Variable-gain control, Nonlinear control, F/A-18			15. NUMBER OF PAGES 152	16. PRICE CODE A08
17. SECURITY CLASSIFICATION OF REPORT Unclassified	18. SECURITY CLASSIFICATION OF THIS PAGE Unclassified	19. SECURITY CLASSIFICATION OF ABSTRACT	20. LIMITATION OF ABSTRACT	